# Glycerol production in *Plasmodium falciparum*: Towards a detailed kinetic model

by

Waldo Wayne Adams

Thesis presented in partial fulfilment of the requirements for the degree of Master of Science in Biochemistry in the Faculty of Science (Biochemistry) at Stellenbosch University

Department of Biochemistry
University of Stellenbosch
Private Bag X1, Matieland, 7602, South Africa

Supervisors:

Prof J.L. Snoep

Department of Biochemistry

University of Stellenbosch

Co-promoter:

Prof M. Rautenbach

Department of Biochemistry

University of Stellenbosch

March 2015

Declaration

By submitting this thesis electronically, I declare that the entirety of the work contained therein is my own, original work, that I am the sole author thereof (save to the extent explicitly otherwise stated), that reproduction and publication thereof by Stellenbosch University will not infringe any third party rights and that I have not previously in its entirety or in part submitted it for obtaining any qualification.

Signature: . . . .
      W.W. Adams

        15/01/2015
Date: . . . .

i

Abstract

Glycerol production in *Plasmodium falciparum*:
Towards a detailed kinetic model

W.W. Adams

Department of Biochemistry
University of Stellenbosch
Private Bag X1, Matieland, 7602, South Africa

Thesis: MSc (Biochemistry)

January 2015

Having caused the deaths of more than 10 million individuals since 2000 with most of them occurring in Africa, malaria remains a serious disease that requires undivided attention. To this end a detailed kinetic model of *Plasmodium falciparum* glycolysis was constructed, validated and used to determine potential drug targets for the development of novel, effective antimalarial therapies.

The kinetic model described the behaviour of the glycolytic enzymes with a set of ordinary differential equations that was solved to obtain the steady state fluxes and concentrations of internal metabolites. The model included a glycerol branch represented in a single fitted equation. This present study set out to detect, characterise, and incorporate into the model the enzymes that constitute the glycerol branch of *P. falciparum* glycolysis.

The kinetic parameters of glycerol 3-phosphate dehydrogenase (G3PDH), the first enzyme in the branch and catalyst of the dihydroxyacetone phosphosate (DHAP) reducing reaction, was determined and added to the detailed kinetic

model. The model was subsequently validated by comparing its prediction of steady state fluxes with experimentally measured fluxes.

Once it was evident that the predictions of the unfitted model agreed with experimentally measured fluxes, metabolic control analysis was performed on this branched system to ascertain the distribution of control over the steady state flux through the glycerol branch. The control G3PDH exercised over its own flux was less than expected due to the enzyme's sensitivity to changes in NADH and thus the redox balance of the cell.

Attempts were made to detect the enzymes responsible for the conversion of glycerol 3-phosphate (G3P) to glycerol. Very low levels of glycerol kinase activity was observed. Although G3P-dependent release of inorganic phosphate was detected results were inconclusive as to whether a non-specific phosphatase also mediated the conversion.

Overall, the expansion of the model to include G3PDH did not affect the steady state metabolite concentrations and flux adversely.

Uittreksel

Gliserol produksie in *Plasmodium falciparum*: Ontwikkeling van 'n uitvoerige kinetiese model

W.W. Adams

Departement Biochemie
Universiteit van Stellenbosch
Privaatsak X1, Matieland 7602, Suid Afrika

Tesis: MSc (Biochemie)

Januarie 2015

Vanaf die jaar 2000 het malaria die dood van meer as 10 miljoen mense veroorsaak. Die meeste sterftes het in Afrika voorgekom —'n aanduiding van hoe ernstige siekte dit is en een wat onverdeelde aandag moet geniet. Om hierdie rede is 'n gedetaileerde kinetiese model van glikoliese in *Plasmodium falciparum* gebou, gevalideer en gebruik om potensiële dwelm teikens te identifiseer vir die ontwikkeling van nuwe, meer effektiewe anti-malaria terapieë.

Die kinetiese model beskryf die gedrag van die glikolitiese ensieme in terme van gewone differensiële vergelykings wat opgelos is om die bestendige toestand fluksies en interne metaboliet konsentrasies te bepaal. Die model sluit 'n gliserol-tak in wat deur 'n enkele aangepaste vergelyking verteenwoordig word. Hierdie studie het voorgeneem om die ensieme van die gliserol-tak van *P. falciparum* glikoliese te identifiseer, karakteriseer en in die model te inkorporeer.

Ons het die kinetiese parameters van die eerste ensiem in die gliserol-tak, gliserol 3-fosfaat dehidrogenase (G3PDH), die katalis van die dihidroksiasetoon

iv

fosfaat(DHAP) reduserende reaksie, bepaal. Die kinetiese parameters is by die gedetaileerde model gevoeg. Validering het plaasgevind deur die model se voorspellings met eksperimenteel bepaalde waardes te vergelyk.

Toe dit duidelik geword het dat die voorspellings van die model met die eksperimenteel bepaalde fluks ooreenstem, is metaboliese kontrole analiese op die vertakte sisteem uitgevoer. Dit is gedoen om vas te stel hoe die bestendige toestand fluks deur die gliserol-tak beheer word. G3PDH het nie volle beheer oor sy eie fluks nie, in teenstelling met ons vergewagtinge.

Daar is gepoog om vas te stel watter ensieme verantwoordelik is vir die produksie van gliserol vanuit gliserol 3-fosfaat (G3P). 'n Lae gliserolkinase aktiwiteit is waargeneem. Alhoewel G3P afhanklike vrystelling van anorganise fosfaat waargeneem is, is dit nie duidelik vanuit die resultate of die proses deur 'n nie-spesifieke fosfatase uitgevoer word nie.

Die uitbreiding van die model om 'n G3PDH vergelyking in te sluit het nie die bestendige toestand metaboliet konsentrasies en fluks negatief geaffekteer nie.

Acknowledgements

I would like to express my sincere gratitude to

- my parents and sister for supporting throughout the course of this study.

- Prof Jacky Snoep for the privilege to study in his laboratory, under his tutelage, and for his patience.

- Prof Marina Rautenbach for advising with the culturing of malaria and sample analysis on HPLC as well as for believing in me.

- Prof Pieter Swart for teaching me more about HPLC, guiding me with the sample analysis on the HPLC and availing his HPLC system.

- Mr Arrie Arends for his technical support and our edifying philosophical discussions.

- Dr Gerald Penkler for imparting his knowledge of enzyme kinetics, malaria culturing and programing in Wolfram Mathematica to me.

- the members of the Triple J Lab for informative discussions.

- the malaria group (Hazel Makowa, Adrienne Leussa, Francios du Toit, Cristiano Macuamule, Francios Brand and Nicolas Walters) for the camaraderie and team work that culturing malaria requires.

- the Lord for giving me wisdom, patience and strength to perform this study.

Dedications

I dedicate this thesis to:
My parents and sister
who supported and loved me throughout my studies and life.

Contents

List of Figures

List of Tables

Abbreviations

1,3-BPG	1,3-Bisphosphoglycerate
2,3-BPG	2,3-Bisphosphoglycerate
2PGA	2-Phosphoglycerate
3PGA	3-Phosphoglycerate
6PGL	6-Phosphogluconolactononase (E.C. 3.1.1.31)
Acetyl-CoA	Acetyl-coenzyme A
ADP	Adenosine diphosphate
AGPAT	1-acyl-glycerol-3-phosphate acyltransferase (E.C. 2.3.1.51)
ALD	Fructose bisphosphate aldolase (E.C. 4.1.2.13)
ATP	Adenosine triphosphate
CDP	Cytidine diphosphate
CDP-DAG	Cytidine diphosphate diacylglycerol
CDS	CDP-DAG synthase (E.C. 2.7.7.41)
CL	Cardiolipin
CLS	Cardiolipin synthase (E.C. 2.7.8.-)
CTP	Cytidine triphosphate
CytB	Cytochalasin B
DAG	Diacylglycerol
DGAT	Acyl-CoA:DAG acyltransferase (E.C. 2.3.1.20)
DHAP	Dihydroxyacetone phosphate
DHODH	Dihydroorotate dehydrogenase (E.C. 1.3.3.1)
dPGM	2,3-Bisphosphoglycerate-dependent phosphoglycerate mutase
iPGM	2,3-Bisphosphoglycerate-independent phosphoglycerate mutase
ENO	Enolase (E.C. 4.2.1.11)
ETC	Electron transport chain
F1,6BP	Fructose-1,6-Bisphosphate
F6P	Fructose-6-Phosphate
G3P	Glycerol-3-phosphate)
G3PDH	Glycerol-3-phosphate dehydrogenase (E.C. 1.1.1.8)
G3Pase	Glycerol-3-phosphate-dependent phosphatase
G6P	Glucose-6-phosphate
G6PD-6PGL	Glucose-6-phosphate dehydrogenase-6-phosphogluconolactonase
G6PDH	Glucose-6-phosphate-1-dehydrogenase (E.C. 1.1.1.49)
GAP	Glyceraldehyde-3-phosphate

GAPDH	Glyceraldehyde-3-phosphate dehydrogenase (E.C. 1.2.1.12)
GK	Glycerol kinase
Glc	D-Glucose
GlcTr	Glucose transporter
Glr	Glycerol
GlrDH	α-Glycerol phosphate dehydrogenase (E.C. 1.1.1.8)
GlrTr	Glycerol transporter
GPAT	Glycerol-3-phosphate acyltransferase (E.C. 2.3.1.15)
HEPES	4-(2-Hydroxyethyl)piperazine-1-ethanesulfonic acid
HILIC	Hydrophilic interaction liquid chromatography
HK	Hexokinase (E.C. 2.7.1.1)
HPLC	High performance liquid chromatography
kDa	kiloDalton
K_m	Michaelis constant
Lac	Lactate
LacTr	Lactate transporter
LDH	L-Lactate dehydrogenase (E.C. 1.1.1.27)
L.O.D.	Limit of detection
lysoPA	Lyso-phosphatidic acid
mRNA	Messenger RNA
MCA	Metabolic control analysis
MCT	Monocarboxylate transporter
MQO	Malate:quinone oxidoreductase (EC 1.1.5.4)
NAD^+	Oxidised nicotinamide adenine dinucleotide
NADH	Reduced nicotinamide adenine dinucleotide
$NADP^+$	Oxidised nicotinamide dinucleotide phosphate
NADPH	Reduced nicotinamide dinucleotide phosphate
PA	Phosphatidic acid
PAP-1	Mg^{2+}-dependent hosphatidic acid phosphatase 1 (E.C. 3.1.3.4)
PAP-2	Mg^{2+}-independent Phosphatidic acid phosphatase 2 (E.C. 3.1.3.4)
PC	Phosphatidyl choline
PE	Phosphatidyl ethanolamine
PEP	Phosphoenolpyruvate
PFK	Phosphofructokinase (E.C. 2.7.1.11)
PfAQP	*Plasmodium falciparum* aquaglyceroporin
PfHT1	*Plasmodium falciparum* Hexose transporter 1
PfNDH2	*Plasmodium falciparum* NADH:ubiquinone oxidoreductase (E.C. 1.6.5.3)
PfPGM1	*Plasmodium falciparum* phosphoglycerate mutase 1 (E.C. 5.4.2.1)
PfPGM2	*Plasmodium falciparum* phosphoglycerate mutase 2
PGI	Phosphoglucoisomerase (E.C. 5.3.1.9)
PGK	Phosphoglycerate kinase (E.C. 2.7.2.3)
PGM	Phosphoglycerate mutase (E.C. 5.4.2.1)
PI	Phosphatidyl inositol

Pi	Inorganic phosphate
PK	Pyruvate kinase (E.C. 2.7.1.40)
PLs	Phospholipids
PPP	Pentose phosphate pathway
PS	Phosphatidyl serine
Pyr	Pyruvate
PyrTr	Pyruvate transporter
RNS	Reactive nitrogen species
ROS	Reactive oxygen species
SDH	Succinate:ubiquinone oxidoreductase (E.C. 1.3.5.1)
SEM	Standard error of the mean
TAG	Triacylglycerol
TPI	Triosphosphate isomerase (E.C. 5.3.1.1)
U	Enzyme units
V_{max}	Maximal specific activity of an enzyme, normalised to total cell protein
WHO	World Health Organization

Prelude

Having caused the deaths of more than 10 million individuals since 2000 with most of them occurring in Africa, malaria remains a serious disease that requires undivided attention[1]. The World Health Organization (WHO), in its *World Malaria Report 2013*[1], reported a decline in malaria incidence and mortality rates worldwide in all age groups since 2000. Despite best efforts to control and eradicate the disease, drug resistance among the *Plasmodium* parasites is growing. Among the five *Plasmodium* species that infect humans, *P. falciparum* is the most lethal.

In an effort to aid the drug discovery process, Penkler[2] constructed a detailed kinetic model of the Emden-Meyerhof-Parnas (glycolysis) pathway of *P. falciparum* D10. Construction of the model (Penkler 1 model), which is available on JWS Online (http://jjj.biochem.sun.ac.za), followed a bottom up approach that required the measurement of the kinetic parameters of each enzyme in the pathway. The ATPase and glycerol dehydrogenase (GlrDH) reactions were the only two reactions that were fitted, the others were determined experimentally. Metabolic control analysis[3,4,5], parameter sensitivity analysis[2] and the differential control approach[6,7] were used to validate the model by determining which enzymes exerted the highest control over the steady state flux and metabolite concentrations, and testing whether an inhibitor of one of these pathogen enzymes could inhibit the flux with little adverse effects on the host system. Cytochalasin B was the inhibitor and the *P. falciparum* hexose transporter 1 (PfHT1) was the chosen enzyme. The model described the behaviour of the system well, thereby passing the validation tests.

However, the glycerol branch of the Penkler model was represented by a single fitted rate equation that was based on K_M values from the scientific literature. The V_{max} value for the glycerol branch was fitted to match the steady state

flux through the branch. This present work aimed to elucidate the kinetic behaviour of the glycerol branch by:

- biochemically characterising glycerol 3-phosphate (G3P) dehydrogenase,

- detecting and kinetically characterising glycerol kinase,

- identifying and characterising any G3P-dependent phosphatase activity

- replacing the single fitted rate equation that represents the glycerol branch in the original model with the kinetic information obtained in this study

- determining the factors involved in the flux control of the glycerol branch.

The results of this study are presented in **Chapter 3** along with a discussion of the results in the context of the background information presented in **Chapter 1**. The materials and methods used to conduct the experiments are explained in **Chapter 2**. This thesis is concluded by a general discussion on the limitations and future research based on this study in **Chapter 4**.

CHAPTER 1

BACKGROUND

This chapter contains an overview of the malarial threat, life cycle of the parasite, glycolysis and the enzymes involved in production and consumption of glycerol and its activated form (i.e. glycerol-3-phosphate) as well as the fundamentals of kinetic modeling.

1.1 Introduction

Malaria, a disease caused by parasites of the genus *Plasmodium*, has plagued the human race for millenia[8]. Of the five *Plasmodium* species that infect humans, *P. falciparum* and *P. vivax* are the most prevalent and *P. falciparum* the most lethal[1].

According to the WHO[1], *P. falciparum* mainly affects Africa while *P. vivax* enjoys a wider distribution range due to its ability to grow at lower temperatures and higher altitudes. It is estimated that 627 000 people died from the disease in 2012 while there were over 200 million new cases worldwide. Africa was the worst affected region with 165 million new cases and 562 000 deaths in 2012. South-East Asia, the second worst affected region, experienced 27 million new cases and 42 000 deaths.

1.2 *Plasmodium falciparum* life cycle

As reviewed by others[9,8 and references therein], the *P. falciparum* life cycle in humans begins when a female *Anopheles* mosquito takes a blood meal. Sporozoites residing in the salivary glands of the *Plasmodium* infected mosquito are deposited in the skin from where they haphazardly make their way to blood vessels where they are transported by the blood stream to the liver[10]. In the

liver the sporozoites infect hepatocytes and mature into schizonts undergoing a substantial amount of nuclear divisions and cytokinesis in the process. After subsequent rupture of the liver cell, thousands of merozoites are released into the blood stream where they subsequently invade erythrocytes. Some *P. vivax* parasites continue to reside in the liver in a dormant hypnozoite form[8].

The intra-erythrocytic asexual phase of the *Plasmodium* life cycle marks the onset of clinical symptoms. Once inside erythrocytes, merozoites develop into trophozoites. During the early trophozoite stage the parasite has a ring-like appearance, the centre of which fills up as the trophozoite matures. During the next 48 hours, the trophozoites mature into schizonts which give rise to up to 32 merozoites, and rupture releasing merozoites into the blood stream once again where they infect new erythrocytes.

Some merozoites develop into male and female gametocytes which remain dormant until they are taken up by an *Anopheles* mosquito during a blood meal[11]. Fertilisation ensues in the mosquito's gut once gametes are formed. The diploid zygote undergoes meiosis producing motile ookinetes that penetrate the midgut and form oocysts which give rise to sporozoites. These migrate to the mosquito's salivary glands, completing the life cycle.

1.3   Parasite energy supply

In addition to the onset of clinical symptoms, the intra-erythrocytic or asexual phase of the *P. falciparum* life cycle is characterised by a 100-fold increase in glucose consumption in the infected erythrocyte[12]. Glucose is the trophozoite's main source of free energy[13].

Although *P. falciparum* possesses a functional electron transport chain (ETC) located in the mitochondrion, the ATP synthase (Complex V) of the ETC does not generate ATP (unlike mammalian ATP synthase) and functions as a proton pump[14,15,16,13]. The ETC has therefore been proposed to act as an electron sink[17] accepting reducing equivalents from its five dehydrogenases[18], viz. NADH:ubiquinone oxidoreductase (PfNDH2), succinate:ubiquinone oxidoreductase (Complex II or SDH), glycerol-3-phosphate dehydrogenase (G3PDH), malate quinone oxidoreductase (MQO) and dihydroorotate dehydrogenase (DHODH). Of these, MQO and PfNDH2 have been identified as drug targets

due to their absence in human mitochondria while the unique molecular differences in DHODH distinguishes it from its human homologue[18]. Despite its lack of contribution to *P. falciparum* energy metabolism, the ETC is essential for the parasite's existence since viable deletion mutants could not be obtained[19].

1.4 Glycolysis

Glycerol (Glr) is produced[2] (Fig. 1.1) when *P. falciparum* hexose transporter 1 (PfHT1) traffics glucose into the parasite cytosol where it is sequentially converted by hexokinase (HK), phosphoglucose isomerase (PGI), phosphofructokinase (PFK) and aldolase (ALD) to glyceraldehyde (GAP) and dihydroxyacetone phosphate (DHAP). Triose phosphate isomerase (TPI) converts DHAP to GAP while NAD^+-dependent glycerol-3-phosphate dehydrogenase (G3PDH) catalyses the reduction of DHAP to glycerol-3-phosphate (G3P) with the concomitant oxidation of NADH. G3P is subsequently dephosphorylated by glycerol kinase (GK) working in reverse or a non-specific phosphatase and the Glr exported via *P. falciparum* aquaglyceroporin (PfAQP)[20,21]. It is believed that maintenance of the redox balance of the cell is the main driving force behind G3P and glycerol production[22,2,23].

Glycolysis[2] continues as GAP dehydrogenase (GAPDH), phosphoglycerate kinase (PGK), phosphoglycerate mutase (PGM), enolase, pyruvate kinase (PK) and lactate dehydrogenase (LDH) convert GAP to lactate which is transported out of the parasite via a proton-coupled lactate transporter[24]. This transporter also transports pyruvate[24,25].

Although most of the glycolytic flux produces lactate, small but significant amounts feed the pentose phosphate pathway as well as the glycerol and carbon dioxide fixation branches[2] .

1.5 Enzymes of the glycerol branch

A closer look will now be taken at the enzymes of the glycerol branch.
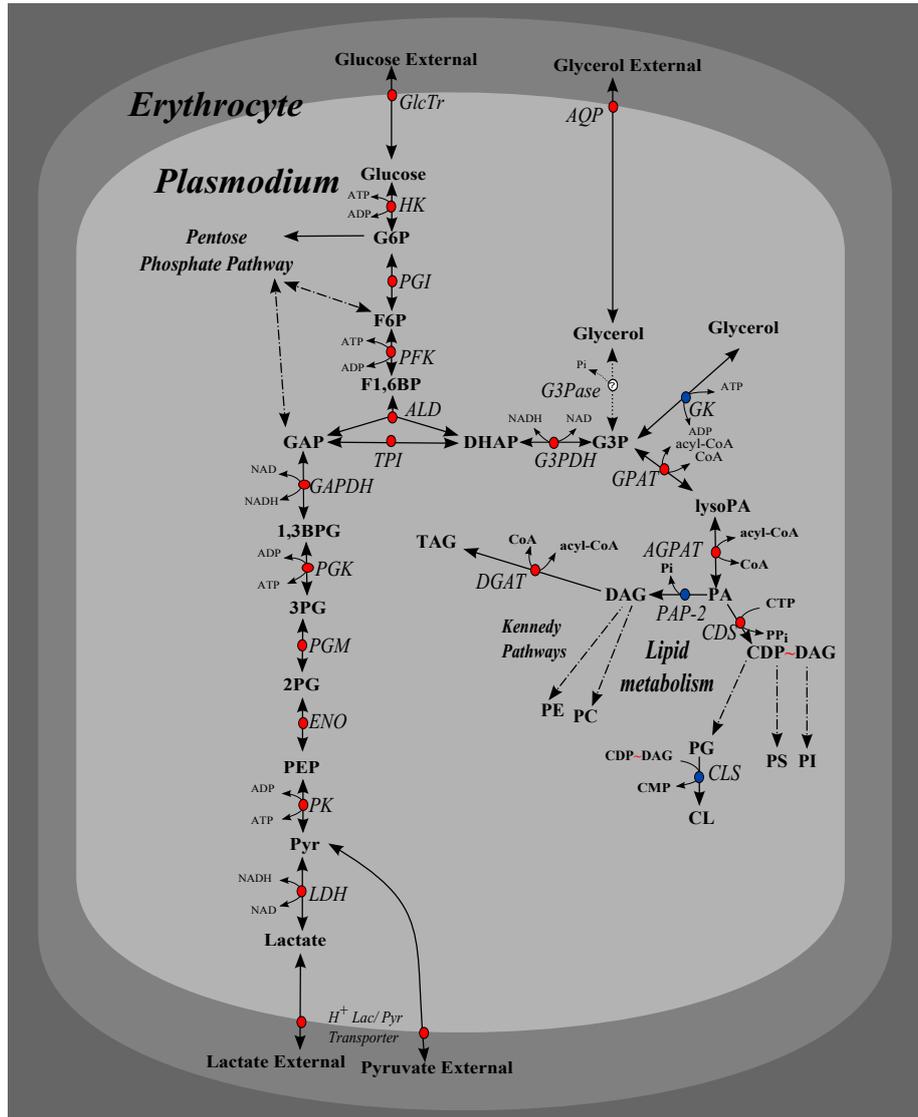
Figure 1.1: Overview of the currently accepted scheme of glycerol metabolism in asexual *Plasmodium falciparum*. The parasite's classic glycolytic pathway processes glucose to lactate, pyruvate and glycerol as well as G3P which is used in lipid metabolism. The red circles indicate enzymes whose genes and activities have been identified while the white circles with a question mark in their centre (accompanied by finely dashed arrows) show enzymes whose genes and activities have not been observed yet in *P. falciparum*. Blue circles mark enzymes whose activities have not been detected but whose genes have been identified. Dashed arrows indicate multi-enzyme pathways. Enzyme names are in italics while metabolites and co-factors are bold faced. *AGPAT*, 1-acyl-glycerol-3-phosphate acyltransferase; *CDS*, CDP-DAG synthase; *CLS*, cardiolipin synthase; *DGAT*, acyl-CoA:diacylglycerol acyltransferase; *ENO*, enolase; *GlcTr*, glucose transporter; *GPAT*, glycerol-3-phosphate acyltransferase; *PAP-2*, phosphatidic acid phosphatase type 2.

1.5.1 Glycerol 3-phosphate dehydrogenase

As stated before and shown in Figure 1.1, *P. falciparum* G3PDH (EC 1.1.1.8) catalyses the conversion of DHAP to G3P while simultaneously oxidising NADH to NAD$^+$[26]. *P. falciparum* G3PDH is not a well-characterised enzyme. However, there is a lot of literature on the biochemical and structural properties of the enzyme in yeast[27,28,29,30,31], *Trypanosoma* spp. and *Leishmania mexicana*[26,32,33,34], and mammalian species[35,36,37,38,39,40,41,42]. Transcription of the two putative *P. falciparum* G3PDH genes (PlasmoDB identifier[1] PF11_0157 and PFL0780w) peak at 37 and 19 hours, respectively[44]. The molecular mass of the dimeric enzyme, as recorded in the scientific literature[45,34,46,26], ranges from 65-80 kDa for a variety of organisms. The crystal structure of *Leishmania mexicana* G3PDH was determined at 1.75 Å and at 1.9 Å with G3PDH bound to DHAP and NADH[26,34]. Michaelis constants (K_M) of G3PDH for DHAP, NADH, G3P and NAD$^+$ are about 0.22 mM, 0.014 mM, 1.3 mM, and 0.35 mM, respectively[27,26,28,32,30].

The exact mechanism by which G3P dephosphorylation occurs is unknown[22,13] as there are conflicting reports regarding *P. falciparum* glycerol kinase activity in the asexual blood stage[47,48] and no G3P specific phosphatase genes have been detected in the genome as yet[13].

1.5.2 Glycerol kinase

Schnick et al.[48] determined the mRNA expression levels of glycerol kinase (GK; EC 2.7.1.30; PlasmoDB identifier: PF13_0269) at various stages of *P. falciparum* development. GK was only expressed in the sexual stages of the life cycle, not in the asexual erythrocyte stage. They also determined the crystal structure of the dimeric 501 amino acid residue enzyme at 1.5 Å. The enzyme catalyses the phosphorylation of glycerol by ATP producing G3P and ADP. For a recombinant construct of the enzyme expressed in *Escherichia coli*, Schnick et al. determined that the K_M values of GK for glycerol and ATP were 18 ± 2 μM and 21 ± 1 μM and V_{max} values of 15.5 ± 0.4 U mg protein^{-1} and 18.3 ± 0.35 U mg protein^{-1}, respectively. The authors also found that GK was not inhibited by fructose-1,6-bisphosphate. The reverse reaction of the enzyme was not studied.

---

[1]PlasmoDB is a functional genomic database for all *Plasmodium* spp. created by Aurrecoechea et al.[43].

Although Naidoo and Coetzer[47] could not detect *P. falciparum* GK activity in the blood stage either, their GK knock-out strain (*3D7ΔPfGK*) grew 43.4% slower than the wild type strain. Only 30% of synchronous ring stage *3D7ΔPfGK* parasites fully matured to late trophozoites/schizonts after 120 hours incubation. The rest of the parasites were still in the ring stage. The GK deletion mutants formed less merozoites compared to wild type. Furthermore, when incubated with ^{14}C-glycerol, relative to the wild type strain, the *3D7ΔPfGK* strain only incorporated $48.4 \pm 10.8\%$ and $53.1 \pm 5.7\%$ of the radiolabelled glycerol into phosphatidylcholine (PC) and phosphatidylethanolamine (PE), respectively. The authors could not detect any other glycerol phosphorylation mechanism to account for the radiolabelled glycerol that was incorporated into these phospholipids (PLs). In a previous study, the group determined that PfGK shared 50% identity with *E. coli* GK[49].

1.5.3 Non-specific phosphatase

Hills et al.[50] investigated a type 2 phosphoglycerate mutase from *P. falciparum* (PfPGM2; PlasmoDB identifier: PFD0660w) comparing its crystal structure and kinetic behaviour to those of *Cryptosporidium parvum* glycolytic dPGM. (The "d" in dPGM indicates that the enzyme is dependent on a 2,3-bisphosphoglycerate co-factor for catalytic activity. Enzymes belonging to the phosphoglycerate mutase family that do not depend on 2,3-bisphosphoglycerate for catalytic activity are designated independent PGMs or iPGMs.) Their study showed that PfPGM2 is an iPGM readily dephosphorylating fructose 6-phosphate (F6P), fructose-1,6-bisphosphate (F1,6BP) and triose phosphates, such as 3-phosphosglycerate (3PG), 2,3-bisphosphoglycerate (2,3-BPG) and phosphoenolpyruvate (PEP). The amino acid sequence and crystal structure of PfPGM2 also differed from that of *C. parvum*, a related Apicomplexan. It is possible that PfPGM2 dephosphorylates G3P to produce glycerol which is subsequently exported out of the cell.

1.5.4 Aquaglyceroporin

Export and import of glycerol to and from the parasitophorous vacuole medium occurs via an aquaglyceroporin unique to *Plasmodium* species. An essential protein of *P. falciparum* metabolism, the *P. falciparum* aquaglyceroporin (PfAQP; PlasmoDB identifier: PF11_0338) plays an important role in osmoregulation

and the influx and efflux of uncharged molecules of low molecular weight such glycerol, water, ammonia, urea, and four- and five-carbon sugar alcohols[20].

The 258 amino acid PfAQP, a member of the major intrinsic protein (MIP) family, is a water and a solute channel which has high affinity for both water and glycerol[20,21]. The homotetrameric nature of PfAQP has not been confirmed to date even though it was modeled as such by Beitz and co-workers[21,51]. The 21 kDa water-glycerol channel is highly similar to, although slightly shorter in length than, *E. coli* glycerol facilitator (GlpF) having 50% similar and 35% identical amino acid residues[20].

Beitz's group[51] expressed PfAQP in *E. coli* by substituting the A-T rich gene with an *E. coli* expressible one while keeping the amino acid sequence constant to obtain a crystal structure. Six transmembrane helices span the parasite plasma membrane while loops B and E each contain half-helices that form the seventh transmembrane helix. These anti-parallel half-helices contain the canonical Asn-Pro-Ala (NPA)-motif typical of aquaporins and aquaglyceroporins. The NPA-motifs in loops B and E are slightly modified to Asn-Leu-Ala and Asn-Pro-Ser, respectively. The asparagines (Asn70 and Asn193) reorient water molecules leading to the disruption of the hydrogen bonds in a file of water[21]. In so doing, the asparagines prevent protons from using the file of water as a proton wire and ions from traversing the pore. Trp124, Glu125 and Thr126 (the WET triad) located on Loop C which dips into the extracellular vestibule of the pore interact with Arg196 to regulate water permeability[21,51]. The 25Å long pore is 3.0Å wide at its narrowest section[51].

1.6   Use in lipid metabolism

The study conducted by Naidoo and Coetzer[47] showed that *P. falciparum* can take up, phosphorylate and use extracellular glycerol since ^{14}C-glycerol was incorporated into phosphatidylcholine (PC) and phosphatidylethanolamine (PE). These two phospholipids (PLs) along with phosphatidylinositol (PI) are the main constituents of the *P. falciparum* plasma membrane[52,53] comprising 40-50%, 35-45% and 4-11%, respectively. The infected erythrocyte membrane experiences a 6, 8 and 14 fold increase in PC, PE, and PI concentrations, respectively[17]. Phosphatidylserine (PS), neutral lipids (i.e. di- and triacylglycerides), cardiolipin (CL) and sphingomyelin make up the rest of the erythrocyte

membrane[17,52].

Glycerophospholipid and acylglycerol synthesis have been extensively reviewed elsewhere[17,54]. They have also been summarised in Figure 1.1. Briefly, glycerol-3-phosphate acyltransferase (GPAT; PlasmoDB identifier: PFL0620c) acylates G3P and acyl-coenzyme A to produce lysophosphatidic acid (lysoPA)[55]. Through the action of 1-acyl-glycerol-3-phosphate acyltransferase (AGPAT) (*PfPlsC*, PlasmoDB identifier: PF14_0421) phosphatidic acid (PA) is formed. PA is incorporated into the structures of PC and PE by the enzymes of the *P. falciparum* Kennedy pathways and into PI and PS through their formation pathways[56,57,58,59,60,61].

Diacylglycerol (DAG) formation follows the dephosphorylation of PA by PA phosphatases, PAP-1 (Mg^{2+}-dependent) and PAP-2 (Mg^{2+}-independent)[17]. CDP-DAG synthase can also activate DAG to CDP-DAG to have it participate in the Kennedy pathways[17,58].

Triacylglycerol (TAG) is formed once acyl-CoA:DAG acyltransferase (DGAT; PlasmoDB identifier: PF3D7_ 0322300) acylates DAG[54]. Palacpac et al.[54] observed a marked increase in TAG production during the late trophozoite, schizont and segmented schizont stages of parasite development. They hypothesized that TAG and the other constituents of lipid bodies might play a key role in schizont rupture and merozoite release.

These enzyme catalysed reactions can be represented by rate equations in a kinetic model. This has been done for phospholipid synthesis in *Plasmodium knowlesi*[62] and glycolysis in *P. falciparum*[2]. A brief explanation of the basic principles of enzyme kinetic modeling follows.

1.7 Principles of kinetic modeling

The principles described below were previously described by Bisswanger[63], Segel[64] and Cornish-Bowden[65]. Consider the metabolic pathway below (Eq. 1.7.1) where enzymes E_1 to E_3 convert external metabolite X_0 to external metabolite X_3. S_1 and S_2 are internal metabolites. The enzymes follow reversible Michaelis-Menten kinetics[66,65,64] where each enzyme has the ability to reversibly convert its substrate into product.

$$X_0 \underset{E_1}{\leftrightharpoons} S_1 \underset{E_2}{\leftrightharpoons} S_2 \underset{E_3}{\leftrightharpoons} X_3 \tag{1.7.1}$$

X_0 serves as the *source* of substrate for the pathway while X_3 is the *sink* into which the metabolites flow. Both external metabolites are parameters of the system while the internal metabolites are free variables. The system is said to be open due to the constant influx of substrate X_0 and efflux of product X_3 keeping these external metabolites that are treated as parameters in the model at a constant concentration and allows the pathway to reach a steady state.

At steady state, metabolite concentrations do not change with time, i.e. their production and consumption rates are exactly balanced. However, the individual enzyme rates are not zero as metabolites are still produced and consumed. It is only under equilibrium conditions that the rate of an enzyme-catalysed reaction would be zero[65]. Rate equations describing the kinetic behaviour of the enzymes in the system can be written as follows:

$$v_1 = \frac{V_{f_1} \frac{x_0}{K_{x_0}} \left(1 - \frac{s_1}{x_0 \cdot K_{eq}} \right)}{1 + \frac{x_0}{K_{x_0}} + \frac{s_1}{K_{s_1}}} \tag{1.7.2}$$

$$v_2 = \frac{V_{f_2} \frac{s_1}{K_{s_1}} \left(1 - \frac{s_2}{s_1 \cdot K_{eq}} \right)}{1 + \frac{s_1}{K_{s_1}} + \frac{s_2}{K_{s_2}}} \tag{1.7.3}$$

$$v_3 = \frac{V_{f_3} \frac{s_2}{K_{s_2}} \left(1 - \frac{x_3}{s_2 \cdot K_{eq}} \right)}{1 + \frac{s_1}{K_{s_1}} + \frac{x_3}{K_{x_3}}} \tag{1.7.4}$$

V_{f_i} ($i \in \{1, 2, 3\}$) represents the forward maximal velocity (also abbreviated V_{max} in the literature) at which enzyme E_i catalyses the conversion of its substrate to its product. s_1 and s_2 denote the concentrations of internal metabolites S_1 and S_2. Similarly, x_0 and x_3 denote the concentrations of external metabolites X_0 and X_3. The equilibrium constant K_{eq} indicates equilibrium conditions. When a *reaction* is at equilibrium its net rate is zero and the product to substrate concentration ratio is equivalent to the K_{eq} value. The Michaelis constants (K_M) in Eq. 1.7.2 (i.e. K_{x_0} and K_{s_1}), for example, indicate the concentration of said metabolite at which half-maximal velocity is achieved in the absence of product, i.e. $v = 0.5V_f$.

The reversible Michaelis-Menten rate equations may also have the following form where V_{r_1} is the maximal velocity of the reverse reaction of enzyme E_1:

$$v_1 = \frac{V_{f_1}\frac{x_0}{K_{x_0}} - V_{r_1}\frac{s_1}{K_{s_1}}}{1 + \frac{x_0}{K_{x_0}} + \frac{s_1}{K_{s_1}}}$$

The system can be described in terms of a series of ordinary differential equations (ODEs; see Eq. 1.7.5-1.7.6) that can be numerically integrated to obtain the concentrations of the internal or variable metabolites. The negative signs in the ODEs indicate reactions that consume the metabolite while those that produce the metabolite have positive signs.

$$\frac{ds_1}{dt} = v_1 - v_2 \tag{1.7.5}$$

$$\frac{ds_2}{dt} = v_2 - v_3 \tag{1.7.6}$$

Solving for metabolite concentrations by equating the ODEs to zero yields steady state concentrations (c) and fluxes (J). At steady state, the rates of all the enzymes will be equal and the flux through the system will equal these: $J = v_1 = v_2 = v_3$.

These principles apply to all multi-reaction systems, e.g. glycolysis, the pentose phosphate pathway, the Kennedy pathways, etc.

With a model of the pathway (Eq. 1.7.1) one can determine which enzymes exert the most control over the steady state flux and concentrations. metabolic control analysis (MCA), a method developed independently by Kacser and Burns[4] and Heinrich and Rapoport[3,5], enables such determinations to be done. For in-depth reviews and analyses see Fell[67] and Hofmeyr[68].

The fractional change in a local rate due to a fractional change in a parameter that interacts with it (e.g. an activator, inhibitor or enzyme concentration) is defined as the *elasticity coefficient*. Thus, when enzyme E_i is isolated from the system and its substrates and products clamped at their steady state concentrations, a small change in a parameter p (δp) will bring about a concomitant change in the local rate v_i (Eq. 1.7.7).

$$\epsilon_p^{v_i} = \frac{\delta \ln v_i}{\delta \ln p} \tag{1.7.7}$$

In living systems, enzymes do not operate in isolation. Any change to the local rate will reverberate throughout the system affecting the steady state flux J and metabolite concentrations c which are *systemic properties*. This sensitivity of a steady state flux to a change in a local rate v_i is known as the *flux control coefficient* ($C_{v_i}^J$; Eq. 1.7.8). The *concentration control coefficient* ($C_{v_i}^c$) can be similarly defined (Eq. 1.7.9).

$$C_{v_i}^J = \frac{\delta J/J}{\delta v_i/v_i} = \frac{\delta J}{\delta v_i}\frac{v_i}{J} = \frac{\delta \ln J}{\delta \ln v_i} \tag{1.7.8}$$

$$C_{v_i}^c = \frac{\delta c/c}{\delta v_i/v_i} = \frac{\delta c}{\delta v_i}\frac{v_i}{c} = \frac{\delta \ln c}{\delta \ln v_i} \tag{1.7.9}$$

A control coefficient shows the dependence of a system variable (e.g. J) on an internal parameter (e.g. enzyme activity) while the *response coefficient* (R_a^J) demonstrates the dependence of a system variable on an external parameter[65]. Thus, a fractional change in the concentration of external effector A (δa) will lead to a fractional change in steady state flux (δJ) or the steady state concentration of a metabolite (δc):

$$R_a^J = \frac{\delta \ln J}{\delta \ln a} \quad \& \quad R_a^c = \frac{\delta \ln c}{\delta \ln a} \tag{1.7.10}$$

External effector A must act on at least one enzyme in the system to produce a systemic response. Therefore, it will have at least one non-zero elasticity coefficient:

$$\epsilon_a^{v_i} = \frac{\delta \ln v_i}{\delta \ln a} \tag{1.7.11}$$

Since a fractional change in the concentration of external effector A will bring about a fractional change in a local rate v_i, this fractional change in v_i will result in a fractional change in the steady state flux (J) such that a flux control coefficient can be defined (see Eq. 1.7.8). It follows that the flux response coefficient as a result of the action of external effector A can be mathematically expressed as the product of elasticity coefficient and flux control coefficient:

$$R_a^J = C_{v_i}^J \epsilon_a^{v_i} = \frac{\delta \ln J}{\delta \ln v_i} \frac{\delta \ln v_i}{\delta \ln a} = \frac{\delta \ln J}{\delta \ln a} \tag{1.7.12}$$

This same relationship applies to any system variable such as the steady state concentration of any metabolite.

Armed with this knowledge one can test the validity of these analyses by inhibiting those enzymes that exert great control over the steady state flux and metabolite concentrations. Such enzymes in pathogens can also serve as drug targets especially when their counterparts in the pathogen's host have less control over the pathway flux or metabolite concentrations. This rationale of *differential control*[6,7] guided Penkler[2] in the construction and validation of a detailed kinetic model on *P. falciparum* glycolysis.

1.8 Model of *P. falciparum* glycolysis

Using a bottom up approach[69], Penkler measured the initial rates of each enzyme in *P. falciparum* glycolysis at various concentrations of substrates, products and effectors (i.e. activators or inhibitors). Fitting appropriate rate equations to each enzyme's data, he obtained K_M-values and V_{max}-values (in the forward and reverse reaction directions where possible). These parameters, along with the initial steady state concentrations of the metabolites, were used to construct a mathematical model (Penkler1 model available on JWS Online, http://jjj.biochem.sun.ac.za) using the principles described above to obtain steady state concentrations of the internal and external metabolites and the steady state flux through the pathway. The steady state predictions of the model were partially validated through isolated trophozoite incubations with labelled and unlabelled glucose.

After the initial validation of the Penkler model further validation was performed based on MCA analysis which indicated that the glucose transporter (GlcTr), HK, PFK, GAPDH and the fitted ATPase exercised the greatest control over the glycolytic flux in *P. falciparum*. The analysis also revealed that, in addition to these enzymes, the fitted glycerol dehydrogenase (GlrDH) exerted high concentration control especially over phospho(enol)pyruvate (PEP) which is an allosteric modulator of many *P. falciparum* glycolytic enzymes.

In applying the differential control approach[6,7], Penkler defined the *scaled effectivity* which takes the logarithm of the response coefficient a drug elicits in a pathogen's host over the logarithm of the response coefficient of a pathogen due to drug treatment (Eq. 1.8.1).

$$\text{scaled effectivity} = \frac{\log\left(|R_{drug}^{J(host)}|\right)}{\log\left(|R_{drug}^{J(pathogen)}|\right)} = \frac{\log\left(|C_{v_i}^{J(host)}\cdot\epsilon_{drug}^{v_i(host)}|\right)}{\log\left(|C_{v_i}^{J(pathogen)}\cdot\epsilon_{drug}^{v_i(pathogen)}|\right)} \quad (1.8.1)$$

Assuming that a drug, such as cytochalasin B, would inhibit an enzyme in host and parasite to the same degree (i.e. the drug is non-selective; $\epsilon_{drug}^{v(host)} = \epsilon_{drug}^{v(pathogen)}$), the scaled effectivity becomes the ratio of the logarithms of the flux control coefficients of host and pathogen. Unlike standard effectivity upon which it is based, scaled effectivity favours reactions with high control in the parasite and low control in the host.

This property of scaled effectivity is counterintuitive when viewing Eq. 1.8.1 but as our example will show is completely logical. If a reaction has a flux control coefficient in the host of 0.001 and a flux control coefficient of 0.1 in the parasite, the logarithms of these flux control coefficients would be -6.9 and -2.3, respectively. Inserting these values into Eq. 1.8.1 yields a scaled effectivity of 3.0. Conversely, a reaction with high flux control in the host (0.9) will yield a logarithm of low value (-0.1). While the flux control coefficient in the parasite might be low (0.0009), the logarithm of the parasite flux control coefficient will be high (-7.0). Substituting these values into the scaled effectivity equation produces a value of 0.015. Therefore, the former reaction will make a better drug target since the reaction in the parasite exerts more control over the flux than the reaction in the host.

Analysis revealed that GAPDH, GlcTr and PFK were the best drug targets of all the enzymes in the *P. falciparum* and erythrocyte[70] glycolysis models with scaled effectivities of 6.41, 5.84 and 3.63, respectively.

The differential control study was performed on GlcTr using cytochalasin B as an inhibitor in *P. falciparum* with the aid of a custom made quench-flow device[2]. The model was adjusted to simulate experimental conditions as Penkler inhibited the GlcTr activity and measured its effect on lactate flux. The model gave a good estimate of the flux control coefficient (a predicted value of 0.2 while 0.3 was experimentally measured).

1.9   This study

The Penkler model of *P. falciparum* glycolysis incorporated the glycerol branch in a single fitted rate equation, termed the glycerol dehydrogenase (GlrDH) reaction, which was fitted to the experimentally measured glycerol flux. The glycerol production pathway in *P. falciparum* consists of at least two enzymes (G3PDH and GK) and a transport protein (aquaglyceroporin) (Fig. 1.1). The present work has as goal to kinetically characterise the enzymes of the glycerol branch with the aim of incorporating the kinetics into the Penkler model.

Chapter 2

Methods

In order to construct a detailed kinetic model on glycerol production in *Plasmodium falciparum*, kinetic parameters (K_M, V_{max}, K_{eq}) had to be obtained. This chapter describes the cultivation and extraction procedures, as well as how the kinetic assays were conducted and how the samples from the red blood cell free trophozoite incubations with glucose were analysed.

2.1   Materials

All reagents, intermediates, and enzymes were purchased from Sigma-Aldrich (Steinheim, Germany) except for Albumax II (Invitrogen Coorp., Auckland, New Zealand), hexokinase/glucose-6-phosphate dehydrogenase (HK/G6PDH; Roche, Mannheim, Germany), acetonitrile (Romil Ltd, Cambridge, United Kingdom), and glycerol (Holpro Lovasz, Gauteng, South Africa). The following reagents were all purchased from Merck (Darmstadt, Germany): sodium chloride, potassium chloride, di-potassium hydrogen orthophosphate, magnesium sulphate heptahydrate, ammonium acetate, and perchloric acid, 70 $\%^v/_v$.

2.2   Cultivation of *Plasmodium falciparum* D10

P. falciparum D10 infected human red blood cells (A$^+$; Western Cape Province Blood Bank) were continuously cultured in RPMI-1640 culture medium[71]. The cultures were incubated at 37 °C under an atmosphere of 3 % oxygen, 4 % carbon dioxide and 93 % nitrogen[19].

The RPMI-1640 culture medium was composed of RPMI medium, 0.5 $\%^w/_v$

Albumax II, 25 mM HEPES, 22 mM glucose, 25 mM sodium bicarbonate, 3 mM hypoxanthine and 0.05 g/L gentamicin sulphate[72]. The pH ranged from 7.2 - 7.3. The medium was sterilised by filtering it through a 0.22 μm pore size filter and used within two weeks after preparation[19].

To ensure that the cultures were synchronised 5 $\%^w/_v$ D-sorbitol was added to 1.5-2.0 mL infected red blood cells[73,19]. The infected red blood cells were centrifuged at 750 $\times$ g for 3 minutes and the supernatant aspirated. Sorbitol (5 $\%^w/_v$; 10 mL) was added to the infected red blood cells. The infected red blood cell-sorbitol suspension was incubated in a 37 °C water bath for 10 minutes (inverted a few times every 2 minutes), centrifuged and aspirated as before. The cells were washed once with culture medium before resuspension in culture medium and deoxygenation with the gas mixture[2]. The cells were periodically checked under the microscope to see whether the cultures were synchronous. Seventy percent of the parasites were typically in the ring phase after synchronisation.

2.3 Isolation of Trophozoite Stage Parasites

Once the parasitemia—the ratio of parasites to red blood cells—reached 10 %, the trophozoites were isolated by centrifugation (750 $\times$ g) of the infected red blood cells and resuspending them in culture medium. Under non-sterile conditions saponin (final concentration 0.05 $\%^w/_v$) was added to the suspension which was centrifuged at 1800 $\times$ g for 7 min at room temperature[74]. The supernatant was discarded and the isolated trophozoites were resuspended in phosphate buffered saline (PBS) or culture medium (for the glucose incubation assays) and centrifuged as before. The cells were washed twice with PBS or culture medium.

For the glucose incubation assays (Section 2.6), the parasites were washed twice with glucose-deficient incubation buffer (i.e. a modified Ringer buffer) that contained 50 mM HEPES, pH 7.16, 120 mM NaCl, 1 mM $MgCl_2.6H_2O$, 10 mM KCl followed by equilibration with glucose-rich incubation buffer (5 mM glucose) followed[2].

Following the two PBS washes, and in preparation for enzyme kinetic assays (Section 2.4), the trophozoites were washed twice with regular kinetic assay

buffer (20 mM HEPES, pH 7.16, 20 mM $MgCl_2.6H_2O$, 10 mM KCl, 20 mM NaCl)[19]. The supernatants of the final two wash steps were retained and functioned as negative controls to ascertain whether uncontrolled lysis of parasites occurred during those wash steps.

2.4 Enzyme Kinetic Assays

The enzyme kinetic assays were all performed in 96 well flat bottomed microtitre plates (Greiner Bio-One GmbH, Frickhouse, Germany) and the reactions monitored online with a PowerWave 340 microtitre plate spectrophotometer (BioTek Instruments Inc., Winooski, VT, USA). The computer program, Gen5 (v.1.05.11, BioTek Instruments Inc., Winooski, VT, USA), was used to record the spectrophotometric data. The final assay volume was 100 μL in all assays except for the Bradford protein determination assays (Section 2.8). The following enzymes were assayed: G3PDH, GK and glycerol 3-phosphate-dependent phosphatase (G3Pase).

2.4.1 Cell extract preparation

Trophozoite extracts of different concentrations were used for the kinetic parameter determinations of the various enzymes. For GK a 2× dilution of trophozoites in kinetic assay buffer (Section 2.3) was made. While for G3PDH and G3Pase the trophozoites were diluted 3 and 6 times, respectively. The extracts were made by subjecting the suspended trophozoites to three freeze-thaw cycles[2] and centrifugation (10,000 × g, 5 min, 4 °C). The supernatant was retained and kept on ice.

2.4.2 Glycerol 3-phosphate dehydrogenase

The methods described below were adapted from Nilsson[30].

G3PDH activity was assayed by varying substrate concentrations NADH (0-0.36 mM) and DHAP (0-5.55 mM). Product inhibition by G3P (0-16.7 mM) in the presence of NADH (0.36 mM) and DHAP (0.22 mM) was measured as well as product inhibition by NAD^+ (0-8.4 mM) with DHAP (5.55 mM) and NADH (0.22 mM). Assays were performed in the presence of 4 mM 1,4-dithio-D-threitol (DTT).

2.4.3   Glycerol kinase

Three methods were used to detect GK activity. Commercial GK from rabbit muscle (0.6 U/mL final concentration) was used as a positive control to make sure that the coupled enzyme system functioned well.

Glycerokinase activity was measured by monitoring the phosphorylation of glycerol (10 mM) spectrophotometrically[75] at 340 nm by linking the enzyme's activity via ADP to pyruvate kinase (PK, 3 U/mL) and L-lactate dehydrogenase (LDH, 3.4 U/mL). The initial concentrations of phosphoenolpyruvate (PEP), NADH and ATP were 1.0 mM, 0.4 mM,and 2.0 mM, respectively.

The second method of detection that used to detect GK activity was adapted from Wieland[76]. Briefly, GK activity, i.e. the phosphorylation of glycerol, was linked to NAD^+ reduction via commercial G3PDH (5 U/mL) and ATP (1.7 mM) with subsequent production of DHAP and ADP. The initial concentration of NAD^+ was 0.7 mM. Absorbance was measured at 340 nm. Hydrazine monohydrate (320 mM) was used to bind irreversibly to DHAP upon formation.

The third GK detection method observed the dephosphorylation of G3P by GK via a hexokinase/glucose 6-phosphate dehydrogenase (HK:G6PDH; 5:2.5 U/mL) enzyme-coupled system. The concentrations of glucose, ADP and NADP were 10, 1 and 10 mM, respectively, while the G3P concentration was 5 mM.

2.4.4   Glycerol 3-phosphate-dependent phosphatase

G3P-dependent phosphatase (G3Pase) activity was measured in two ways. With the first method the aim was to (1) determine whether there was a marked reproducible G3P-dependent increase in the concentrations of glycerol and inorganic phosphate over the incubation period since reaction was expected to be at equilibrium at the times when samples were taken and (2) shorten the incubation time and the duration of the intervals between sampling times to determine the initial rate of the reaction once reproducible results were obtained in aim 1.

Trophozoite extract was therefore incubated with G3P (0, 5, 10, 20 mM) in the presence of 4 mM DTT over a 50 minute period. Samples were taken at 0, 10, 20, 35, and 50 minutes after the reaction was initiated by the addition of extract. Perchloric acid (6 % $^v/_v$ final concentration) was used to quench the

reaction and the samples were neutralised with 7 N KOH prior to centrifugation (10000 $\times$g, 1 min). The samples were stored on ice and centrifuged collectively. The supernatants of the samples were retained and diluted 5, 10 and 15 times with kinetic assay buffer (Section 2.3).

The method of Barnett et al.[77] was used to colorimetrically analyse the inorganic phosphate content of the samples' supernatants. To a 50 μL sample in a well of a Greiner Bio-One 96 well flat-bottomed microtiter plate was added 50 μL colour reagent (1 vol. 3 M H_2SO_4 : 1 vol. 2.5 % $^w/_v$ ammonium molybdate : 2 vol. d.i. H_2O : 1 vol. 10 % $^w/_v$ ascorbic acid). The plate was then incubated for 90 minutes at 37 °C and read at 660 nm. To determine the concentration of inorganic phosphate in the samples, a standard curve of K_2HPO_4 (0-2 mM) was constructed.

The second method involved the online monitoring of inorganic phosphate evolution by coupling the dephosphorylation of G3P (5 mM) to GAPDH (3.2 U/mL) reaction (see Fig. 1.1). The GAPDH reaction oxidises GAP (5 mM) to 1,3-bisphosphoglycerate (1,3BPG) while simultaneously reducing NAD^+(2.5 mM) and phosphorylating the substrate with inorganic phosphate.

2.5   Model Construction

The original model for *P. falciparum* glycolysis was constructed by Penkler[2,23]. The models were constructed in Wolfram Mathematica 8.0® and are available on JWS Online (http://jjj.biochem.sun.ac.za)[78,79]. The data files and models are also available on the SEEK platform[80] in Mathematica notebook and SBML formats[23]. The models are a set of ordinary differential equations that are numerically integrated to obtain the steady state flux and internal metabolite concentrations. In this study we followed a similar technique to incorporate our experimentally measured enzyme kinetics in the existing model.

2.6   Model Validation

In order to validate the predictions of the model, isolated, erythrocyte-free trophozoites were incubated in a ^{14}C-glucose-rich incubation buffer (Section 2.3) to determine the change in external metabolite (i.e. glucose, lactate, pyruvate

and glycerol) concentration over time. The experiment was repeated with unlabelled glucose-rich incubation buffer.

2.6.1 Incubation with ^{14}C-glucose

Isolated trophozoites were incubated with ^{14}C-glucose[1] in order to determine the concentrations of external metabolites more accurately with the aid of hydrophilic interaction liquid chromatography (HILIC)[81]. Once the trophozoites were mixed with glucose-rich incubation buffer, 10 μL of the suspension was sampled for cell counting (Improved Neubauer Haemocytometer). Another aliquot was taken for total protein determination (Section 2.8). The incubation was immediately mixed with the ^{14}C-glucose (1:80 ratio) after which a sample was taken (time point zero), centrifuged (5000 $\times$ g, 1 min) and the supernatant added to acetonitrile (70 % $^{v}/_{v}$ final concentration). Samples were taken in 15 and 30 minute intervals.

2.6.2 Sample analysis with HPLC

The method of Antonio et al.[82] was used to determine the concentrations of the external metabolites: glucose, lactate, pyruvate and glycerol. Briefly, a ZIC®-HILIC column (150 $\times$ 7.5mm, 5μm, 200Å, SeQuant™, Merck, Darmstadt, Germany) fitted with a guard column (20 $\times$ 2.1mm, 5 μm, SeQuant™, Merck, Darmstadt, Germany) on a high performance liquid chromatography (HPLC) system was used to separate the analytes. The components of the HPLC system were a SpectraSYSTEM P4000 pump (Thermo Separation™ products, San Jose, CA, USA), a SpectraSYSTEM AS3000 auto-sampler (Thermo Separation™ products, San Jose, CA, USA) and a Flo-One liquid scintillation spectrophotometer (Radiomatic, Tampa, FL, USA). The radioactive emissions of the samples were recorded with HPLC Flo-One/Beta Data Acquisition software (v. 2.0). The analogue intensity (V) data was analysed with Wolfram Mathematica 8.0 ®.

The flow rate and injection volume were 1.0 mL/min and 100 μL. Separation occurred at room temperature (25 °C). Mobile phase A consisted of acetonitrile (0.1 % $^{v}/_{v}$ formic acid) and mobile phase B of 5 mM ammonium acetate, pH 4 (0.1 % $^{v}/_{v}$ formic acid). Before initiating the gradient elution profile, 90 %

---

[1]Samples were provided by Dr. Gerald Penkler.

$^v/_v$ A was pumped through the system for 1 minute—altering the method of Antonio et al. [82] minutely.

2.6.3 Incubation with unlabelled glucose

The cells were packed by centrifugation (10000 ×g, 5 min) at room temperature. The supernatant was discarded and the parasites resuspended in glucose-rich incubation buffer. At time point (t_0) two 10 μL aliquots for cell counting (Improved Neubauer Haemocytometer) and total protein determination (Section 2.8) were taken immediately. Additional samples were taken 15, 30, 45, 60 and 90 minutes after initiation. The trophozoites in these time point samples were pelleted by centrifugation (13000 rpm, 5 min) and the supernatant drawn off and flash frozen with liquid nitrogen. The samples were stored at -80 °C and enzymatically assayed. The cell pellets were frozen too and subjected to a Bradford total protein determination assay (Section 2.8).

2.6.4 Enzymatic analyses of samples

External glucose concentration

In order to determine the concentration of glucose in the samples that were taken during the incubation with unlabelled glucose, a standard curve was constructed [19]. A series of standards ranging from 0 mM to 10 mM glucose was made. Glucose standard (5 μL) was incubated with 95 μL glucose determination buffer for 30 minutes at 25 °C. The glucose determination buffer was composed of 150 mM HEPES, pH 7.6, 15 mM $MgSO_4.7H_2O$, 4.5 mM ATP, 0.63 mM NADP, and 0.5 % $^v/_v$ hexokinase/glucose-6-phosphate dehydrogenase. Absorbance was read after 30 minutes of incubation on a PowerWave 340 microtiter plate spectrophotometer (BioTek Instruments, Winooski, VT, USA). Likewise, 5 μL of sample (or dilution of sample) was incubated with 95 μL glucose determination buffer and absorbance read at 340 nm after 30 minutes.

External lactate concentration

Lactate concentrations were determined in a similar manner (adapted from Penkler [19]). A standard curve was set up with concentrations ranging from 0-10 mM sodium lactate. The lactate determination buffer was composed of 320 mM hydrazine monohydrate, 4 mM NAD^+ and 20 U/mL L-lactate

dehydrogenase in addition to 150 mM HEPES, pH 7.6, and 15 mM $MgSO_4.7H_2O$. Lactate determination buffer (95 μL) was added to 5 μL standard or sample and the absorbance read after 90 minutes at 340 nm and 25 °C. Hydrazine monohydrate binds irreversibly to pyruvate which, then, drives the reaction in the direction of pyruvate formation.

External pyruvate concentration

The concentration of pyruvate in samples and standards were determined in a manner similar to the way in which lactate concentrations were obtained. The pyruvate determination buffer was composed of 150 mM HEPES, pH 7.6, 15 mM $MgSO_4.7H_2O$, 0.8 mM NADH, and 15.8 U/mL L-lactate dehydrogenase. The standard/sample was incubated at 25 °C for 30 minutes before the absorbance was read at 340 nm. The pyruvate standard dilution series ranged from 0 to 2 mM.

External glycerol concentration

An adaptation of the method developed by Eggstein and Kuhlmann[75] was used to determine the glycerol concentration of standards (0-2 mM) and in samples. After 30 minutes incubation at room temperature of a 5 μL sample/standard with 95 μL glycerol determination buffer, the absorbance was read at 340 nm. For the glycerol determination buffer, the HEPES/$MgSO_4.7H_2O$ (150 mM/15 mM) buffer (pH 7.6) was supplemented with 1 mM PEP, 0.4 mM NADH, 1 mM ATP, 3 U/mL PK, 3.6 U/mL LDH and 2 U/mL GK.

From absorbance to concentration

To determine the concentration of an external metabolite in a given sample, a linear standard curve of known concentrations is constructed. Upon obtaining the slope of the standard curve via linear regression, the metabolite-dependent absorbance values of the samples are converted to concentration with the Beer-Lambert law[83].

Because glycerol and pyruvate standards absorbance values decrease with increasing metabolite concentration as NADH is oxidised to NAD^+, negative concentration values arise when a sample's absorbance value (A_s) is greater than that of the 0 mM metabolite standard (A_0) (Eq. 2.6.1). This standard's

absorbance value is subtracted from the absorbance value of all the other standards and samples. Thus, negative concentration values are merely an artefact of data processing and should not affect the product formation rate adversely in any way.

$$\Delta Abs = -(A_s - A_0) \qquad (2.6.1)$$

2.7   Metabolic Control analysis

Steady state analysis and metabolic control analysis were performed on the model on JWS Online (http://jjj.biochem.sun.ac.za) by the author.

2.8   Bradford protein determination

The total protein in an extract was determined via the method of Bradford[84] as modified by Penkler[19]. Briefly, a standard curve of bovine serum albumin (0-1 mg/mL) was constructed by incubating 5 μL standard with 180 μL Bradford Reagent (0.1g/L Coommassie Brilliant Blue G-250, 0.05 % $^v/_v$ methanol, 8.5 % $^w/_v$ H_3PO_4) for 15 minutes (at room temperature) and reading the plate 595 nm at the end of the 15 minute period. A dilution series of the extract was made and incubated in the same way. The absorbance values were converted to concentration with the aid of the standard curve and thus the protein concentration in the extract was determined.

CHAPTER 3

RESULTS AND DISCUSSION

This chapter presents the experimental results of the kinetic characterisation of glycerol 3-phosphate dehydrogenase (G3PDH), detection of glycerol kinase (GK) and G3P-dependent phosphatase activity as well as the partial validation of the kinetic model which was constructed by Penkler et al.[23]. A description of the kinetic model is presented along with the findings of metabolic control analysis that was performed on the model.

3.1 Enzyme Kinetics

3.1.1 Glycerol 3-phosphate dehydrogenase

Glycerol 3-phosphate dehydrogenase (G3PDH) reduces DHAP to G3P while simultaneously oxidising NADH to NAD$^+$. A random order bi-substrate rate equation[85] (Eq. 3.1.1) was fitted simultaneously to all the data.

$$vG3PDH = \frac{V_{f_{G3PDH}} \frac{dhap}{Kdhap} \frac{nadh}{Knadh}}{(1 + \frac{dhap}{Kdhap} + \frac{g3p}{Kg3p})(1 + \frac{nadh}{Knadh} + \frac{nad}{Knad})} \tag{3.1.1}$$

P. falciparum G3PDH was not observed to be sensitive to inorganic phosphate, in contrast to yeast G3PDH[28,29], as seen by the maximum specific activity measured in the presence and absence of 1 mM KH$_2$PHO$_4$: 0.0351 ± 0.005 μmol.min^{-1}.mg^{-1} protein vs. 0.0345 ± 0.006 μmol.min^{-1}.mg^{-1} protein.

The fitting of Eq. 3.1.1 to the kinetic data yielded K_{DHAP} and K_{NADH} values of 0.340 ± 0.040 mM and 0.090 ± 0.009 mM, respectively (Table 3.2). The substrate saturation curves are shown in Fig. 3.1 A & B. No kinetic data for G3PDH of *P. falciparum* could be found in the scientific literature. The kinetic data for a number of other organisms (*T. brucei* (blood stream forms),

L. mexicana (recombinant), *Debaromyces hansenii* and rabbit muscle) was collected from the scientific literature[27,32,30] and the average values of the kinetic constants for these organisms were calculated. Compared to the values from the scientific literature, the K_{DHAP} and K_{NADH} values determined in this present study were 1.5 to 3 times higher.

For the forward reaction, i.e. the reduction of DHAP to G3P, the maximum specific activity of G3PDH was measured to be 0.0423 ± 0.0052 μmol.min^{-1}.mg^{-1} protein (n = 5). However, the maximum specific activity of G3PDH in the manuscript in Appendix A was measured to be 0.06 ± 0.01 μmol.min^{-1}.mg^{-1} protein. A possible for this discrepancy might be the higher hemoglobin contents of the extracts used in the determination of the maximum specific activity in this present study. The maximum specific activity that appears in the manuscript was measured independently from this present work.

The maximum specific activity of the reverse reaction was 0.0034 ± 0.0003 μmol.min^{-1}.mg^{-1} protein (n = 4). It comes as no surprise since the K_{eq} (32600[86]) indicates that the enzyme favours the forward reaction. This finding was corroborated by previous studies in a variety of organisms[29,30,87].

Since the reverse reaction was very slow compared to the forward reaction, the K_M of G3PDH for its products were determined via product inhibition studies. Product inhibtion by G3P was measured at 0.22 mM DHAP and 0.358 mM NADH while that by NAD$^+$ was determined at 0.22 mM NADH and 5.55 mM DHAP. These yielded a K_{G3P} of 3.98 ± 1.93 mM and a K_{NAD} of 0.513 ± 0.123 mM which are more than those of *L. mexicana*, *T. brucei* and rabbit muscle[32], for example (Table 3.1). The fits are shown in Fig. 3.1 C & D.

3.1.2   Glycerol kinase

Three different assay methods were used to detect GK activity. Two of these assay methods measured the activity of GK in the direction of glycerol to G3P conversion. The first assay method linked ADP formation to NADH oxidation through the action of pyruvate kinase and lactate dehydrogenase assay. The second assay method linked G3P formation directly to NADH oxidation through the action of G3PDH. The third assay method detected GK activity by coupling ATP formation (and thus the dephosphorylation of G3P) to NADPH formation through the activity of hexokinase and glucose-6-phosphate dehydrogenase.

Table 3.1: Summary of the kinetic parameters for *P. falciparum* glycerol-3-phosphate dehydrogenase. The kinetic data of G3PDH were combined, normalised to V_{max} (Fig. 3.1) and fitted simultaneously to Eq. 3.1.1. In addition to the fitted parameters ($\pm$ asymptotic error) shown below, K_M of G3PDH for its substrates and products were taken from the literature. These values are presented as mean $\pm$ standard error of the mean (SEM).

Parameter	Fitted Value	Literature Value[a]	Reference
$V_{f_{G3PDH}}$ [b]	0.0423 ± 0.0052[c]	—	—
K_{DHAP} (mM)	0.340 ± 0.040	0.222 ± 0.082	[27,32,30]
K_{NADH} (mM)	0.090 ± 0.009	0.014 ± 0.004	[27,32,30]
K_{G3P} (mM)	3.98 ± 1.93	1.333 ± 0.088	[27,32,30]
K_{NAD} (mM)	0.513 ± 0.123	0.347 ± 0.440	[27,32,30]
K_{eq}	—	32600	[86]

[a] Values from 5 different organisms (i.e. *T. brucei* (blood stream form), *L. mexicana* (recombinant enzyme), *Debaromyces hansenii*, *Saccharomyces cerevisiae* and rabbit (muscle)) were used to compute the literature value of K_{DHAP} and K_{NADH} while K_{G3P} and K_{NAD} are the mean $\pm$ SEM of 4 independent organisms.

[b] Specific activity was measured in μmol.min^{-1}.mg^{-1} protein.

[c] The maximal specific activity from five independent experiments. Mean $\pm$ SEM shown.

Table 3.2: Comparison of *P. falciparum* K_{G3P} and K_{NAD} to values from the scientific literature. The K_{G3P} and K_{NAD} of *P. falciparum* G3PDH generated in this study are compared to those obtained by Marché et al.[32] for the indicated organisms.

	K_{G3P} (mM)	K_{NAD} (mM)	Reference
P. falciparum	3.98	0.513	-
L. mexicana	1.7	0.42	[32]
T. brucei	2.25	0.32	[32]
rabbit muscle	0.18	0.012	[32]

A

B

C

D

Figure 3.1: Biochemical characterisation of *P. falciparum* G3PDH. G3PDH catalyses the NADH-dependent reduction of dihydroxyacetone phosphate to form glycerol 3-phosphate and NAD^+. Saturation curves with DHAP (A) and NADH (B) are shown in addition to the inhibition of G3P (C) and NAD^+ (D). A random order bi-substrate rate equation (Eq. 3.1.1) was fitted simultaneously to all the data and described the data well (adjusted R^2 = 0.94). Parameter values obtained from the fitting are shown in Table 3.2. The error bars represent SEM, where n = 4 (A), n = 4 (B), n = 5 (C) and n = 2 (D) independent experiments and the shaded area indicates the 95% confidence interval.

GK activity could not be measured with the two methods for the reaction in the direction of glycerol to G3P. Positive controls were made for both methods using commercial GK. A minimal activity of 0.003 μmol.min^{-1}.mg^{-1} protein would have been detected in the assay.

When the dephosphorylation of 5 mM G3P was monitored using commercial hexokinase and glucose-6-phosphate dehydrogenase as coupling enzymes, low level GK activity was observed (Fig. 3.2). The background activity was high (0.0301 $\pm$ 0.0008 μmol.min^{-1}.mg^{-1} protein) in the first 7 minutes of the reaction after which it increased to 0.0377 $\pm$ 0.0004 μmol.min^{-1}.mg^{-1} protein. Subtracting the background activity from the G3P-dependent activity yielded a GK rate of 0.0034 μmol.min^{-1}.mg^{-1} protein.

With the aid of an ATP standard curve, it was determined that the enzyme-coupled system used was sensitive enough to measure ATP concentrations as low as 10 μM. To fully convert 10 μM G3P to 10 μM ATP will take GK (with a specific activity of 0.0034 μmol.min^{-1}.mg^{-1} protein) at least 7.5 minutes.

Naidoo and Coetzer[47] knocked out the GK gene in the *P. falciparum* 3D7 strain to determine whether GK is essential to parasite growth. In their radiolabel study, they incubated late stage trophozoite wild type and 3D7ΔPfGK parasites with ^{14}C-glycerol for 4 hours at 37°C. The knockout parasites incorporated 50 % less ^{14}C-glycerol into PE and PC than the wild type strain. This suggests that GK plays a role in glycerol incorporation but is not essential, and that another pathway for the incorporation of ^{14}C-glycerol exists.

3.1.3 G3P-dependent phosphatase

The measured activity of 0.0034 μmol.min^{-1}.mg^{-1} protein for GK in the direction of glycerol formation is very low compared to specific activities for glycolytic enzymes in *P. falciparum*. Although the flux through the glycerol pathway is much lower than the glycolytic flux an attempt was made to detect G3P-dependent phosphatase activity in trophozoite extracts.

With a colorimetric assay for inorganic phosphate[77] and an enzyme-coupled assay for glycerol[75], the G3P-dependent release of inorganic phosphate and glycerol could be detected in two independent experiments (Fig. 3.3). Figure 3.3 A clearly shows inorganic phosphate formation in the presence of G3P and none in the absence of this substrate. Specific activities ranging from

Figure 3.2: Progress curve of *P. falciparum* glycerol kinase activity. Shown are lysate activities in the presence (■) and absence (●) of G3P (5 mM). The error bars represent SEM of two independent experiments each conducted in triplicate.

0.3174 to 0.4326 μmol.min^{-1}.mg^{-1} protein in the presence of G3P (5-20 mM) were observed (Table 3.3). The enzyme showed little G3P dependence above 5 mM. This might be due to the enzyme being saturated at G3P concentrations exceeding 5 mM.

The glycerol formation progress curves (Fig. 3.3 B) did not follow the same pattern as inorganic phosphate formation neither do they agree stoichiometrically.

The first experiment was performed in a technical triplicate but it was not possible to fully reproduce the results (Fig. 3.3 A & B) in a second independent experiment (Fig. 3.3 C & D). A 5 fold decrease in inorganic phosphate concentration was observed which might be due to a lower parasite yield than expected or an experimental error. There was little stiochiometric consistency between inorganic phosphate and glycerol concentration measurements within an experiment as well as between the two experiments.

Table 3.3: Glycerol-3-phosphate-dependent inorganic phosphate and glycerol formation rates. G3P was added to trophozoite extract. Samples were taken at 0, 5, 10, 15, 35 and 50 minutes. The inorganic phosphate concentrations in the samples were determined colorimetrically[77] while their glycerol concentration were obtained via a coupled enzyme assay[75]. The two independent experiments were conducted in singleton.

G3P (mM)	Experiment 01		Experiment 02	
	Pi Rate[a]	Glycerol Rate	Pi Rate	Glycerol Rate
0	0.0027	0.5615	0.0057	-0.1549
5	0.3174	1.2626	-0.0352	-0.2766
10	0.3993	-0.6285	0.1668	0.8436
20	0.4326	0.0966	0.09420	0.3122

[a] The rates shown here have units of μmol.min^{-1}.mg^{-1} protein.

Due to the unreliability of this data, our findings of G3P-dependent phosphatase activity in the extract of *P. falciparum* trophozoites are inconclusive and merely preliminary.

When G3P-dependent release of inorganic phosphate was coupled to glyceraldehyde 3-phosphate dehydrogenase, enzyme activity was not detected.

3.2   Incorporation into glycolysis model

For the G3PDH rate equation (Eq. 3.1.1) to be incorporated[1] into the detailed kinetic model (Penkler 1 model[23]), it was rewritten in the form:

$$vG3PDH = \frac{V_{G3PDH} \cdot V_{Pf} \cdot \alpha \cdot \frac{DHAP[t]}{K_{DHAP} \cdot V_{Pf}} \frac{NADH[t]}{K_{NADH} \cdot V_{Pf}} \left(1 - \frac{G3P[t] \cdot NAD[t]}{DHAP[t] \cdot NADH[t] \cdot Keq}\right)}{\left(1 + \frac{DHAP[t]}{K_{DHAP} \cdot V_{Pf}} + \frac{G3P[t]}{K_{G3P} \cdot V_{Pf}}\right)\left(1 + \frac{NADH[t]}{K_{NADH} \cdot V_{Pf}} + \frac{NAD[t]}{K_{NAD} \cdot V_{Pf}}\right)} \quad (3.2.1)$$

where the factor α is the ratio of parasite cytosolic volume to total protein (4.67 μL cytosol.mg protein^{-1}) and V_{Pf} is the trophozoite cytosolic volume (assumed to be 28 fL)[2]. By multiplying the V_{max} by these factors its units change from μmol.min^{-1}.mg^{-1} protein to mmol.min^{-1}.L cytosol^{-1}. By dividing each metabolite by V_{Pf}, one can model in terms of mole quantity instead of (molar) concentration which simplifies the incorporation of the *P. falciparum* glycolysis

---

[1]The modelling work in Section 3.2 was performed by G. Penkler, Ph.D., who uploaded the model onto JWS Online (http://jjj.biochem.sun.ac.za).

A

B

C

D

Figure 3.3: Progress curves of glycerol 3-phosphate-dependent inorganic phosphate and glycerol formation. The assays were initiated when 0 (●), 5 (■), 10 (♦) or 20 (▲) mM G3P was added to trophozoite extracts at 37°C. Samples were taken at 0, 10, 20, 35 and 50 minutes, and subjected to inorganic phosphate [77] (A & C) and glycerol [75] (B & D) analyses. Two independent experiments were performed in singleton while samples were analysed in triplicate. The error bars indicate SEM of these technical triplicates.

model as a compartment in an erythrocyte glycolysis model. The metabolites are represented as time-dependent variables[2].

Because of the low GK rate, G3P dephosphorylation to glycerol (Glr) was modeled as a mass action equation (Eq. 3.2.2) that also incorporates Glr export since *P. falciparum* aquaglyceroporin relies on mass-action kinetics[20,21]. Operating under the assumption of rapid G3P dephosphorylation and transport of Glr, the k_{GlrTr} was set to 1 min^{-1}[23].

$$vGlrTr = k_{GlrTr} \cdot \left(\frac{G3P[t]}{V_{Pf}} - \frac{Glr_{ext}[t]}{V_{RBC}} \right) \tag{3.2.2}$$

where V_{RBC} is the external volume. In the model all external metabolites (i.e. in the erythrocyte) are divided by V_{RBC}.

The model consists of 19 ordinary differential equations (ODEs)[23] which describe changes in external (i.e. glucose, lactate, pyruvate and glycerol) and internal (e.g. DHAP, G3P) metabolite concentrations as a function of time and enzyme rates.

In this section only the ODEs and rate equations for the metabolites in the glycerol branch are shown. Equations 3.2.3 - 3.2.5 are the ODEs of DHAP, G3P and Glr$_{ex}$ while Eq. 3.2.6 and 3.2.7 are the time-dependent rate equations of aldolase (ALD) and triose phosphate isomerase (TPI). Aldolase cleaves fructose-1,6-bisphosphate (F1,6BP) into DHAP and GAP while TPI catalyses the isomerisation of DHAP to glyceraldehyde-3-phosphate (GAP).

$$DHAP'[t] = vALD - vTPI - vG3PDH \tag{3.2.3}$$

$$G3P'[t] = vG3PDH - vGlrTr \tag{3.2.4}$$

$$Glr'_{ex}[t] = vGlrTr \tag{3.2.5}$$

$$vALD = \frac{V_{ALD} \cdot V_{Pf} \cdot \alpha \cdot \frac{F1,6BP[t]}{K_{F1,6BP} \cdot V_{Pf}} \cdot \left(1 - \frac{DHAP[t] \cdot GAP[t]}{F1,6BP.Keq}\right)}{1 + \frac{F1,6BP[t]}{K_{F1,6BP} \cdot V_{Pf}} + \frac{DHAP[t]}{K_{DHAP} \cdot V_{Pf}} + \frac{GAP[t]}{K_{GAP} \cdot V_{Pf}} + \frac{DHAP[t] \cdot GAP[t]}{K_{DHAP} \cdot V_{Pf} \cdot K_{GAP} \cdot V_{Pf}}} \tag{3.2.6}$$

$$vTPI = \frac{V_{TPI} \cdot V_{Pf} \cdot \alpha \cdot \frac{DHAP[t]}{K_{DHAP} \cdot V_{Pf}} \cdot \left(1 - \frac{GAP[t]}{Keq \cdot DHAP[t]}\right)}{1 + \frac{DHAP[t]}{K_{DHAP} \cdot V_{Pf}} + \frac{GAP[t]}{K_{GAP} \cdot V_{Pf}} \frac{PEP[t]}{Ki_{PEP} \cdot V_{Pf}}} \qquad (3.2.7)$$

3.3 Model validation

To validate the model (Penkler 1 model), it was adapted to function as a closed system (Penkler 2 model) so that its predictions of the glucose consumption and product formation rates could be compared to experimentally determined rates[23]. The validation evaluates the accuracy of the enzyme kinetics upon which the model (Penkler 1 model) is based.

The external metabolites (glucose, lactate, pyruvate, and glycerol) were made time-dependent variables, i.e. *metabolite*[*t*]. The initial external glucose concentration was raised to 5 mM while the other external metabolites were set to zero. The initial concentrations of the internal metabolites were all set to 0.1 mM while the ATP and NADH moieties remained equal to 3 mM. The initial ratios of ATP:ADP and NADH:NAD were set to 1.

The model predicted the glucose flux J_{GLC} to be 0.05 μmol.min^{-1}.mg^{-1} protein, J_{LAC} 0.092 μmol.min^{-1}.mg^{-1} protein, J_{PYR} 0.004 μmol.min^{-1}.mg^{-1} protein and J_{GLR} 0.004 μmol.min^{-1}.mg^{-1} protein. These predictions agree well with the experimentally measured fluxes that were obtained when erythrocyte-free, intact trophozoites were incubated with ^{14}C radiolabelled and unlabelled glucose (see Table 3.4).

Erythrocyte-free, intact trophozoites were incubated with ^{14}C-glucose for 90 minutes during which samples were taken to quantify the external metabolite concentrations (see Section 2.6.1). These samples were provided by G. P. Penkler for HPLC analysis by the author. The retention times of the external metabolites lactate, pyruvate, glycerol and glucose were 6.5, 10.1, 10.4 and 13.4 minutes, respectively. In Fig. 3.4 one can clearly see the elution profiles of the external metabolites changing over time with total decrease om the glucose forming predominantly lactate, with glycerol and pyruvate as minor metabolites.

The analysis showed a pyruvate:glycerol ratio close to 1, i.e. 0.92 ± 0.23 (SD, n =7)[2]. Therefore, when the peaks of these two closely eluting metabolites

Table 3.4: Comparison between experimental and model predictions of the steady state fluxes. The external metabolites produced during an incubation of intact trophozoites with 5 mM glucose were measured via enzyme-coupled assays. The steady state fluxes ($\pm$ SEM; for ^{12}C-glucose, n =3; for ^{14}C-glucose, n = 2) were determined by linear regression, sampling at least 30 minutes. The experimental fluxes are compared to the predictions of Penkler's model of *P. falciparum* glycolysis[23]. Model predictions were obtained by setting the concentrations of external glucose (5 mM), lactate (1 mM), glycerol (0.2 mM) and pyruvate (0.15 mM).

Flux	^{12}C-Glucose Incubation Mean (SEM) $\frac{\mu\text{mol}}{\text{min·mg protein}}$	^{14}C-Glucose Incubation Mean (SEM) $\frac{\mu\text{mol}}{\text{min·mg protein}}$	Model Prediction $\frac{\mu\text{mol}}{\text{min·mg protein}}$
J_{GLC}	0.050 (0.006)	0.045 (0.002)	0.05
J_{LAC}	0.109 (0.005)	0.081 (0.003)	0.092
J_{PYR}	0.004 (0.001)	0.004 (0.0007)	0.004
J_{GLR}	0.003 (0.001)	0.005 (0.0005)	0.004
J_{PYR}: J_{GLR}	1.5	0.8	1

were inseparable, a ratio of 1:1 was assumed. The ratio of their production rates was close to 1 too, i.e. J_{PYR}: J_{GLR} = 0.8.

Integration of the chromatograms yielded metabolite concentrations. Linear regression over a minimum period of 30 minutes yielded consumption and production rates of 0.045 $\pm$ 0.002 μmol.min^{-1}.mg^{-1} protein for J_{GLC}, 0.081 $\pm$ 0.003 μmol.min^{-1}.mg^{-1} protein for J_{LAC}, 0.004 $\pm$ 0.0007 μmol.min^{-1}.mg^{-1} protein for J_{PYR} and 0.005 $\pm$ 0.0005 μmol.min^{-1}.mg^{-1} protein for J_{GLR}. These are the average rates (mean $\pm$ SEM) of two independent incubations. It was assumed that the system was in steady state after 30 minutes' incubation.

Similar rates were obtained for the incubations with unlabelled glucose (n = 3): J_{GLC} = 0.050 $\pm$ 0.006 μmol.min^{-1}.mg^{-1} protein, J_{LAC} = 0.109 $\pm$ 0.005 μmol.min^{-1}.mg^{-1} protein, J_{PYR} = 0.004 $\pm$ 0.001 μmol.min^{-1}.mg^{-1} protein and J_{GLR} = 0.003 $\pm$ 0.001 μmol.min^{-1}.mg^{-1} protein.

These rates, however, were normalised to previous lactate production rate measurements due to a 3-fold overestimation of these rates which resulted from an inherent error to account for all viable trophozoites. Figure 3.5 shows the changes in external metabolite concentrations over time.

0 minutes
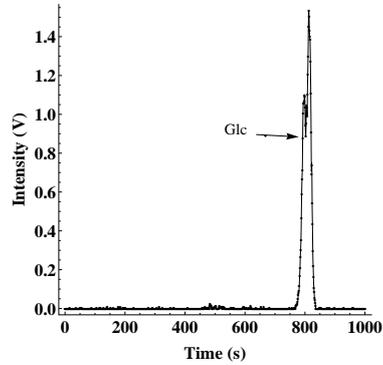
45 minutes
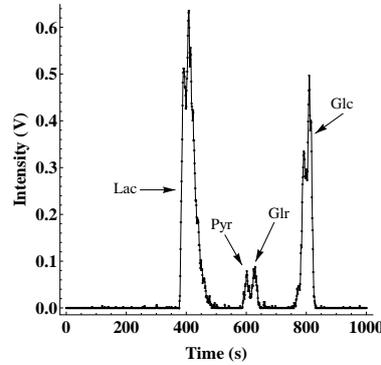
15 minutes
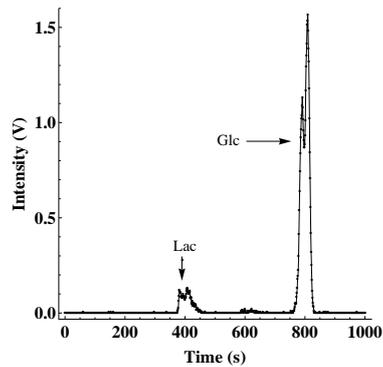
60 minutes
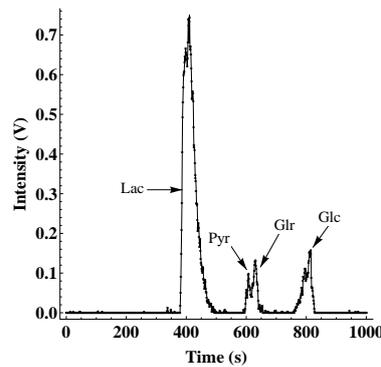
30 minutes
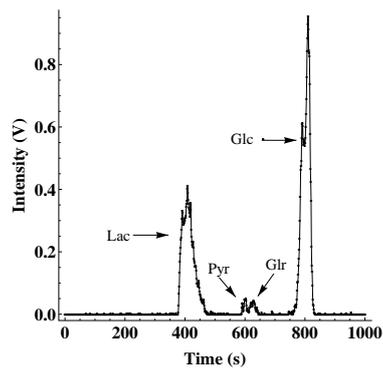
135 minutes
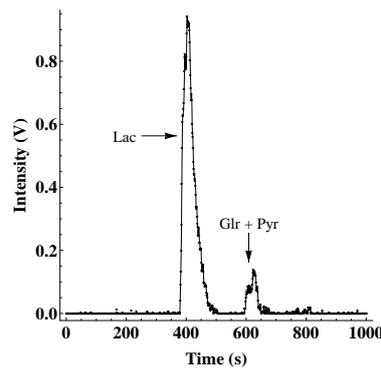
Figure 3.4: Representative time progression HPLC chromatograms following the metabolism of ^{14}C-glucose (Glc) in *P. falciparum* trophozoites to the ^{14}C-labelled intermediates lactate (Lac), pyruvate (Pyr) and glycerol (Glr).

Although the pyruvate:glycerol flux ratio was close to 1, i.e. $J_{PYR} : J_{GLR} = 1.5$, the absolute concentration of pyruvate and glycerol differ strongly, in contrast to measurements in the radioisotope experiments above. This discrepancy between the radiolabelled and unlabelled experiments can be ascribed to the negative pyruvate concentration values, an artefact of the enzymatic analysis process. Yet despite this disagreement, the experimentally measured fluxes agreed well with the model predictions. The concentration ranges of glycerol and pyruvate have been offset by -0.69 mM and 0.37 mM, respectively, in Fig. 3.5 to facilitate the comparison between the experimentally determined fluxes and those predicted by the model. The model prediction for glycerol and pyruvate production rates are quite accurate, although the model prediction for the final concentration is lower. The model prediction for glucose consumption and lactate production is not as accurate, mostly due to a difference in initial conditions for glucose: an initial concentration of 5 mM was chosen and products were initialised at 0 mM.

3.4   Metabolic Control Analysis

This thesis mainly focused on the kinetics of *P. falciparum* G3PDH and the steady state pathway flux to glycerol. To understand the importance of G3PDH on the flux through the pathway, metabolic control analysis (MCA) was performed on the system.

Presented in Table 3.5 are the steady state predictions of the detailed kinetic (Penkler 1) model. These steady state predictions were generated on JWS Online (http://jjj.biochem.sun.ac.za) by the author. Of interest are the steady state concentrations of DHAP, G3P, NADH and NAD$^+$ which are 1.271, 0.557, 0.059 and 2.941 mM, respectively, as well as the steady state fluxes of glucose transporter (GlcTr), ALD, TPI and G3PDH which have values of 0.04929, 0.04929, 0.04549, and 0.0038 μmol.min^{-1}.mg^{-1} protein, respectively.

One can reduce the system to three reactions centred around the branch point metabolite DHAP: the supply block of upper glycolysis (represented by $J_{GlcTr} = J_{ALD}$) and the two branches of the glycerol pathway (represented by J_{G3PDH}) and lower glycolysis (represented by J_{TPI}). This rationale was presented by Snoep et al.[88] and Sauro[89][90,91] when they analysed branched systems.

A

B

C

D

Figure 3.5: Progress curves of external metabolite concentrations. Isolated *P. falciparum* trophozoites were incubated with glucose and the concentrations of external metabolites were determined from samples taken over a 90 minute period. External glucose (A), lactate (B), glycerol (C) and pyruvate (D) concentrations were measured spectrophotometrically at 340 nm via enzyme-coupled assays. The concentration ranges of glycerol (C) and pyruvate (D) were offset by -0.69 mM and 0.37 mM, respectively, due to a glycerol concentration of 0.69 mM and a pyruvate concentration of -0.37 mM at 0 minutes. The mean $\pm$ SEM of three independent experiments are shown. The solid line represents the model prediction over this 90 minute time period.

Table 3.5: Kinetic model predictions of steady state concentrations and fluxes. Summarised below are the predictions of the *P. falciparum* glycolysis (Penkler1) model for the steady state fluxes and metabolite concentrations. These steady state predictions were generated on JWS Online (http://jjj.biochem.sun.ac.za) by the author.

Metabolite	Concentration (mM) mM	Flux	Rate μmol.min^{-1}.mg^{-1} protein
ADP	0.51	J_{ALD}	0.04929
ATP	2.49	J_{ATPASE}	0.09098
B1,3PG	0.001	J_{ENO}	0.09478
DHAP	1.271	J_{G3PDH}	0.0038
F1,6BP	1.372	J_{GAPDH}	0.09478
F6P	0.297	J_{GLCtr}	0.04929
G3P	0.557	J_{GlrTr}	0.0038
G6P	0.967	J_{HK}	0.04929
GAP	0.055	J_{LACtr}	0.09098
GLC	1.001	J_{LDH}	0.09098
LAC	2.902	J_{PFK}	0.04929
NAD$^+$	2.941	J_{PGI}	0.04929
NADH	0.059	J_{PGK}	0.09478
P2G	0.056	J_{PGM}	0.09478
P3G	0.578	J_{PK}	0.09478
PEP	0.061	J_{PYRtr}	0.0038
PYR	1.125	J_{TPI}	0.04549

In their respective treatises they highlighted an important feature of branched systems, i.e. when the flux through a downstream branch is much smaller than the main flux, the enzymes in that branch will tend to have a high control of the flux through that branch. Thus, the sum of the flux control coefficients of the enzymes in a branch with negligible flux will be 1[88]. It is tempting to think that the glycerol pathway is such a negligible branch but with a flux that is 7.7% of the GlcTr flux, the pathway is not quite negligible. This shows the importance of flux ratios in control analysis, another feature of branched systems. In linear systems flux ratios are irrelevant since there is only one steady state flux through the system.

Analysis of G3PDH yielded a flux control coefficient of 0.6552, a value much lower than 1. By using the approach set out by Sauro[89] (see Equation 3.4.1), one

can calculate the flux control coefficient of G3PDH for its own flux ($C_{vG3PDH}^{J_{vG3PDH}}$). The approach does not assume that the flux through the glycerol pathway is negligible and makes use of flux ratios ($\alpha = \frac{J_{vG3PDH}}{J_{ALD}}$ and $1 - \alpha = \frac{J_{vTPI}}{J_{ALD}}$) and elasticitiy coefficients (where $\epsilon_{DHAP}^{vALD} = -1.810$, $\epsilon_{DHAP}^{vG3PDH} = 0.234$ and $\epsilon_{DHAP}^{vTPI} = 17.687$). Application of this approach yielded a predicted flux control coefficient of 0.99, still closer to 1 and higher than the actual $C_{vG3PDH}^{J_{vG3PDH}}$.

$$C_{vG3PDH}^{J_{vG3PDH}} = \frac{\epsilon_{DHAP}^{vALD} - \epsilon_{DHAP}^{vTPI} \cdot (1 - \alpha)}{\epsilon_{DHAP}^{vALD} - \epsilon_{DHAP}^{vG3PDH} \cdot \alpha - \epsilon_{DHAP}^{vTPI} \cdot (1 - \alpha)} \tag{3.4.1}$$

The discrepancy between the actual flux control coefficient and the predicted value may be attributed to the theory assuming that only one branch point metabolite (DHAP) exists when the pathways really share more than one (i.e. NAD(H)). Thus, any analysis will have to consider NAD(H) too.

For an enzyme to have a flux control of 1 over its own flux, all its substrates, products and effects have to remain constant when a small perturbation in the enzyme is made. This means that for any change that occurs in G3PDH, the concentrations of its substrates (DHAP and NADH) and products (G3P and NAD$^+$), the enzyme's only effectors, have to remain constant. One can therefore determine how much each effector contributes to the lessening of the control G3PDH exerts over its own flux. One does this by adding the effects of changes in DHAP, NADH, G3P and NAD$^+$ to the flux control coefficient of 1. In MCA terms this translates to adding the product of the concentration control coefficient and elasticity of G3PDH for each of its effectors to the predicted G3PDH flux control coefficient of 1 (as in Equation 3.4.2). The elasticity and concentration control coefficients are presented in Table 3.6.

$$C_{vG3PDH}^{J_{vG3PDH}} = 1 + C_{vG3PDH}^{DHAP} \cdot \epsilon_{DHAP}^{vG3PDH} + C_{vG3PDH}^{G3P} \cdot \epsilon_{G3P}^{vG3PDH}$$
$$+ C_{vG3PDH}^{NADH} \cdot \epsilon_{NADH}^{vG3PDH} + C_{vG3PDH}^{NAD} \cdot \epsilon_{NAD}^{vG3PDH} \tag{3.4.2}$$

Our analysis shows that the contribution of NADH (-0.2955) strongly dominates those of DHAP (-0.0302), G3P (-0.0141) and NAD$^+$ (-0.0051) (see Table 3.6). Thus, NADH is responsible for lessening the control G3PDH exerts over its own flux due to the enzyme's high elasticity for this metabolite and the reasonably strong concentration control on this metabolite.

Table 3.6: Contribution of each G3PDH substrate and product to the enzyme's flux control coefficient. Presented here are elasticities of G3PDH for each substrate or product and the concentration control coefficients of G3PDH on these metabolites. The elasticities and concentration control coefficients were determined on JWS Online (http://jjj.biochem.sun.ac.za). The contribution each metabolite makes to lessing the control of G3PDH over the enzyme's own flux is determined by the product of the elasticity and concentration contol coefficients of G3PDH for that metabolite.

ϵ_{DHAP}^{vG3PDH}	0.2343	C_{vG3PDH}^{DHAP}	-0.1289	$\epsilon_{DHAP}^{vG3PDH} \cdot C_{vG3PDH}^{DHAP}$	-0.0302
ϵ_{NADH}^{vG3PDH}	0.9121	C_{vG3PDH}^{NADH}	-0.3240	$\epsilon_{NADH}^{vG3PDH} \cdot C_{vG3PDH}^{NADH}$	-0.2955
ϵ_{G3P}^{vG3PDH}	-0.0294	C_{vG3PDH}^{G3P}	0.4788	$\epsilon_{G3P}^{vG3PDH} \cdot C_{vG3PDH}^{G3P}$	-0.0141
ϵ_{NAD}^{vG3PDH}	-0.7774	C_{vG3PDH}^{NAD}	0.0065	$\epsilon_{NADH}^{vG3PDH} \cdot C_{vG3PDH}^{NAD}$	-0.0051

CHAPTER 4

GENERAL DISCUSSION

The present work set out to: 1) determine the kinetic parameters (K_M and V_{max}) of *Plasmodium falciparum* glycerol 3-phosphate dehydrogenase (G3PDH), 2) detect glycerol kinase (GK) activity in asexual *P. falciparum* and determine whether the parasite uses a phosphatase mechanism to dephosphorylate glycerol 3-phosphate (G3P), 3) update the existing Penkler model with the measured kinetic data, and finally to 4) ascertain the distribution of control over the steady state flux through the glycerol branch.

The kinetic characterisation of G3PDH was successfully completed. To the author's knowledge, this study marks the first kinetic description of the NAD^+-dependent G3PDH of *P. falciparum* in the scientific literature.

The results concerning the conversion of G3P to glycerol were inconclusive. Although low level GK activity was detected, the background activity was very high. If it is the case that *P. falciparum* GK does function in reverse, i.e. dephosphorylating G3P to glycerol, in the intra-erythrocytic stage of the parasite's life cycle, the behaviour would be similar to that of *T. brucei* GK which also catalyses the thermodynamically unfavourable reverse reaction in the blood stage form of *T. brucei*[92,93]. A reason for *T. brucei* GK catalysing the thermodynamically unfavourable reaction was advanced by Krakow and Wang[93] who proposed that GK dephosphorylated G3P by mass action due to high concentrations of G3P and ADP and an efficient ATP trap in the glycosome. Králová et al.[94] found that *T. brucei* only used GK to dephosphorylate G3P under anaerobic conditions. Under aerobic conditions, a G3P:DHAP shuttle functioned to recycle DHAP.

Efforts to detect G3P-dependent phosphatase activity in the extract were irreproducible and inconclusive. Given a shorter incubation time and intervals

between sampling times, one might have been able to compare the initial rates of the reaction and draw conclusions from the comparison. However, one cannot rule out the activity of the non-specific phosphatase discovered by Hills et al.[50].

The kinetic parameters that were obtained during the biochemical characterisation of G3PDH were incorporated into an existing model of *P. falciparum* glycolysis (Penkler 1 model; Appendix A) which is available on JWS Online[23,78,79] (http://jjj.biochem.sun.ac.za). For model validation, the Penkler 1 model was changed to reflect experimental conditions (Penkler 2 model —also available on JWS Online) during which saponin-derived trophozoites were incubated with radiolabelled and unlabelled glucose. The model predicted the steady state fluxes of external metabolites glucose, lactate, pyruvate and glycerol. These predictions compared well with the experimentally measured fluxes.

This glycolysis model is the first of its kind for *P. falciparum.* Similar bottom up approach kinetic models of glycolysis exist, e.g. in yeast[95], human erythrocyte[70] and *T. brucei*[96,92]. A kinetic model describing the glycerophospholipid metabolism of *P. knowlesi* exists, but the researchers constructed the model based on flux balance analysis[62].

Metabolic control analysis was used to determine the distribution of flux control over the glycerol branch in the updated Penkler 1 model. The analysis showed that the NADH concentration greatly influenced the control of G3PDH over the enzyme's own flux. In this way glycolysis is able to control the magnitude of the flux flowing through the glycerol branch. Unlike the simple pathway used by Snoep et al.[88] and Sauro[89] to explain the theory of branch point analysis, the glycerol branch is not negligible as shown by its elasticity coefficients for DHAP and NADH as well as its flux ratio.

The fact that NADH exercises a significant amount of control over the flux through G3PDH means that an increase in its concentration will result in an increase in the flux through G3PDH thereby recycling the NAD^+ for use by glycolysis. *P. falciparum* also possesses mitochondrial G3PDH which implies the presence of a G3P Shuttle. The G3P Shuttle, first reconstructed in rat kidney mitochondria[97], functions to transport reducing equivalents from cytosolic NADH to mitochondrial NADH where they are used by the parasite's electron transport chain. Cytosolic NAD^+ is recycled in the process[22].

In a purely linear pathway, e.g. glucose conversion to lactate, there is no degree

of freedom in terms of redox balancing. All glucose must be converted to lactate or else there is no redox balance. A branched pathway in which the final product has a different degree of reduction than glucose, offers different ways of maintaining the redox balance. For instance, if a cell needs to make lipids via G3P, then there would quickly be a shortage of NADH and the cell would not be able to make lactate as the final product. Pyruvate would accumulate. Via the flexibility of glycerol and pyruvate production the parasite can balance redox metabolism, even if products are made that do not have the same degree of reduction as glucose.

A similar situation is observed in Trypanosomatids (*T. brucei, T. gambiense, T. equiperdum* and *T. evansi*) that convert glucose to glycerol and pyruvate in equimolar amounts under anaerobic conditions[94,98]. Under aerobic conditions when the G3P:DHAP shuttle is active in the micro-aerophilic parasite, *T. brucei brucei* produced pyruvate and glycerol in a 3:1 ratio[98].

Would G3PDH serve as a good drug target since the enzyme and the glycerol branch (of which it is a part) are at a junction between glucose catabolism and lipid metabolism? Based on the MCA results, inhibition of G3PDH would have a significant effect on the flux through the lactate transporter (and therefore lower glycolysis) because of the accumulation of DHAP and NADH in the parasite. Whether lipid metabolism will be affected adversely requires further study since Naidoo and Coetzer[47] showed that *P. falciparum* is able to acquire and use glycerol from the surrounding medium even in the absence of GK.

Although not particularly relevant to the systems biology approach, further study is needed to ascertain biophysical and other biochemical properties of *P. falciparum* G3PDH since very little information in the literature exists on the enzyme. *P. falciparum* aquaglyceroporin and GK have been extensively characterised but not G3PDH.

Future studies also include expanding the Penkler model of *P. falciparum* glycolysis to include the pentose phosphate pathway, making the model a compartment of erythrocyte glycolysis, formatting it to simulate parasite growth, and studying how malaria affects its human host's homeostasis.

Appendices

Appendix A

Published Results

The G3PDH kinetic data generated during this study was incorporated into Penkler et al.[23]. I was responsible for generating the kinetic data which was combined with those of the first and second authors of this paper.

Construction and validation of a detailed kinetic model of glycolysis in *Plasmodium falciparum*

Gerald Penkler[1,2], Francois du Toit[1], Waldo Adams[1], Marina Rautenbach[1],
Daniel C. Palm[1], David D. van Niekerk[1] & Jacky L. Snoep[1,2,3*]

December 11, 2014

1 Abstract

The enzymes in the Embden-Meyerhof-Parnas pathway of *Plasmodium falciparum* trophozoites were kinetically characterised and their integrated activities analysed in a mathematical model. For validation of the model we compared model predictions for steady state fluxes and metabolite concentrations of the hexose phosphates with experimental values for intact parasites. The model, which is completely based on the experimentally determined enzyme kinetic parameters, gives an accurate prediction of the steady state fluxes and intermediate concentrations. This is the first detailed kinetic model for glucose metabolism in *P. falciparum*, one of the most prolific malaria-causing protozoa, and the high predictive power of the model makes it a strong tool for future drug target identification studies. The modelling workflow is transparent and reproducible and completely documented in the EuroSEEK platform, where all experimental data and models are available for download.

Database

2 Abbreviations

enzymes: ALD, fructose-bisphosphate aldolase (EC 4.1.2.13); GAPDH, glyceraldehyde-3-phosphate dehydrogenase (phosphorylating) (EC 1.2.1.12); GLYDH, glycerol-3-phosphate dehydrogenase (EC 1.1.99.5); HK, hexokinase (EC 2.7.1.1); PGI, glucose-6-phosphate isomerase (EC 5.3.1.9); LDH, lactate dehydrogenase (EC 1.1.1.27); PFK, 6-phosphofructokinase (EC 2.7.1.11); PGK, phosphoglycerate kinase (EC 2.7.2.3); PGM, phosphoglycerate mutase (EC 5.4.2.12); ENO, phosphopyruvate

---

[*]corresponding author,

[1] Department of Biochemistry, Stellenbosch University, Private Bag X1, Matieland 7602, South Africa, e-mail: jls@sun.ac.za, phone: +27218085844, fax: +27218085863; [2] Molecular Cell Physiology, Vrije Universiteit Amsterdam, The Netherlands; [3] MIB, University of Manchester, UK.

hydratase (EC 4.2.1.11); PK, pyruvate kinase (EC 2.7.1.40); TPI, triose-phosphate isomerase (EC 5.3.1.1).
intermediates: G6P, glucose 6-phosphate; F6P, fructose 6-phosphate; F16BP, fructose 1,6-bisphosphate; DHAP, glycerone phosphate; G3P, glycerol 3-phosphate; GAP, d-glyceraldehyde 3-phosphate; B13PG, 1,3-bisphosphoglycerate;
3PG, 3-phosphoglycerate; 2PG, 2-phosphoglycerate; PEP, phosphoenolpyruvate; PYR pyruvate; LAC lactate; GLC glucose.

3 Introduction

Despite several attempts at a complete eradication of the disease, malaria is still killing more than half a million people per year, mostly small children in sub-saharan Africa (World Health Organisation report 2013). The disease is caused by parasitic protozoa of the *Plasmodium* genus, which have a complicated life cycle consisting of an insect vector and vertebrate host (for a recent review see [1]). In the human host, parasite sporozoites first invade liver cells, but the malaria disease symptoms manifest only at a later stage during multiplication of the asexual stages of the parasite in red blood cells (RBCs). The blood life-cycle consists of ring, trophozoite and schizont stages and after RBC lysis leads to the formation of merozoites, which can further infect RBCs, or differentiate to sexual gametocytes, which invade the insect vector upon a mosquito bite.

The aetiology of the disease is not well-understood, but the best predictors for poor chances of survival, hypoglycaemia and lactic acidosis, are directly linked to glucose (GLC) metabolism in the infected host [2], although it is not known to what extent the glycolytic activity of the parasite contributes to this. With the ultimate aim to deeply understand changes in GLC metabolism during malaria infection and to identify potential drug targets in the parasite, we have started a detailed study in central carbon metabolism of *Plasmodium falciparum*. Our strategy is to use a hierarchical modelling approach, starting with modelling of the *Plasmodium* trophozoite stage, then linking the parasite model with a red blood cell model for glucose metabolism [3, 4], and extending to the other blood stages of the parasite, including bursting and reinvasion of erythrocytes. We will have separate construction and validation data sets for each of these stages. Ultimately these hierarchies will include whole body glucose metabolism during *Plasmodium* infection, first in animal models and eventually for human malaria patients. By comparing the parasite with human cell models a differential control analysis approach will be used to identify potential drug targets [5].

Central carbon metabolism of *P. falciparum* consists of glycolysis and the pentose phosphate pathway. The parasite is dependent on glycolysis for ATP production [6] and does not store any reduced carbon reserves [7, 8]. Although a modified form of the tricarboxylic acid (TCA) cycle exists, it is not directly linked to glycolysis due to localisation of the pyruvate dehydrogenase complex in the apicoplast. Instead, the TCA cycle utilises primarily glutamine and glutamate as its carbon sources [9]. It was initially thought that *P. falciparum* glycolysis was homolactic, which was supported by the finding of an almost 2:1 ratio of lactate (LAC) produced per GLC consumed [8]. However, this is inconsistent with several reports of pyruvate (PYR) and glycerol (GLY) production [10, 11]. The pentose phosphate pathway flux is low in asexual *P. falciparum* [8, 12] and for this study we focused on the enzymes of the classic Embden-Meyerhof-Parnas pathway, including GLY production and transport reactions (see Fig. 1).

Most of the glycolytic enzymes have been kinetically characterised for a variety of *Plasmodium* species, often as pure enzymes (after cloning, expression and isolation), under conditions optimal for the respective enzymes. Despite the multitude of reports on kinetics of individual enzymes
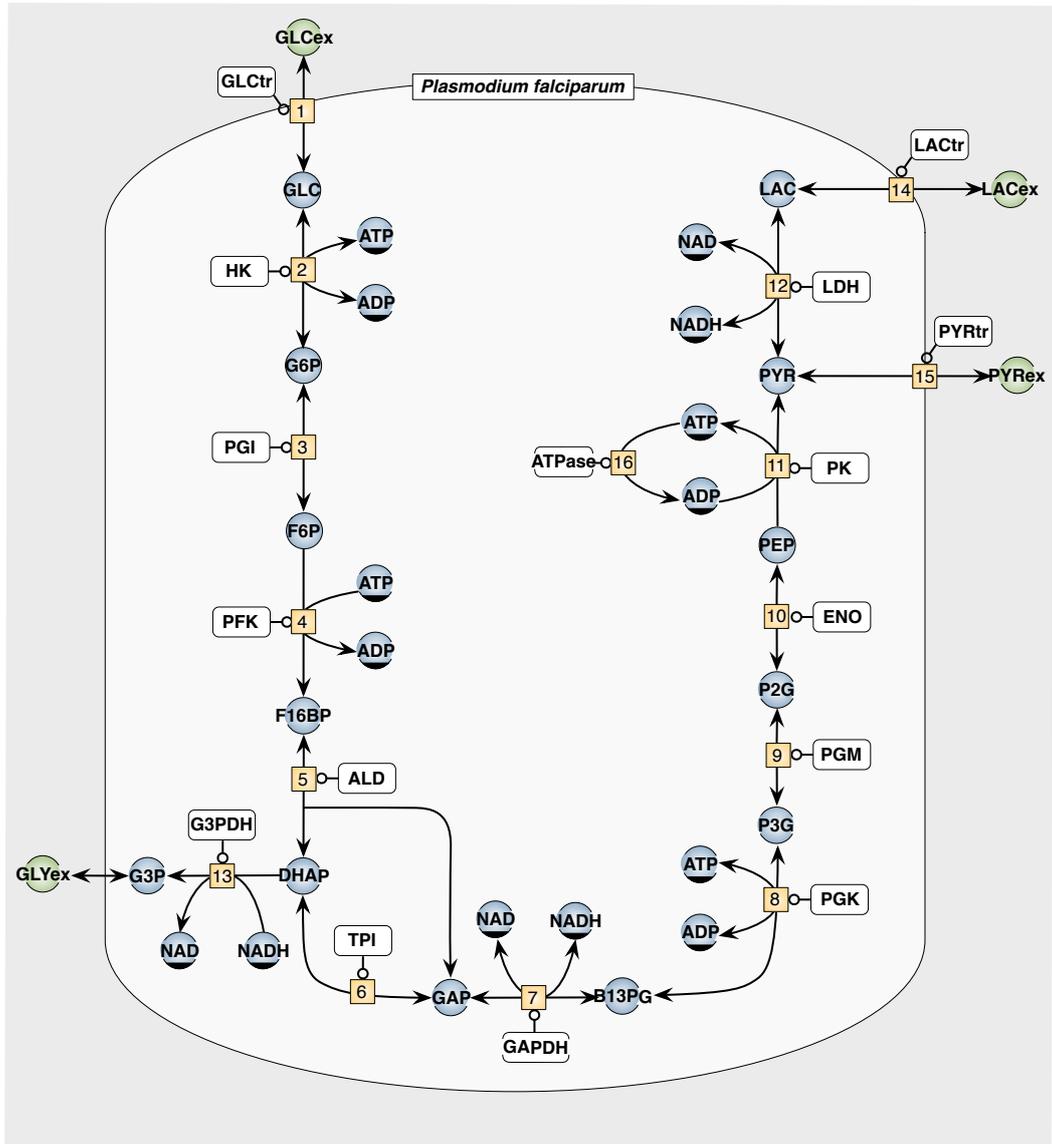
Figure 1: Glycolysis and metabolite transport reactions in *P. falciparum* as included in the kinetic model.

of the glycolytic pathway of *Plasmodium*, to the best of our knowledge no study has been published on an integrated analysis of the enzyme kinetics. Ideally, for such an integrated analysis the kinetic parameters should be determined under physiologically relevant conditions [13]. Typically, for integration of enzyme kinetics a mathematical model would be constructed, which can be validated by its predictive strength of (non-fitted) complete system data-sets, a process described in the Silicon Cell initiative [14]. Many mathematical models have been constructed for central carbon metabolism in a number of organisms (for examples of glycolytic models see [4, 15, 16]).

Different types of rate equations are used for mathematical modelling of enzyme reaction networks. These range from simple rate equations (e.g. mass action kinetics and lin-log kinetics [17]) to very detailed rate equations (e.g. kinetics defined in terms of elementary rate constants [3]). Whereas the simple rate equations have the advantage that they contain few parameters, they are often limited in their applicability to a narrow range around a steady state reference state. The detailed rate equations give a close representation of the enzyme kinetic mechanism, but have many kinetic parameters, which are often difficult to quantify. For modelling studies of reaction networks an interesting in-between level of detail for rate equations has been suggested in the form of "convenience kinetics" [18], and as generic rate equations [19]. The generic rate equations have a mechanistic basis, i.e. they can be derived assuming a random-order equilibrium-binding mechanism, but have been shown to be able to capture the kinetic behaviour of various other enzyme kinetic mechanisms [19]. In mathematical models it is important to chose a correct level of detail to describe a system, and generic rate equations with operationally defined parameters, have been shown to be adequate for many modelling studies focussing on steady state behaviour of reaction networks.

In this study we test whether the integrated kinetics of the glycolytic enzymes of *P. falciparum* can predict steady state pathway fluxes and metabolite concentrations in the intact trophozoite blood stage form. We first present the biochemical characterisation of each of the glycolytic enzymes and fit the kinetic behaviour with generic kinetic equations, based on random-order equilibrium-binding mechanisms. The equations are then integrated in an ordinary differential equations (ODEs) based model. The steady state of the kinetic model is analysed and compared to experimental fluxes and metabolite concentrations that were obtained with intact *P. falciparum* cells. The complete workflow, including data sets and model files are made available in the SEEK data and model management platform [20], making the modelling process completely transparent and reproducible.

4   Results and Discussion

4.1   Kinetic characterization

We used a bottom-up systems biology approach for the construction of a detailed kinetic model of glycolysis in the malaria parasite *P. falciparum*, to test whether the *in vitro* enzyme kinetics can be used to predict *in vivo* steady state behaviour. In this section we present the kinetic characterization for each of the glycolytic enzymes, including the parameterisation of rate equations and comparison to literature values of parameters (if available). The enzyme kinetic experiments were performed in cell free extracts, and activities are expressed in units per mg total protein. We use generic rate equations, based on equilibrium binding, random order mechanisms, for the description of the enzyme kinetic experiments. These mechanisms do not necessarily reflect the real enzyme kinetic mechanism but the rate equations can describe the kinetic data well, and have operationally defined parameters with an unambiguous interpretation. For special cases, such as enzymes subject to substrate inhibition, we have derived additional rate equations and

4

give the assumptions for the derivation in the text.

For this study we focus on the trophozoite stage of *Plasmodium falciparum* and on a single physiological reference state of pH 7.2 and a temperature of 37°C. In section 4.2 we present the specific activity data for the glycolytic enzymes as measured in cell extracts of *P. falciparum* trophozoites. In section 4.3 we give details on the model construction and finally in section 4.4 we compare model predictions with experimental flux and metabolite values obtained with intact trophozoites.

4.1.1 Hexokinase

Hexokinase (HK) catalyses the ATP dependent phosphorylation of GLC to glucose 6-phosphate (G6P) and ADP. The enzyme showed hyperbolic saturation kinetics for GLC, and the product inhibition by G6P and ADP followed monotonous trends, while ATP displayed substrate inhibition (Fig. 2) which became very pronounced at concentrations above 5 mM. For fitting of the enzyme kinetic parameters, we only took the experimental data for ATP concentrations up to 5 mM into account, considering any higher concentrations as non-physiological. For HK and all other kinases we assumed that Mg-ATP is the active ATP complex, and since Mg^{2+} was always maintained at least at twice the concentration of ATP we assumed all ATP in the assays in the Mg-ATP form.

$$vHK = \frac{V_{f_{HK}} \cdot \frac{atp}{K_{ATP}} \cdot \frac{glc_{in}}{K_{GLC_{in}}} \cdot \left(1 - \frac{adp \cdot g6p}{atp \cdot glc_{in} \cdot K_{eq}}\right)}{\left(1 + \frac{adp}{K_{ADP}} + \frac{atp}{K_{ATP}}\right) \cdot \left(1 + \frac{g6p}{K_{G6P}} + \frac{glc_{in}}{K_{GLC_{in}}}\right) \cdot \left(1 + \frac{atp}{K_{i_{ATP}}}\right)} \tag{1}$$

For the fitting of the kinetic data we used Eqn 1, derived assuming a random order bi-bi mechanism with equilibrium binding of substrates, products and effectors. In this and subsequent equations we use the following symbols: V_x maximal rate of enzyme x, expressed in (μmol·min^{-1}·mg^{-1} total protein), K_x dissociation constant of x in mM, K_{i_x} inhibitor dissociation constant in mM, and K_{eq} equilibrium constant. The lower case abbreviations denote concentrations (e.g. atp=[ATP]). These notations will be used throughout the manuscript. The kinetic mechanism of ATP inhibition is not known and we assumed that ATP can bind to each of the enzyme complexes. This equation could describe the kinetics quite well (Fig. 2), although the dissociation constants for GLC and ATP are lower than the K_M values determined by Roth *et al.* [21]. In [21] no kinetic data or rate equations are given, and the reported K_M value for ATP is measured in infected erythrocyte lysates and thus reflects a combination of parasite and

Table 1: Kinetic parameters for *P. falciparum* hexokinase. The parameter values ($\pm$ asymptotic standard error) were obtained by fitting Eqn. 1 to the normalised combined HK data set (Fig. 2). Literature values are given for HK as determined in *P. falciparum* infected erythrocyte lysates [21]. The maximal specific activity, $V_{f_{HK}}$ was determined independently in cell extracts and is expressed per mg total protein (see Fig. 15).

Parameter	Fitted Value	Literature Value	Reference
$V_{f_{HK}}$ (μmol·min^{-1}·mg^{-1})	0.39 ± 0.09	-	
K_{GLC} (mM)	0.17 ± 0.02	0.43 ± 0.02	[21]
K_{ATP} (mM)	0.70 ± 0.03	3 ± 1	[21]
$K_{i_{ATP}}$ (mM)	26 ± 5	-	-
K_{ADP} (mM)	0.8 ± 0.1	-	-
K_{G6P} (mM)	0.04 ± 0.01	-	-
K_{eq}		1310	[22]

erythrocyte HK kinetics, although predominantly determined by parasite kinetics (erythrocyte hexokinase: $K_{M_{ATP}}$ (mM) = 2.5 ± 1.0 [21] and $K_{M_{Glc}}$ (mM) = 0.098 ± 0.0010 [21]). One must be careful to compare kinetic constants that were determined for different rate equations as they might not have the same mechanistic interpretation.

4.1.2 Phosphoglucoisomerase

Phosphoglucoisomerase (PGI) catalyses the conversion of G6P to fructose 6-phosphate (F6P). Hyperbolic saturation kinetics were obtained for both G6P and F6P and a reversible Michaelis-Menten equation (Eqn. 2) fitted the combined data set well (Fig. 3). The parameter values for the fit are listed in Table 2. For the model we expressed $V_{r_{PGI}}$ in the rate equation as a function of $V_{f_{PGI}}$, K_{G6P}, K_{F6P} and K_{eq} using the Haldane equation with a K_{eq} value of 0.33 [23, 24].

$$v\text{PGI} = \frac{V_{f_{\text{PGI}}} \cdot \frac{\text{g6p}}{K_{\text{G6P}}} - V_{r_{\text{PGI}}} \cdot \frac{\text{f6p}}{K_{\text{F6P}}}}{1 + \frac{\text{f6p}}{K_{\text{F6P}}} + \frac{\text{g6p}}{K_{\text{G6P}}}} \tag{2}$$

Table 2: Kinetic parameters for *P. falciparum* PGI. Eqn 2 was fitted to the normalised combined PGI data and the fitted parameters are indicated with asymptotic standard error. The forward and reverse maximal specific activities ($V_{f_{PGI}}$ and $V_{r_{PGI}}$) were determined in separate experiments in cell extracts and are expressed per mg total protein (Fig. 15). K_{eq} value was calculated with the Haldane relation.

Parameter	Fitted Value	Literature Value	Reference
$V_{f_{PGI}}$ (μmol·min^{-1}·mg^{-1})	3.7 ± 0.2	-	-
$V_{r_{PGI}}$ (μmol·min^{-1}·mg^{-1})	1.4 ± 0.3	-	-
K_{G6P} (mM)	1.0 ± 0.1	-	-
K_{F6P} (mM)	0.10 ± 0.01	0.26 ± 0.03	[25]
K_{eq}	0.3 ± 0.1	0.33	[23, 24]

Srivastava *et al.* identified and characterised three PGI isoenzymes of *P. falciparum* each with a similar K_M for fructose 6-phosphate [25], for which the average value and SEM are given in Table 2. The expression profile of the three isozymes during the asexual development phase of the *P. falciparum* life cycle is not known and in our model we simulate PGI activity as an average activity of the three isozymes.

4.1.3 Phosphofructokinase

PFK catalyses the ATP-dependent phosphorylation of F6P to fructose 1,6-bisphosphate (F16BP). The enzyme showed hyperbolic saturation kinetics for F6P and monotonous curves for the inhibition by F16BP and ADP but displayed substrate inhibition for ATP (Fig. 4). ATP inhibition was also observed for PFK of *P. berghei* [26–29], but we did not observe regulation by PEP and F16BP in *P. falciparum*, which is in agreement with [30]. In Fig. 4 the specific activities were normalised to a control rate determined with 1.25 mM ATP and 10 mM F6P.

We fitted an irreversible, random order binding mechanism with substrate inhibition for ATP, assuming that ATP can bind to all enzyme forms (see Eqn. 3).

$$v\text{PFK} = \frac{V_{\text{PFK}} \cdot \frac{\text{atp}}{K_{\text{ATP}}} \cdot \frac{\text{f6p}}{K_{\text{F6P}}}}{(1 + \frac{\text{atp}}{K_{i_{\text{ATP}}}}) \cdot (1 + \frac{\text{f6p}}{K_{\text{F6P}}} + \frac{\text{f16bp}}{K_{\text{F16BP}}}) \cdot (1 + \frac{\text{atp}}{K_{\text{ATP}}} + \frac{\text{adp}}{K_{\text{ADP}}})} \tag{3}$$

6
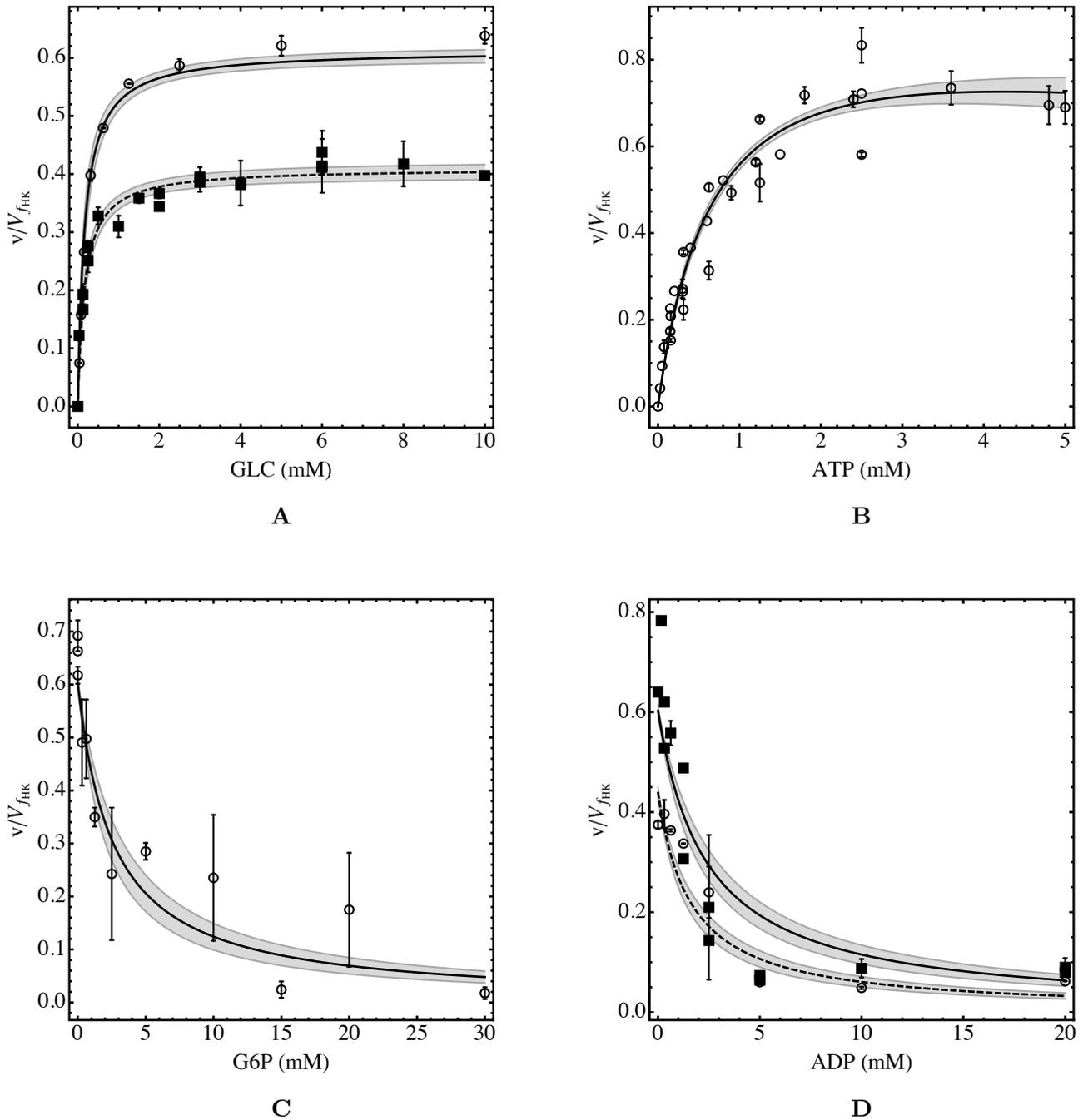
Figure 2: Kinetic characterisation of *P. falciparum* hexokinase. Panel A, saturation of HK with GLC (0.5 mM ATP, squares and dashed line; 1.25 mM ATP, circles and solid line). Panel B, saturation with ATP (10 mM GLC). Panel C, inhibition by G6P (10 mM GLC and 1.25 mM ATP). Panel D inhibition by ADP (1.25 mM ATP and 10 mM GLC, squares and solid line; 0.625 mM ATP and 3.125 mM GLC, circles and dashed line). Eqn 1 was fitted to the complete dataset, equation fits (lines) and 90% mean prediction confidence intervals (shaded areas) are indicated, (fitted parameters values are presented in Table 1). Specific activities are normalised to $V_{f_{HK}}$. The error bars represent SEM of technical triplicates, with the number of independent experiments: 3, 4, 3, 2 for panels A, B, C and D respectively.

7

A   **B**
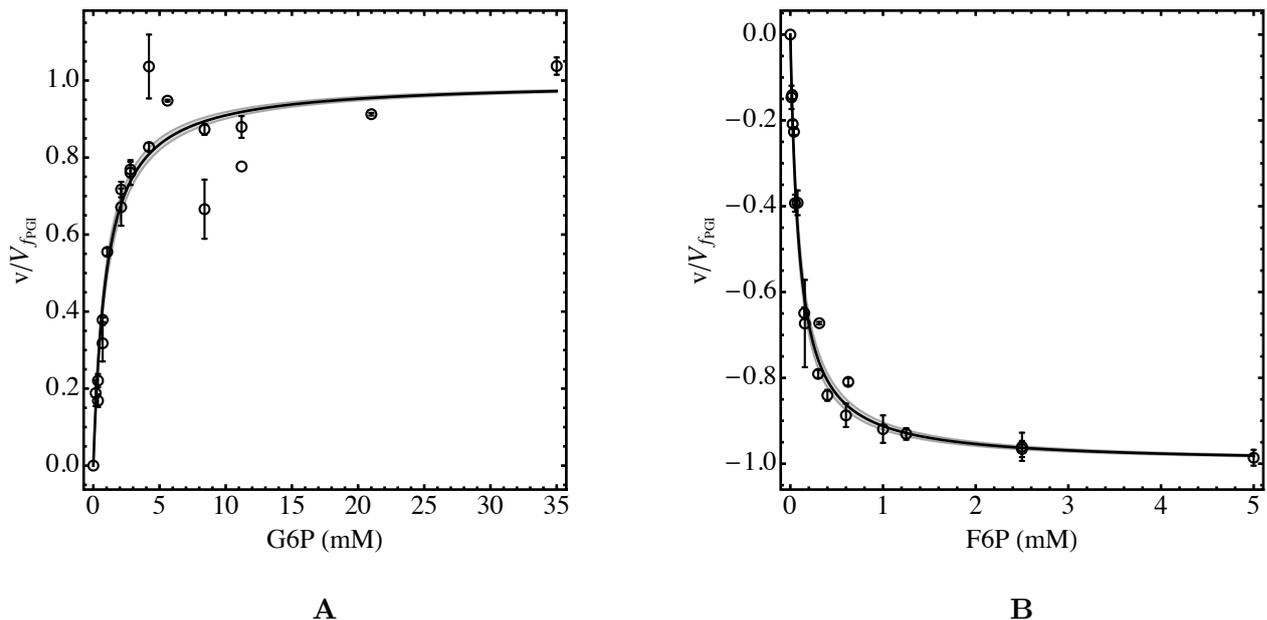
Figure 3: Kinetic characterisation of *P. falciparum* phosphoglucoisomerase. The fit to Eqn 2 and the 90% mean prediction confidence intervals (shaded areas) are shown for the saturation kinetics of PGI with G6P (A) and F6P (B). The data comprise five independent experiments (two for the forward reaction and three for the reverse reaction). Error bars represent SEM of technical triplicates. Specific activities are normalised to $V_{f_{\mathrm{PGI}}}$.

When fitting Eqn. 3 to the experimental data set we observed that K_{ATP} and $K_{i_{ATP}}$ had similar values and could not be estimated independently. We therefore set the values of the two constants as equal.

Table 3: Summary of kinetic parameter values for *P. falciparum* phosphofructokinase. The parameters (± asymptotic standard error) were obtained by fitting Eqn. 3 to the combined kinetic data set (Fig. 4). $V_{f_{PFK}}$ was calculated from the specific activity (measured in cell extracts and expressed per mg total protein) and Eqn. 3, see Fig. 15 and Section 4.2.

Parameter	Fitted Value
$V_{f\mathrm{PFK}}$ (μmol·min^{-1}·mg^{-1})	1.9 [1]± 0.3
K_{ATP} (mM)	0.79 ± 0.04
K_{F6P} (mM)	1.07 ± 0.06
K_{F16BP} (mM)	3.6 ± 0.5
K_{ADP} (mM)	0.7 ± 0.1

[1] Note that this value is highly dependent on the specific rate equation used.

4.1.4 Aldolase

Aldolase catalyses the aldol cleavage of F16BP into GAP and DHAP. The forward reaction for *P. falciparum* aldolase was characterised for its substrate, F16BP (Fig 5), for which it displayed a high affinity, which is in agreement with earlier findings [31], although our K_{F16BP} value was higher (see Table 4). Since we use enzyme linked assays we could not analyse product inhibition for the forward reaction, and neither could we analyse the reverse reaction due to

A

B

C

D
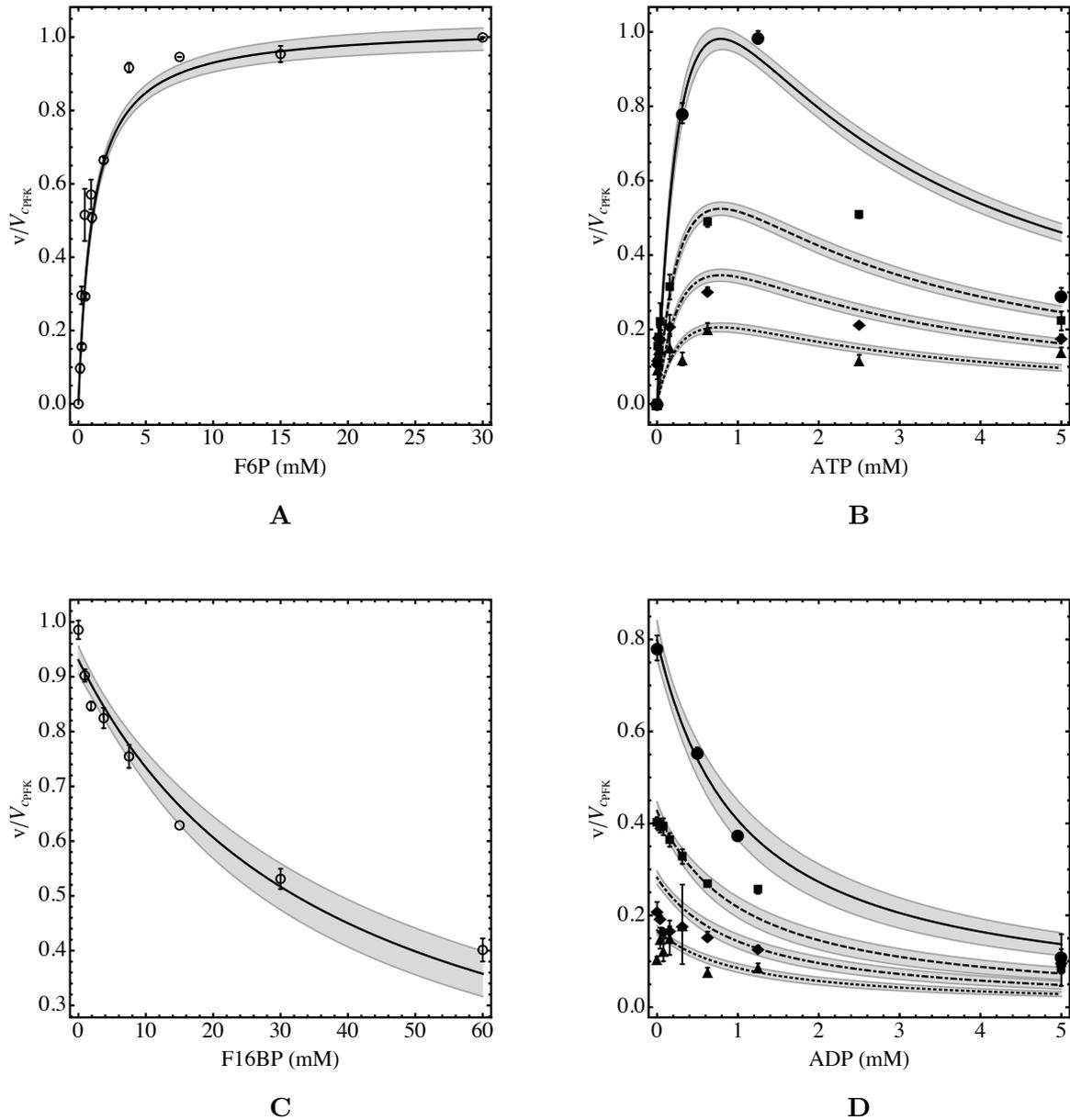
Figure 4: Kinetic characterisation of *P. falciparum* phosphofructokinase. The enzyme was characterised in terms of its substrates: Panel A, F6P (with 1.25 mM ATP) and Panel B, ATP (with 0.25 mM F6P, triangles and dotted line; 0.5 mM F6P, diamonds and dot-dashed line; 1 mM F6P, squares and dashed line; 10 mM F6P, circles and solid line) as well as its products, Panel C, F16BP (with 10 mM F6P and 1.25 mM ATP) and Panel D, ADP (with 0.3125 mM ATP, and varying F6P concentrations: 0.25 mM, triangles and dotted line; 0.5 mM diamonds and dot-dashed line; 1 mM squares and dashed line; 10 mM circles and solid line). Eqn. 3 was fitted simultaneously to the complete dataset, equation fits (lines) and 90% mean prediction confidence intervals (shaded areas) are indicated and fitted parameters values are presented in Table 3. The data are a combination of 8 independent experiments and error bars represent SEM (n >3). Specific activities are normalised to a control rate $V_{c\text{PFK}}$, see Materials and Methods for assay conditions.

9
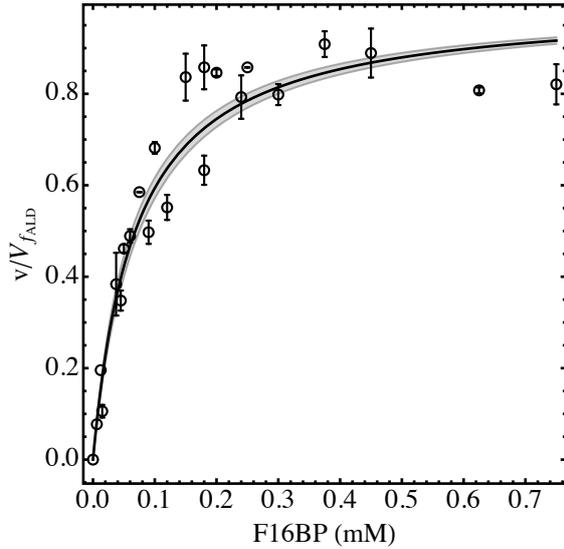
Figure 5: Kinetic characterisation of *P. falciparum* aldolase. Saturation kinetics of ALD with F16BP was fitted to Eqn 4 and the fit and 90% mean prediction confidence intervals (shaded areas) are shown. The data are a combination of two independent experiments. Error bars represent SEM of technical triplicates. Specific activities are normalised to $V_{f_{\text{ALD}}}$.

the absence of good linking reactions. The dissociation constants for the products, K_{GAP} and K_{DHAP} were estimated by averaging the values published for *T. brucei*, *Lactococcus lactis* and human erythrocytes [32–34], listed in Table 4. The kinetic data were described by a random order uni-bi mechanism (Eqn. 4), and the parameters are summarised in Table 4.

$$v\text{ALD} = \frac{V_{f_{\text{ALD}}} \cdot \frac{\text{f16bp}}{K_{\text{F16BP}}} \cdot \left(1 - \frac{\text{dhap} \cdot \text{gap}}{K_{\text{eq}} \cdot \text{f16bp}}\right)}{1 + \frac{\text{dhap}}{K_{\text{DHAP}}} + \frac{\text{f16bp}}{K_{\text{F16BP}}} + \frac{\text{gap}}{K_{\text{GAP}}} + \frac{\text{dhap} \cdot \text{gap}}{K_{\text{DHAP}} \cdot K_{\text{GAP}}}} \tag{4}$$

Table 4: Kinetic parameters for *P. falciparum* ALD. Eqn 4 was fitted to the normalised combined ALD data and the fitted parameters are indicated with asymptotic standard error. The maximal specific activity, $V_{f_{ALD}}$ was determined in separate experiments in cell extracts and is expressed per mg total protein (Fig. 15).

Parameter	Fitted Value	Literature Value	Reference
$V_{f_{ALD}}$ (μmol·min^{-1}·mg^{-1})	0.27 ± 0.01	-	
K_{F16BP} (mM)	0.068 ± 0.004	0.025 ± 0.006	[31]
K_{GAP} (mM)	-	0.05 ± 0.02[1]	[32–34]
K_{DHAP} (mM)	-	0.11 ± 0.09[1]	[32–34]
K_{eq} (mM^{-1})	-	0.090	[35]

[1] Average value of affinities in *T. brucei*, *L. lactis* and human erythrocytes (Mean ± SEM).

4.1.5 Triosephosphate Isomerase

Triosephosphate isomerase (TPI) catalyses the isomerisation of DHAP and GAP. Hyperbolic saturation kinetics were obtained for DHAP and GAP, and for the inhibition by PEP. We used

10

a reversible Michaelis-Menten equation with a competitive inhibitor (Eqn. 5) to fit the kinetic data (Fig. 6). The fitted parameters for the equation are shown in Table 5. The binding constant for GAP is in good agreement with the literature but we measured a lower affinity for DHAP [36, 37]. The inhibition of TPI with PEP has not been described for *P. falciparum* but has been observed in a number of organisms [38, 39] and binding of PEP was shown to be competitive to DHAP and GAP [40].

$$v\text{TPI} = \frac{V_{f_\text{TPI}} \cdot \frac{\text{dhap}}{K_\text{DHAP}} - V_{r_\text{TPI}} \cdot \frac{\text{gap}}{K_\text{GAP}}}{1 + \frac{\text{dhap}}{K_\text{DHAP}} + \frac{\text{gap}}{K_\text{GAP}} + \frac{\text{pep}}{\text{Ki}_\text{PEP}}} \tag{5}$$

Table 5: Kinetic parameters for *P. falciparum* TPI. Eqn 5 was fitted to the normalised combined TPI data and the fitted parameters are indicated with asymptotic standard error. The forward and reverse maximal specific activities ($V_{f_{TPI}}$ and $V_{r_{TPI}}$) were determined in separate experiments in cell extracts and are expressed per mg total protein (Fig. 15). K_{eq} value was calculated with the Haldane relation.

Parameter	Fitted Value	Literature Value	Reference
V_{f_TPI} (μmol·min^{-1}·mg^{-1})	7 ± 1	-	-
V_{r_TPI} (μmol·min^{-1}·mg^{-1})	15 ± 1	-	-
K_GAP (mM)	0.34 ± 0.04	0.4 ± 0.2	[36, 37]
K_DHAP (mM)	2.0 ± 0.3	0.59	[36]
K_{i_PEP} (mM)	0.016 ± 0.002	-	-
K_{eq}	0.08 ± 0.03	0.046	[41]

4.1.6 Glyceraldehyde-3-Phosphate Dehydrogenase

Glyceraldehyde-3-phosphate dehydrogenase (GAPDH) catalyses the conversion of GAP, P$_i$ and NAD$^+$ to 1,3-bisphosphoglycerate (B13PG) and NADH. The enzyme showed hyperbolic saturation kinetics for all reactants and products (Fig. 7). P$_i$ kinetics were not analyzed and a concentration of 10 mM was used in the assays. The K_eq calculated with the Haldane equation is in reasonable agreement with the literature value adjusted for pH = 7.2 (Table 6).

$$v\text{GAPDH} = \frac{V_{f_\text{GAPDH}} \cdot \frac{\text{gap} \cdot \text{nad}}{K_\text{GAP} \cdot K_\text{NAD}} - V_{r_\text{GAPDH}} \cdot \frac{\text{nadh} \cdot \text{b13pg}}{K_\text{NADH} \cdot K_\text{B13PG}}}{\left(1 + \frac{\text{nad}}{K_\text{NAD}} + \frac{\text{nadh}}{K_\text{NADH}}\right)\left(1 + \frac{\text{gap}}{K_\text{GAP}} + \frac{\text{b13pg}}{K_\text{B13PG}}\right)} \tag{6}$$

For fitting of the kinetic data we used Eqn 6, which was derived assuming a random ordered bi-bi mechanism and could describe the experimental data well (Fig. 7). The fitted parameters are summarised in Table 6.

For the B13PG saturation kinetics we produced B13PG in a linked PGK assay which was assumed to be in equilibrium (see Materials and Methods). GAPDH of *P. falciparum* has not been extensively characterised before, but the binding constant for GAP is in good agreement with the literature [42].

4.1.7 Phosphoglycerate kinase

Phosphoglycerate kinase (PGK) catalyses the conversion of B13PG to 3-phosphoglycerate (3PG) with substrate level phosphorylation of ADP to ATP. The *P. falciparum* PGK was characterised

11
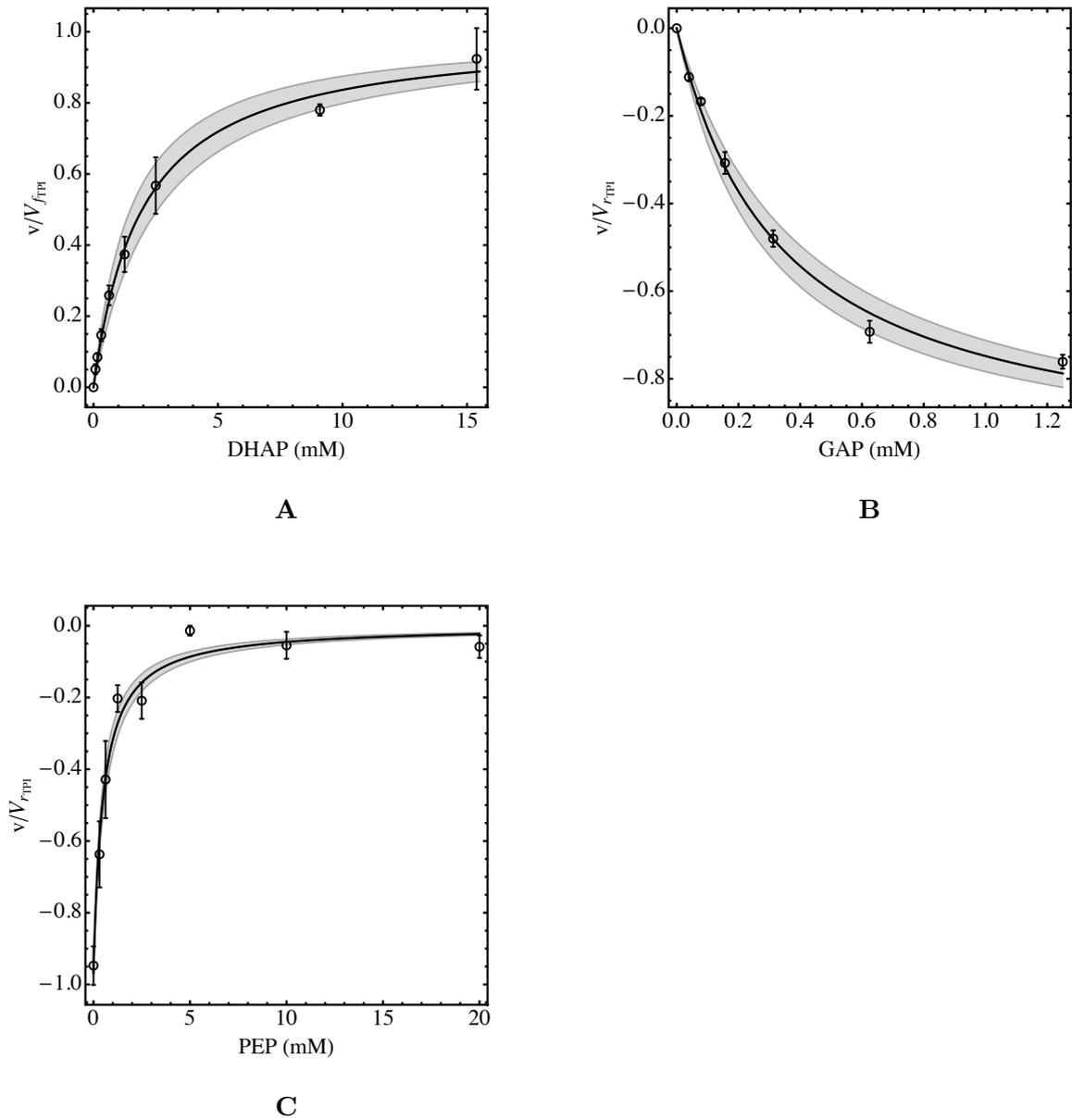
Figure 6: Kinetic characterisation of *P. falciparum* TPI. Saturation kinetics of the enzyme is shown in Panel A for DHAP, in Panel B for GAP. In Panel C the inhibition by PEP (vTPI measured in reverse direction with 10 mM GAP) is shown. The combined data set was fitted to Eqn 5 and the fit and 90% mean prediction confidence intervals (shaded areas) are indicated. The data are a combination of two independent experiments. Error bars represent SEM of technical replicates (n=6). Specific activities are normalised to $V_{f_{\text{TPI}}}$ or $V_{r_{\text{TPI}}}$ for the forward or reverse rates respectively.

in the reverse direction, with saturation curves for ATP and 3PG, and inhibition by ADP (Fig. 8). For the binding constant of B13PG (K_{B13PG}) we used a literature value of 0.013 mM [44]. The kinetic data (Fig. 8) were described by a random order bi-bi mechanism (Eqn. 7) with
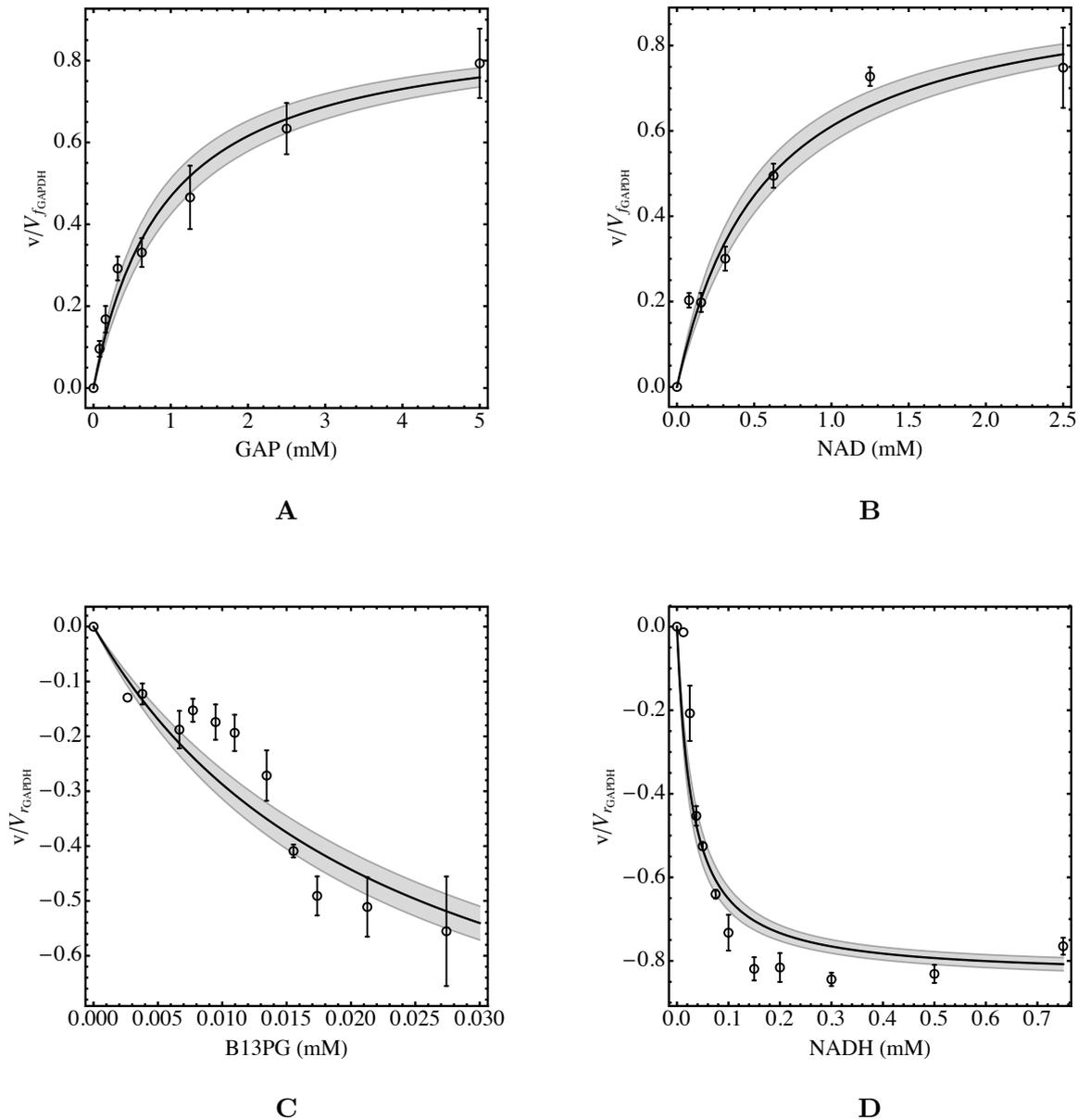
Figure 7: Kinetic characterisation of *P. falciparum* GAPDH. Saturation of the enzyme is shown in Panel A for GAP (5 mM NAD) and in Panel B for NAD$^+$ (20 mM GAP) in the forward direction and in Panel C for B13PG (0.8 mM NADH) and in Panel D for NADH (0.12 mM B13PG) in the reverse direction. Eqn 6 was fitted to the complete dataset, fits and 90% mean prediction confidence intervals (shaded areas) are shown, (fitted parameters values are presented in Table 6). The error bars represent SEM of technical triplicates of 2 independent experiments. B13PG is not commercially available and we calculated equilibrium concentrations for B13PG produced in a linked assay with saturating concentrations of PGK. Specific activities are normalised to $V_{f_{\text{GAPDH}}}$ or $V_{r_{\text{GAPDH}}}$ for the forward or reverse rates respectively.

Table 6: Kinetic parameters for *P. falciparum* GAPDH. Eqn 6 was fitted to the normalised combined GAPDH data and the fitted parameters are indicated with asymptotic standard error. The forward and reverse maximal specific activities ($V_{f_{GAPDH}}$ and $V_{r_{GAPDH}}$) were determined in separate experiments in cell extracts and are expressed per mg total protein (Fig. 15). K_{eq} was calculated for 10 mM phosphate concentration and a pH of 7.2.

Parameter	Fitted Value	Literature Value	Reference
$V_{f_{\text{GAPDH}}}$ (μmol·min^{-1}·mg^{-1})	3.1 ± 0.2	-	-
$V_{r_{\text{GAPDH}}}$ (μmol·min^{-1}·mg^{-1})	1.2 ± 0.3	-	-
K_{GAP} (mM)	0.9 ± 0.1	1.0	[42]
K_{B13PG} (mM)	0.024 ± 0.002	-	-
K_{NAD} (mM)	0.57 ± 0.06	-	-
K_{NADH} (mM)	0.029 ± 0.004	-	-
K_{eq} (mM)	0.0035	0.0089	[43]

Table 7: Kinetic parameters for *P. falciparum* PGK. Eqn 7 was fitted to the normalised combined PGK data and the fitted parameters are indicated with asymptotic standard error. The reverse maximal specific activity $V_{r_{PGK}}$ was measured in separate experiments in cell extracts and is expressed per mg total protein. $V_{f_{\text{PGK}}}$ was calculated using the Haldane relationship.

Parameter	Fitted Value	Literature Value	Reference
$V_{r_{\text{PGK}}}$ (μmol·min^{-1}·mg^{-1})	1.7 ± 0.2	-	
$V_{f_{\text{PGK}}}$ (μmol·min^{-1}·mg^{-1})	30	-	
K_{ADP} (mM)	0.15 ± 0.01	0.30^{1}	[44]
K_{ATP} (mM)	0.77 ± 0.05	0.68^{1}, 0.63^{2}	[44], [45]
K_{3PG} (mM)	0.27 ± 0.02	0.17^{1}, 0.52^{2}	[44], [45]
K_{B13PG} (mM)	-	0.013^{1}	[44]
K_{eq}	-	3200	[46]

^{1} Determined for PGK-deficient erythrocytes infected with *P. falciparum*.

^{2} Determined for recombinant *P. falciparum* PGK.

fitted parameters as given in Table 7.

$$v\text{PGK} = \frac{V_{r_{\text{PGK}}} \cdot \frac{\text{3pg·atp}}{K_{\text{3PG}} \cdot K_{\text{ATP}}} \cdot \left(\frac{\text{adp·b13pg} \cdot K_{\text{eq}}}{\text{atp·3pg}} - 1 \right)}{\left(1 + \frac{\text{adp}}{K_{\text{ADP}}} + \frac{\text{atp}}{K_{\text{ATP}}} \right) \left(1 + \frac{\text{b13pg}}{K_{\text{B13PG}}} + \frac{\text{3pg}}{K_{\text{3PG}}} \right)} \tag{7}$$

Since we measured the PGK in reverse direction we have expressed the $V_{f_{PGK}}$ in terms of $V_{r_{PGK}}$, the dissociation constants and K_{eq} as derived from the Haldane relation.

Two isoenzymes of PGK have been isolated from *P. falciparum* [8], but the role of these isoenzymes and their expression profiles during the different life stages are not known. The kinetic parameters determined here are weighed averages of both isoenzymes. The kinetic parameters determined by us are in fair agreement with published values, although we obtained a higher affinity for ADP.

4.1.8   Phosphoglycerate Mutase

Phosphoglycerate mutase (PGM) catalyses the conversion of 3PG to 2PG. Hyperbolic saturation kinetics were obtained for 3PG and 2PG. We used a reversible Michaelis-Menten equation (Eqn.

A

B

C
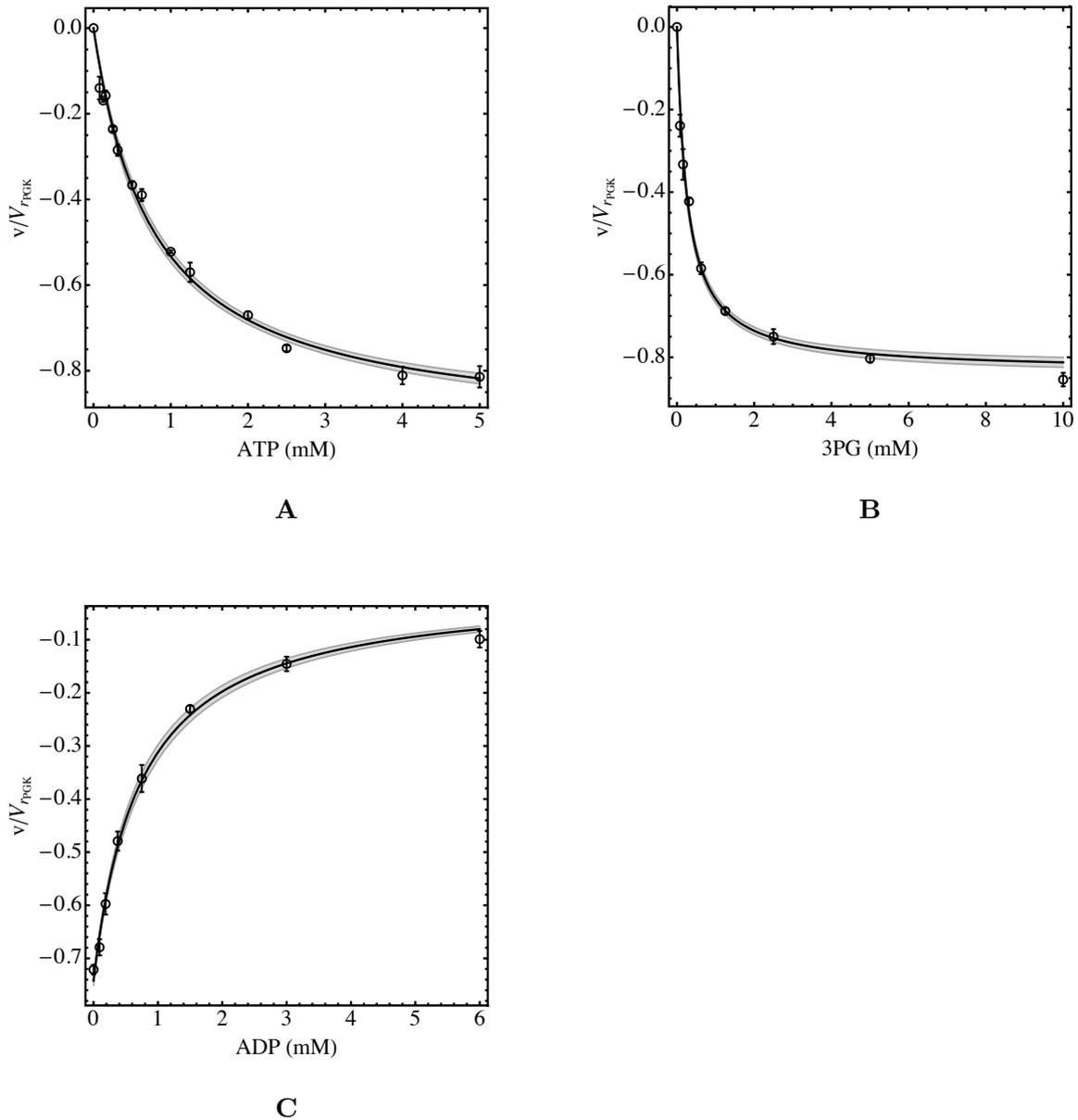
Figure 8: Kinetic characterisation of *P. falciparum* PGK. The reaction was measured in the reverse direction, and saturation of the enzyme with ATP (A, 5 mM 3PG) and 3PG (B, 4 mM ATP) and inhibition by ADP (C, 4 mM 3PG, and 3 mM ATP) is shown. Eqn 7 was fitted to the complete dataset, fits and 90% mean prediction confidence intervals (shaded areas) are shown, (fitted parameters values are presented in Table 7). The error bars represent SEM of technical triplicates, of 2 independent experiments. The specific activities are normalised to $V_{r_{\mathrm{PGK}}}$.
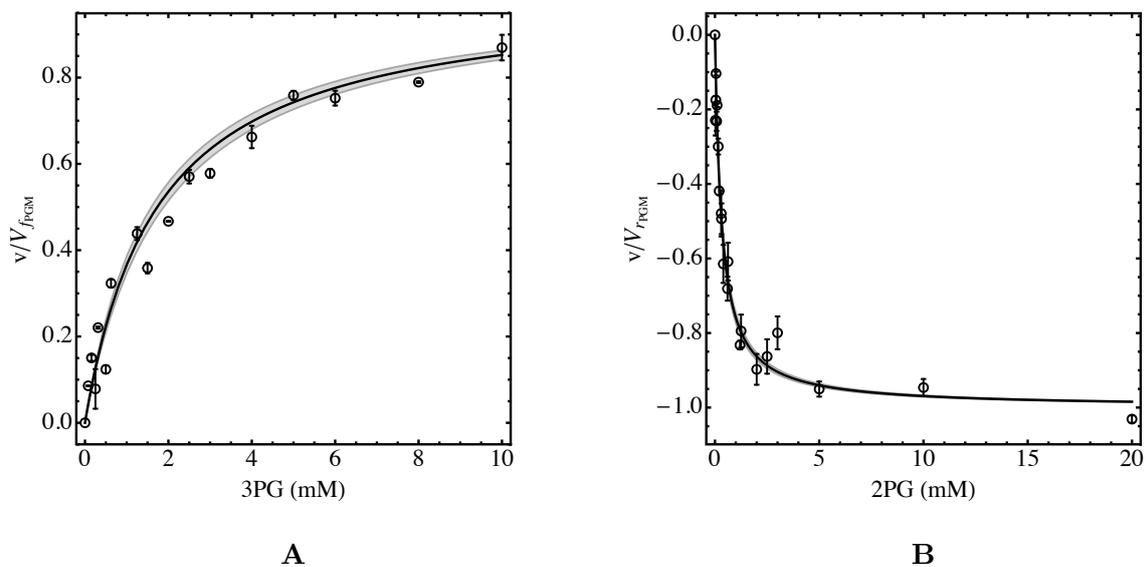
Figure 9: Kinetic characterisation of *P. falciparum* PGM. Saturation kinetics of the enzyme with 3PG (A) and 2PG (B) was fitted to Eqn 8 and the fit and 90% mean prediction confidence intervals (shaded areas) are shown. The data are a combination of two independent experiments. Error bars represent SEM of technical triplicates. The specific activities are normalised to $V_{f_{PGM}}$ or $V_{r_{PGM}}$ for the forward or reverse rates respectively.

8) to fit the kinetic data. The parameterised rate equation described the data set well (Fig. 9), although our binding constants were higher than published values (Table 8).

$$v\text{PGM} = \frac{V_{f_{PGM}} \cdot \frac{3\text{pg}}{K_{3PG}} - V_{r_{PGM}} \cdot \frac{2\text{pg}}{K_{2PG}}}{1 + \frac{2\text{pg}}{K_{2PG}} + \frac{3\text{pg}}{K_{3PG}}} \tag{8}$$

4.1.9   Enolase

Enolase (ENO) catalyses the conversion of 2PG to phosphoenolpyruvate (PEP). Hyperbolic saturation kinetics were obtained for 2PG and PEP. A reversible Michaelis-Menten equation (Eqn. 9) was fitted to the kinetic data (Fig. 10), resulting in the parameters given in Table 9.

Table 8: Kinetic parameters for *P. falciparum* PGM. Eqn 8 was fitted to the normalised combined PGM data and the fitted parameters are indicated with asymptotic standard error. The forward and reverse maximal specific activities ($V_{f_{PGM}}$ and $V_{r_{PGM}}$) were determined in separate experiments in cell extracts and are expressed per mg total protein (Fig. 15).

Parameter	Fitted Value	Literature Value	Reference
$V_{f_{PGM}}$ (μmol·min^{-1}·mg^{-1})	0.87 ± 0.09	-	-
$V_{r_{PGM}}$ (μmol·min^{-1}·mg^{-1})	0.4 ± 0.1	-	-
K_{3PG} (mM)	1.7 ± 0.1	0.85	[47]
K_{2PG} (mM)	0.32 ± 0.02	0.041	[47]
K_{eq}	0.14 - 0.45[1]	0.10	[35]

[1] Estimated with the Haldane relationship for the experimental error range of the parameters.

16

A **B**
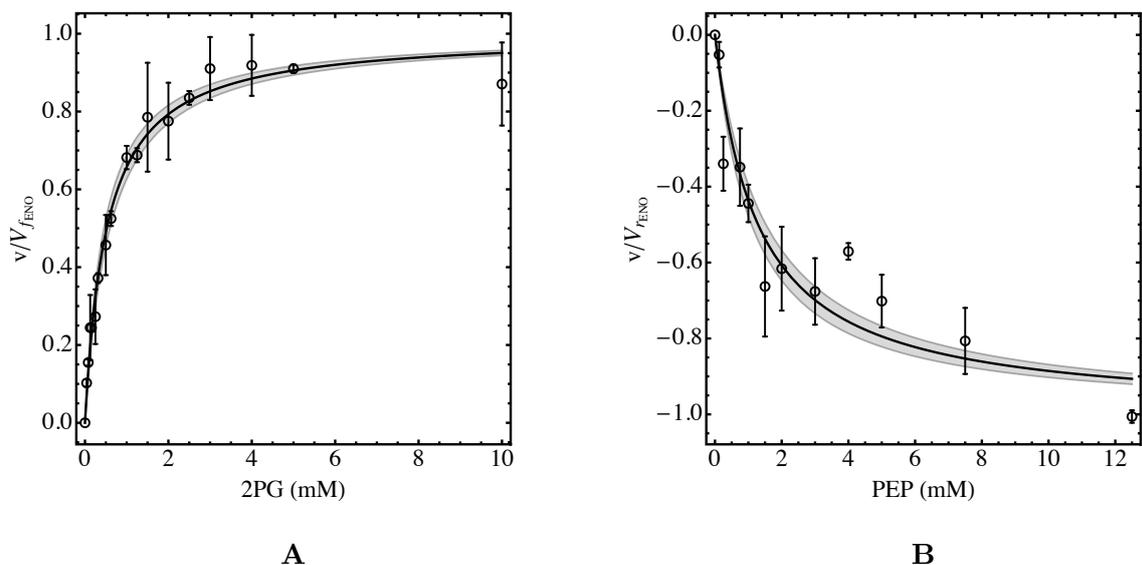
Figure 10: Kinetic characterisation of *P. falciparum* ENO. Saturation kinetics of the enzyme is shown in Panel A for 2PG and in Panel B for PEP. The data was fitted to Eqn 9 and the fit and 90% mean prediction confidence intervals (shaded areas) are indicated. The data are a combination of two independent experiments. Error bars represent SEM of technical triplicates. The specific activities are normalised to $V_{f_{\mathrm{ENO}}}$ or $V_{r_{\mathrm{ENO}}}$ for the forward or reverse rates respectively.

$$v\mathrm{ENO} = \frac{V_{f_{\mathrm{ENO}}}\frac{2\mathrm{pg}}{K_{2\mathrm{PG}}} - V_{r_{\mathrm{ENO}}}\cdot\frac{\mathrm{pep}}{K_{\mathrm{PEP}}}}{1 + \frac{2\mathrm{pg}}{K_{2\mathrm{PG}}} + \frac{\mathrm{pep}}{K_{\mathrm{PEP}}}} \tag{9}$$

The affinities for PEP and 2PG determined in this work are lower than determined by Pal-Bhowmick *et al.*, (see Table 9), for recombinantly expressed purified enzyme [48]. Although these literature values were determined at optimal pH for the enzyme (7.4) and 20 °C, while we measured at physiological temperature and pH values (37 °C and 7.2), it is unlikely that these relatively small differences in conditions would cause a significant effect on the affinity of ENO for 2PG and PEP.

Table 9: Kinetic parameters for *P. falciparum* ENO. Eqn 9 was fitted to the normalised combined ENO data and the fitted parameters are indicated with asymptotic standard error. The forward and reverse maximal specific activities ($V_{f_{ENO}}$ and $V_{r_{ENO}}$) were determined in separate experiments in cell extracts and are expressed per mg total protein (Fig. 15).

Parameter	Fitted Value	Literature Value	Reference
$V_{f_{\mathrm{ENO}}}$ (μmol·min^{-1}·mg^{-1})	1.3 ± 0.4	-	-
$V_{r_{\mathrm{ENO}}}$ (μmol·min^{-1}·mg^{-1})	0.9 ± 0.4	-	-
$K_{2\mathrm{PG}}$ (mM)	0.52 ± 0.04	0.041 ± 0.004	[48]
K_{PEP} (mM)	1.3 ± 0.1	0.25 ± 0.03	[48]
K_{eq}	1.8 - 9.6[1]	4.6	[35]

[1] Estimated with the Haldane relationship for the experimental error range of the parameters.

17

4.1.10 Pyruvate Kinase

Pyruvate kinase (PK) catalyses the conversion of PEP to pyruvate (PYR) with substrate level phosphorylation of ADP to ATP. The *P. falciparum* PK was characterised in the forward direction, with saturation curves for PEP and ADP, and inhibition by PYR and ATP. From the saturation curves (Fig. 11) it is apparent that the PK is under kinetic regulation, inhibited by both of its substrates at higher concentrations and inhibited cooperatively by its product ATP.

We used a random order bi-bi irreversible Monod-Wyman-Changeux rate equation to model the PK reaction. It was assumed that the R and T conformations have equal affinities for the substrates ADP and PEP, but that neither conformation binds the products ATP and PYR to an appreciable extent at the active site. Finally, two additional independent allosteric sites exist for the ADP/ATP pair and the PEP/PYR pair to which they bind with infinite cooperativity (all-or-none). The enzyme is assumed to be tetrameric (n=4). These assumptions yield Eqn. 10 that could describe the kinetic data well (Fig. 11), with fitted parameters as given in Table 10.

$$v\text{PK} = \left(\frac{V_{f\text{PK}} \cdot \frac{\text{adp}}{K_{\text{ADP}}} \cdot \frac{\text{pep}}{K_{\text{PEP}}} \cdot (1 + \frac{\text{adp}}{K_{\text{ADP}}})^{n-1} \cdot (1 + \frac{\text{pep}}{K_{\text{PEP}}})^{n-1}}{(1 + \frac{\text{adp}}{K_{\text{ADP}}})^n \cdot (1 + \frac{\text{pep}}{K_{\text{PEP}}})^n} \right) \cdot \left(\frac{1}{1 + L} \right) \qquad (10)$$

$$L = L_0 \left(1 + \left(\frac{\text{adp}}{K_{i_{\text{ADP}}}} + \frac{\text{atp}}{K_{i_{\text{ATP}}}} \right)^n \right) \cdot \left(1 + \left(\frac{\text{pyr}}{K_{i_{\text{PYR}}}} + \frac{\text{pep}}{K_{i_{\text{PEP}}}} \right)^n \right)$$

Table 10: Kinetic parameters for *P. falciparum* PK. Eqn 10 was fitted to the normalised combined PK data and the fitted parameters are indicated with asymptotic standard error. The forward maximal specific activities ($V_{f_{PK}}$ was determined in separate experiments in cell extracts and is expressed per mg total protein, Fig. 15).

Parameter	Fitted Value	Literature	Reference
$V_{f\text{PK}}$ (μmol·min^{-1}·mg^{-1})	3.6 ± 0.2		
K_{ADP} (mM)	0.32 ± 0.05	0.13 ± 0.04	[49]
K_{PEP} (mM)	0.41 ± 0.05	0.19 ± 0.03	[49]
$K_{i_{\text{Pyr}}}$ (mM)	105 ± 12	-	-
$K_{i_{\text{ATP}}}$ (mM)	1.8 ± 0.2	-	-
$K_{i_{\text{ADP}}}$ (mM)	2.0 ± 0.2	-	-
$K_{i_{\text{PEP}}}$ (mM)	2.9 ± 0.2	-	-
L_0	0.26 ± 0.11	-	-
n	4		

P. falciparum possesses two homotetrameric pyruvate kinases (PK1 and PK2). Both are expressed during the asexual phase [50], but PK1 expression is constant and continually high throughout the asexual phase and thought to be part of glycolysis, whereas PK2 correlates with the expression of lipid synthesis genes. Since the enzyme characterisation is in trophozoite lysates, both isozymes would be present and the kinetic parameters determined here would therefore be weighed averages of both isoenzymes, where it is to be expected that PK1 has a much stronger contribution than PK2 [50]. Chan et al., [49] reported higher affinities for ADP and PEP than were determined by us but it is hard to compare the values as they are dependent on the experimental conditions and the kinetic mechanism assumed for their determination.

A

B

C

D
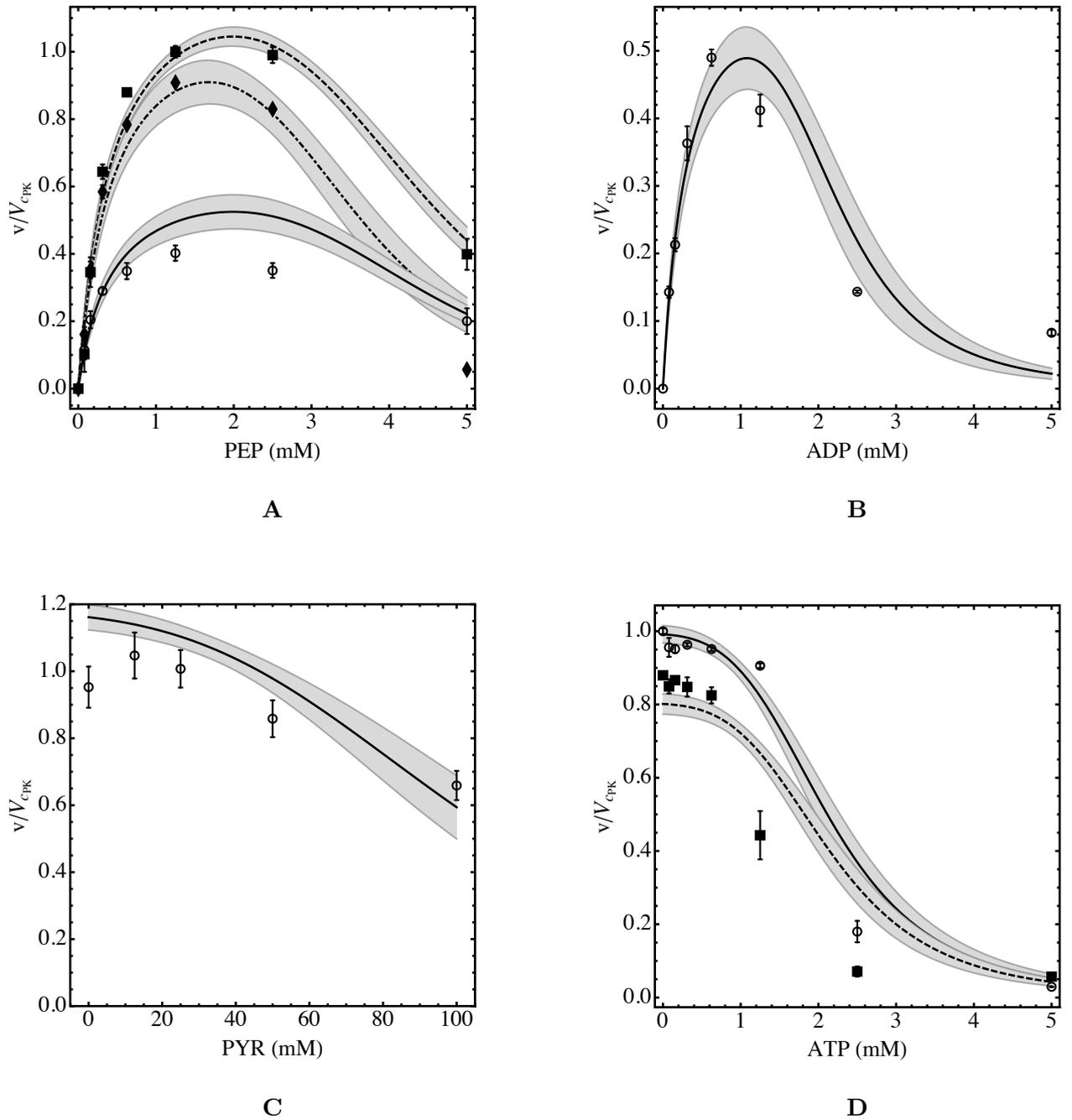
Figure 11: Kinetic characterisation of *P. falciparum* PK. Saturation kinetics of the enzyme is shown in Panel A for PEP (with ADP = 0.156, 0.613 and 2.5 mM respectively for the solid, dashed and dash-dotted lines) and in Panel B for ADP (with 5 mM PEP). Inhibition of the PK is shown in Panel C for PYR (with 1.25 mM PEP and 1.0 mM ADP) and in Panel D for ATP (with 0.625 mM PEP and 0.625 mM ADP). The combined data set was fitted to Eqn 10 and the fit and 90% mean prediction confidence intervals (shaded areas) are indicated. The data are a combination of seven independent experiments. Error bars represent SEM of technical triplicates. The specific activities are normalised to a control rate $V_{c_{PK}}$, see Materials and Methods for PK assay conditions.

4.1.11   Lactate Dehydrogenase

P. falciparum lactate dehydrogenase (LDH) reduces PYR to lactate (LAC) with the concomitant oxidation of NADH to NAD^+. The enzyme was characterised in the forward and reverse direction (Fig. 12). Pyruvate has been shown to inhibit the enzyme at high concentrations with a K_i of 140 mM [51], but this inhibition is negligible at physiological concentrations of pyruvate and thus excluded. The combined kinetic data were described successfully (Fig. 12) with a random order bi-bi mechanism (Eqn. 11) and the fitted parameters are indicated in Table 11. These parameter values are higher than the published values for purified LDH characterised under optimal conditions for the enzyme [51, 52].

$$v\text{LDH} = \frac{V_{f\text{LDH}} \cdot \frac{\text{nadh} \cdot \text{pyr}}{K_{\text{NADH}} \cdot K_{\text{Pyr}}} - V_{r\text{LDH}} \cdot \frac{\text{lac} \cdot \text{nad}}{K_{\text{LAC}} \cdot K_{\text{NAD}}}}{\left(1 + \frac{\text{nad}}{K_{\text{NAD}}} + \frac{\text{nadh}}{K_{\text{NADH}}}\right)\left(1 + \frac{\text{lac}}{K_{\text{LAC}}} + \frac{\text{pyr}}{K_{\text{PYR}}}\right)} \tag{11}$$

We choose to use a generic rate equation, based on a random order binding mechanism for the description of the LDH kinetics, even though the enzyme most likely follows an ordered bi-bi mechanism. The most important reason for this was that the detailed ordered bi-bi mechanism would introduce an additional four parameters (K_i values for each of the substrates and products), which would make the rate equation unnecessary complicated. We have shown before that the kinetic behaviour of an ordered bi-bi mechanism can be described adequately with our generic equation [19]. The dissociation constants that we obtained for PYR and NADH are higher than those published for LDH before, while the K value for LAC is lower and the K value for NAD is close to published values (see Table 11).

Table 11: Kinetic parameters for *P. falciparum* LDH. Eqn 11 was fitted to the normalised combined LDH data and the fitted parameters are indicated with asymptotic standard error. The forward and reverse maximal specific activities ($V_{f_{LDH}}$ and $V_{r_{LDH}}$) were determined in separate experiments in cell extracts and are expressed per mg total protein (Fig. 15).

Parameter	Fitted Value	Literature Value	Reference
$V_{f_{LDH}}$ (μmol·min^{-1}·mg^{-1})	2.5 ± 0.1	-	-
$V_{r_{LDH}}$ (μmol·min^{-1}·mg^{-1})	1.4 ± 0.2	-	-
K_{Pyr} (mM)	0.13 ± 0.01	0.030, 0.055	[51, 52]
K_{NADH} (mM)	0.046 ± 0.003	0.0070, 0.011	[51, 52]
K_{Lac} (mM)	3.6 ± 0.3	12, 47	[51, 52]
K_{NAD} (mM)	0.23 ± 0.02	0.086, 0.18	[51, 52]
K_{eq}	150 - 430[1]	227 - 7194	[53, 54]

[1] Estimated with the Haldane relationship for the experimental error range of the parameters.

4.1.12   Glycerol-3-phosphate dehydrogenase

Glycerol-3-phosphate dehydrogenase (G3PDH) reduces DHAP to glycerol 3-phosphate (G3P) with the concomitant oxidation of NADH to NAD^+. The enzyme activity was determined in the forward direction and the saturation kinetics for DHAP and NADH, and the inhibition by G3P and NAD^+ are shown in Fig. 13. The reaction has a large equilibrium constant (K_{eq}=32600) [55] and we could not assay the enzyme in the reverse direction. A product sensitive, irreversible, random order mechanism was used to derive a rate equation for the G3PDH activity (Eqn. 12). The rate equation was fitted to the combined data set for the estimation of the binding
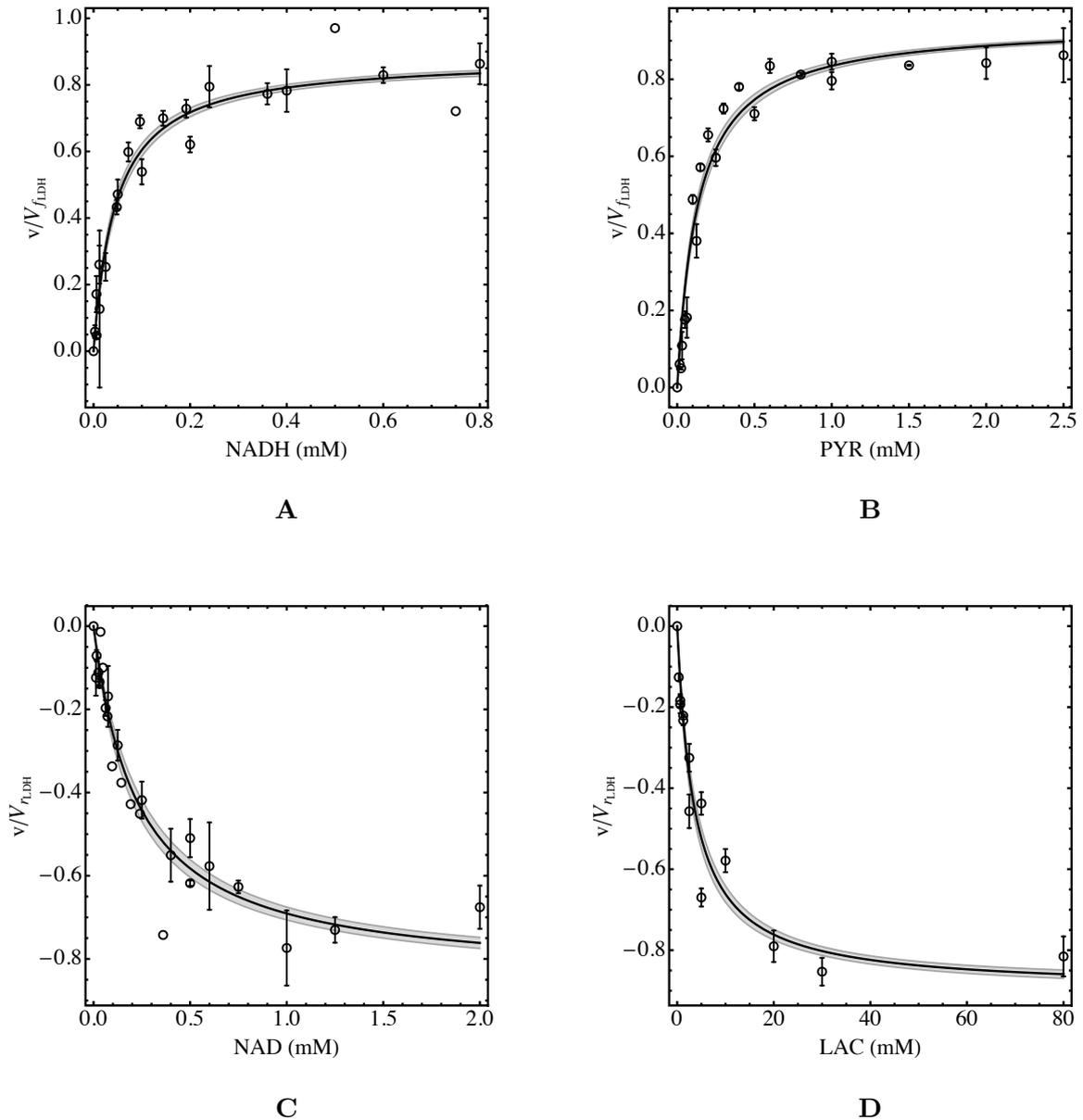
Figure 12: Kinetic characterisation of *P. falciparum* LDH. Saturation kinetics of the enzyme in the forward direction is shown in Panel A for with NADH (with 1 mM PYR) and in Panel B for PYR (with 0.8 mM NADH) and in the reverse direction in Panel C for NAD^+ (with 20 mM LAC) and in Panel D for LAC (with 2 mM NAD^+). The complete data set was fitted to Eqn 11 and the fit and 90% mean prediction confidence intervals (shaded areas) indicated. The data are a combination of three independent experiments. Error bars represent SEM of technical triplicates. The specific activities are normalised to $V_{f_{LDH}}$ or $V_{r_{LDH}}$ for the forward or reverse rates respectively.

constants (Table. 12), the V_{max} value was estimated from specific activity measurements in separate experiments (Fig. 15).

$$v\text{G3PDH} = \frac{V_{f\text{G3PDH}} \cdot \frac{\text{dhap}\cdot\text{nadh}}{K_{\text{DHAP}}\cdot K_{\text{NADH}}}}{\left(1 + \frac{\text{nad}}{K_{\text{NAD}}} + \frac{\text{nadh}}{K_{\text{NADH}}}\right) \cdot \left(1 + \frac{\text{g3p}}{K_{\text{G3P}}} + \frac{\text{dhap}}{K_{\text{DHAP}}}\right)} \tag{12}$$

Table 12: Kinetic parameters for *P. falciparum* G3PDH. Eqn. 12 was fitted to the normalised combined G3PDH data and the fitted parameters are indicated with their asymptotic standard error. The maximal specific activity, $V_{f\text{G3PDH}}$, was obtained from separate experiments in cell extracts and is expressed per mg total protein (Fig. 15).

Parameter	Fitted Value	Reference
$V_{f\text{G3PDH}}$ (μmol·min^{-1}·mg^{-1})	0.06 ± 0.01	
K_{DHAP} (mM)	0.34 ± 0.04	
K_{NADH} (mM)	0.09 ± 0.01	
K_{G3P} (mM)	4 ± 2	
K_{NAD} (mM)	0.5 ± 0.1	
K_{eq}	32600	[55]

The production of glycerol (GLY) by asexual *P. falciparum* was reported by Lian *et al.* [11], but there is still uncertainty about the exact metabolic route via which GLY is produced from G3P [56]. The parasite possesses a glycerol kinase that was suggested to be active predominantly in gametocytes [57], but a role in the a-sexual stages has been shown too [58]. However, the enzyme is suggested to be mostly active in the phosphorylation of GLY to G3P and has not been shown to be reversible. Furthermore, no putative genes for glycerol-3-phosphatase have been identified in the *P. falciparum* genome [59]. However, there is a PGM isozyme, PGM2 [47], which has phosphatase activity and it may be able to utilise G3P as a substrate to produce glycerol. The parasite does posses a aquaglyceroporin and transport of glycerol is probably fast but kinetics in the parasite are not known [60].

Whereas we could detect G3PDH activity in cell extracts of *P. falciparum*, we could not detect glycerol-3-phosphate kinase or phosphatase activity. We simulated the combined dephosphorylation and transport reactions with a single mass-action equation (Eqn. 13), with a k_{GLYtr} of 1 min^{-1} assuming a rapid dephosphorylation of G3P and transport of GLY.

$$v\text{GLYtr} = k_{\text{GLYtr}} \cdot (\text{g3p} - \text{gly}_{\text{ex}}) \tag{13}$$

4.1.13   Glucose transport

In *P. falciparum* GLC first crosses the parasitophorous vacuolar membrane via high-capacity non-selective channels [61–63] after which it is transported across the parasite plasma membrane via a saturable, sodium-independent and stereo-specific hexose transporter [64, 65]. Hexose transporters have been characterised for several *Plasmodium* species [64–69], for *P. falciparum* mostly after expressing the enzyme in *Xenopus laevis* oocytes. In these studies cells are typically incubated for 5 to 20 minutes with GLC to determine uptake. It is hard to interpret GLC transport studies in *P. falciparum* infected erythrocytes [61, 62] in terms of GLC transporter kinetics of the isolated parasite. Saliba *et al.* [70] investigated the uptake of 2-deoxy-D-glucose (2DOG) in isolated parasites but using incubation times greater than 20 s, which may not reflect
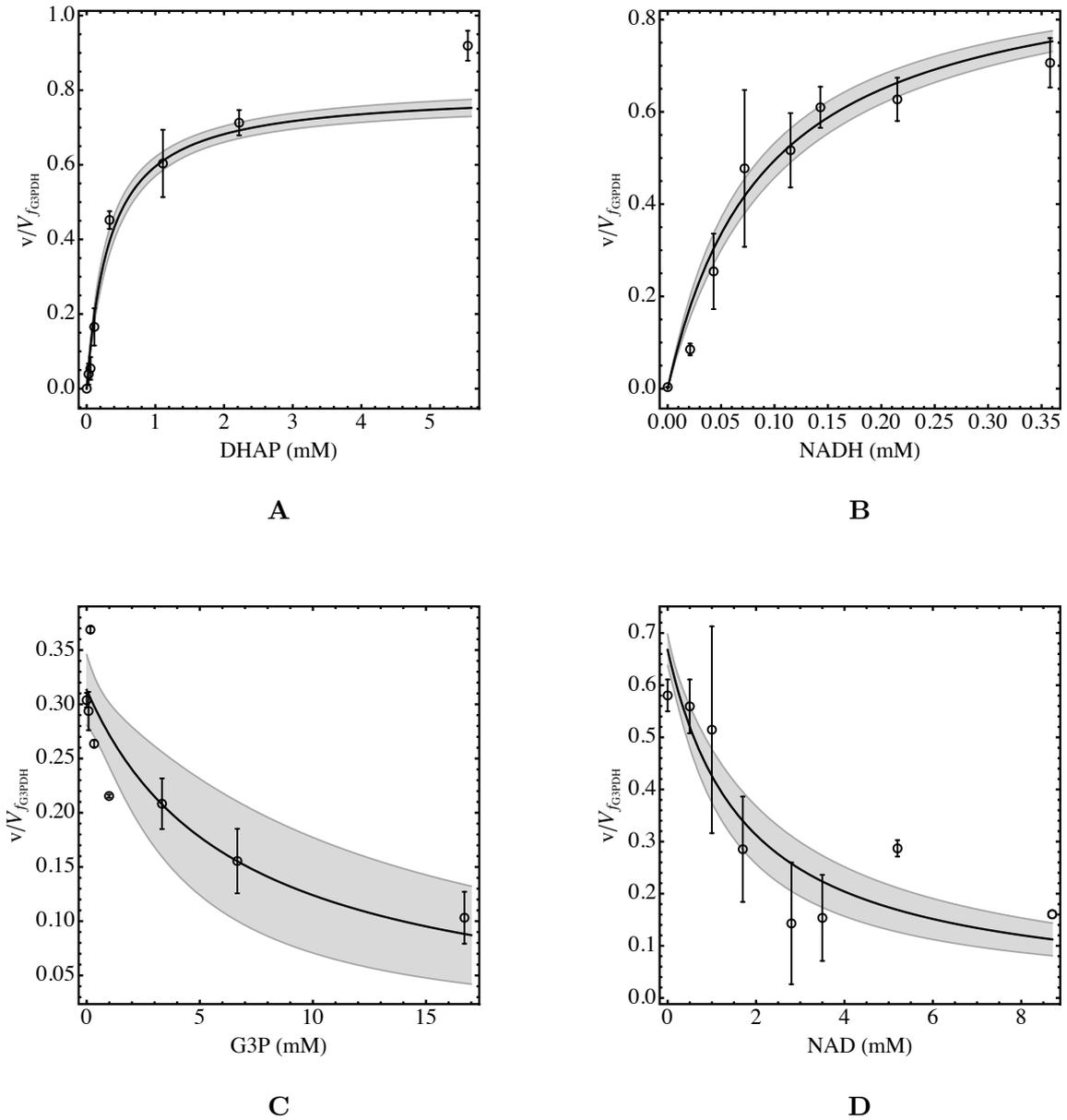
Figure 13: Kinetic characterisation of *P. falciparum* G3PDH. Saturation kinetics of the enzyme is shown in Panel A for DHAP (with 0.358 mM NADH) and in Panel B for NADH (with 5.55 mM DHAP). Product inhibition of the enzyme is shown in Panel C for G3P (with 0.22 mM DHAP and 0.358 mM NADH) and in Panel D for NAD$^+$ (with 5.55 mM DHAP and 0.22 mM NADH). The complete data set was fitted to Eqn 12 and the fit and 90% mean prediction confidence intervals (shaded areas) are shown. The data are a combination of at least two independent experiments. Error bars represent SEM of technical triplicates. The specific activities are normalised to $V_{f_{\text{G3PDH}}}$.

zero-trans influx kinetics. We studied GLC transport in isolated *P. falciparum* trophozoites using short incubation times (0.2 to 20s) of ^{14}C labelled D-GLC (Fig. 14 A).

A

B
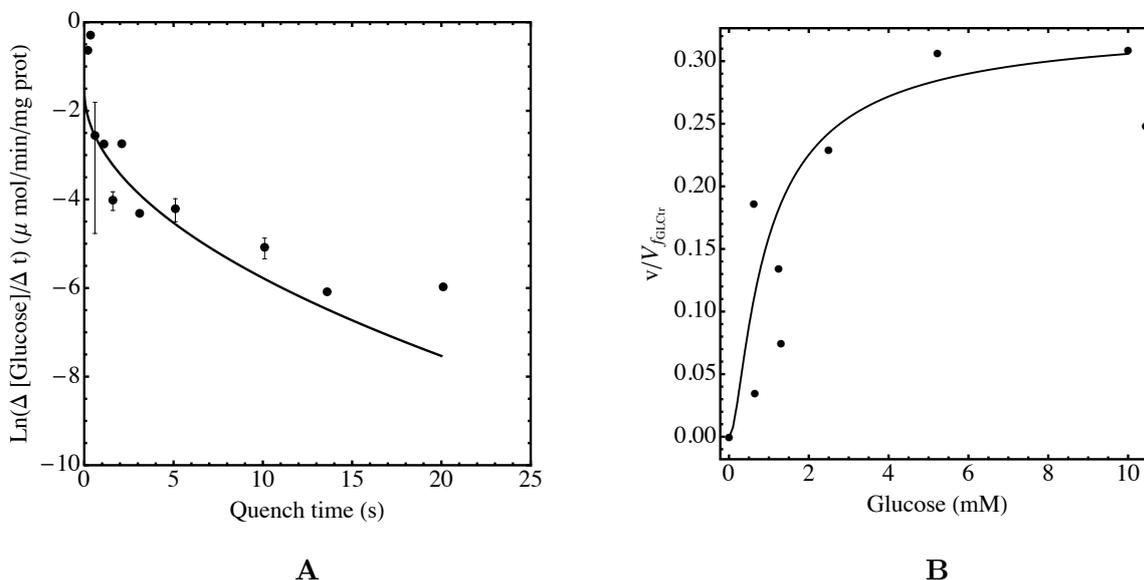
Figure 14: Kinetic characterisation of GLC transport in *P. falciparum*. A quench flow device was used to study uptake of labelled D-GLC into isolated trophozoites. Intracellular ^{14}C label concentration was measured as a function of incubation time and normalised per time and protein concentration (Panel A). The incubation time was varied between 0.2 and 20 s, and the fitted line was used to estimate the specific uptake rate at zero seconds quench time. The data are combined sets of four biological repeats. Error bars represent the mean $\pm$ SEM (n >2). In Panel B, GLC transport as a function of GLC concentration was determined after 2 s incubation time. Activities were normalised to the specific uptake rate at 2 s as determined in (A). Data represent two independent experiments. To estimate the binding constant for GLC (K_{GLC}), the data were fitted to GLC transport rate equation, taking the internal GLC that has accumulated after 2s into account. The fitted line was calculated with Eqn. 14 with parameter values as in Table 13 taking the calculated internal GLC concentrations into account.

We used a quench flow device (see Materials and Methods) to measure uptake rates over a range of incubation times (0.2 - 20 s), which allowed us to extrapolate uptake rates back to a 0 s incubation time which reflect zero-trans influx kinetics. The calculated uptake rates were normalised to total protein and are presented as the concentration increase in labelled GLC divided by the time period of the incubation and plotted on a logarithmic scale for the different incubation times in Fig. 14 A. The uptake rate of labelled GLC decreases strongly with incubation time, already at very small quench times, clearly illustrating the effect of inhibition of transport due to accumulation of internal GLC (Fig. 14 A). There is significant experimental error in the determination of the GLC transport rate, which might reflect lysis of a fraction of the cells during the washing step, and at short incubations times we operate the quench flow device close to its dead-time period of 0.15 s. We estimated lower and upper boundaries for GLC transport rates of 0.1, and 0.5 μmol/min/mg protein and a best fit value 0.21 μmol/min/mg protein (Fig. 14 A), for the zero trans influx GLC transport rate at 5 mM GLC.

To measure GLC transport rates at the short quench times, high concentrations of biomass and labelled GLC were needed and we had to work close to the dead-time of the quench flow device. To study glucose saturation kinetics, we decided to work with a 2 s incubation time and measured transport activities at different GLC concentrations (Fig. 14 B). Clearly at a

2 s incubation time the internal GLC cannot be ignored, and to estimate the affinity of the transporter we fitted Eqn. 14 to the experimental data, taking a 2 s integration of the activity to calculate the internal GLC concentration into account. For the GLC transporter a reversible kinetic equation was used (Eqn. 14) assuming a symmetrical transporter (i.e. $K_{\mathrm{GLC_{in}}} = K_{\mathrm{GLC_{ex}}}$) with an interactive constant α of 0.91 as determined for yeast [71].

$$v\mathrm{GLCtr} = \frac{V_{f_{\mathrm{GLCtr}}} \cdot (\mathrm{glc_{ex}} - \mathrm{glc_{in}})}{K_{\mathrm{GLC}} + \mathrm{glc_{ex}} + \mathrm{glc_{in}} + \alpha \cdot \frac{\mathrm{glc_{in}} \cdot \mathrm{glc_{ex}}}{K_{\mathrm{GLC}}}} \tag{14}$$

Table 13: Summary of the kinetic parameters for *P. falciparum* hexose transport. The *P. falciparum* hexose transporter has been characterised in terms of its maximal specific activity and affinity for GLC. $V_{f_{\mathrm{GLCtr}}}$ was calculated from Fig. 14 (see text for details) and is expressed per mg total protein.

Parameter	Fitted Value	Literature Value	Reference
$V_{f_{\mathrm{GLCtr}}}$ (μmol·min^{-1}·mg^{-1})	0.23	-	-
K_{GLC} (mM)	0.37	0.48, 1.0, 0.97	[64, 65, 68]
α	-	0.91	[71]

In most kinetic analyses of GLC transport in *P. falciparum* the internal GLC concentration is ignored when estimating the affinity for GLC (K_{GLC}). Even in the short time incubations of 2s, as employed in our study there is already a significant build-up of internal GLC, inhibiting GLC transport (see Fig. 14 A). Ignoring internal GLC in the analysis would lead to a significant overestimation of the K_{GLC}. If one would naively fit a Michaelis-Menten equation (i.e. assuming the internal GLC concentration to be zero) to the data set in Fig. 14, this would give a K_m value of 1.8 mM, while we obtained a K_{GLC} value of 0.37 mM with Eqn. 14, taking the internal GLC into account. To calculate the internal glucose built up during the assay we assumed that none of the transported glucose was further metabolised in the 2 s incubation. This assumption leads probably to an overestimation of the internal GLC concentration. However, since the trophozoites are kept on ice without energy source before the assay, the internal ATP concentration is most likely very low, leading to a low HK activity. To test the effect of HK activity on our estimation of K_{GLC}, we simulated the accumulation of glucose during the 2 s uptake experiments with an active HK (eq 1), and a fixed ATP/ADP ratio of 5 and G6P concentration of 1 mM (i.e. physiological conditions). The inclusion of HK in the analyses led to a lower estimated K_{GLC} of 0.23 mM. In our model we used the value of 0.37 mM as estimated in the original analysis since this is closer to the estimated values in the literature.

4.1.14 Lactate and pyruvate transporters

LAC and PYR are secreted from the parasite into the RBC cytosol via a proton symport transporter [10], which shares many characteristics of the monocarboxylate transporter (MCT) family [72]. Elliot *et al.* [10] characterised the *P. falciparum* transporter for LAC and PYR influx as a saturable H$^+$ symport system with a 1:1 stoichiometry. They fitted the transporter kinetics to Eqn. 15, where monocarboxylate refers to either LAC or PYR, and obtained values for the Michaelis-Menten constant (K_m) of 3.8 mM and 16 mM, and maximal specific activity (V_{max}) of 94 and 34 (mmol H$^+$·min^{-1} ·L cell water^{-1}) for LAC and PYR respectively. Eqn. 15 also contains a non-saturable component for which k_d values of 0.80 and 0.11 min^{-1} were fitted for LAC and PYR [10].

$$v\mathrm{MCT} = \frac{V_{max} \cdot [\mathrm{monocarboxylate}]}{K_m + [\mathrm{monocarboxylate}]} + k_d \cdot [\mathrm{monocarboxylate}] \tag{15}$$

A couple of changes needed to be made to Eqn. 15 to be able to use it in our study. Firstly, Elliot *et al.* varied monocarboxylate at a fixed pH gradient ($\text{pH}_{out} = 7.2$ and $\text{pH}_{in} = 7.1$) and protons are not explicit in their rate equations, and secondly they assumed a zero trans-influx transport of the monocarboxylate, i.e. internal concentration of the monocarboxylate is assumed to be zero. These assumptions reduced their rate equation to a simple Michaelis-Menten equation (with an additional non saturable component) for monocarboxylate transport into the parasite. Under physiological conditions LAC and PYR are exported from the parasite into the cytosol of the RBC, and we needed to adapt the rate equation to reflect a reversible process, for which we needed to use an explicit pH gradient to correctly reflect the equilibrium point where: $[\text{monocarboxylate}_{in}] \cdot [\text{H}^+_{in}] = [\text{monocarboxylate}_{ex}] \cdot [\text{H}^+_{ex}]$. The intracellular pH of *P. falciparum* strains has been shown to vary between 7.17 and 7.4 [73–77]. The average pH was taken as 7.2 and the erythrocyte cytosolic pH set to 7.1 [74, 75, 77], which is close to the pH value of the incubations used in the validation experiments. Lactate and pyruvate bind competitively to the monocarboxylate transporter [78]. We assumed a symmetrical transporter, with identical dissociation constants for internal and external LAC and PYR and equal maximal rates for influx and efflux, leading to the following equations:

$$v\text{LACtr} = \frac{V_{\text{LACtr}} \cdot \frac{\text{lac}_{\text{in}}}{K_{\text{LAC}}} \left(1 - \frac{10^{\text{-pH}_{ex} \cdot \text{lac}_{\text{ex}}}}{10^{\text{-pH}_{in} \cdot \text{lac}_{\text{in}}}}\right)}{1 + \frac{\text{lac}_{\text{in}}}{K_{\text{LAC}}} + \frac{\text{lac}_{\text{ex}}}{K_{\text{LAC}}} + \frac{\text{pyr}_{\text{in}}}{K_{\text{PYR}}} + \frac{\text{pyr}_{\text{ex}}}{K_{\text{PYR}}}} + k_{d_{LAC}} \cdot \text{lac}_{\text{in}}\left(1 - \frac{10^{\text{-pH}_{ex}} \cdot \text{lac}_{\text{ex}}}{10^{\text{-pH}_{in}} \cdot \text{lac}_{\text{in}}}\right) \quad (16)$$

$$v\text{PYRtr} = \frac{V_{\text{PYRtr}} \cdot \frac{\text{pyr}_{\text{in}}}{K_{\text{PYR}}} \left(1 - \frac{10^{\text{-pH}_{ex} \cdot \text{pyr}_{\text{ex}}}}{10^{\text{-pH}_{in} \cdot \text{pyr}_{\text{in}}}}\right)}{1 + \frac{\text{lac}_{\text{in}}}{K_{\text{LAC}}} + \frac{\text{lac}_{\text{ex}}}{K_{\text{LAC}}} + \frac{\text{pyr}_{\text{in}}}{K_{\text{PYR}}} + \frac{\text{pyr}_{\text{ex}}}{K_{\text{PYR}}}} + k_{d_{PYR}} \cdot \text{pyr}_{\text{in}}\left(1 - \frac{10^{\text{-pH}_{ex}} \cdot \text{pyr}_{\text{ex}}}{10^{\text{-pH}_{in}} \cdot \text{pyr}_{\text{in}}}\right) \quad (17)$$

In addition to changing the kinetic rate equations we also needed to adapt some of the parameter values to convert to the correct units and experimental conditions. Using a cytosolic volume of 4.67 μL cytosol·mg protein^{-1} (see Materials and Methods), the measured V_{max} values for lactate and pyruvate influx [10] were converted to 0.44 and 0.16 μmol·min^{-1} · mg protein^{-1} respectively for LAC and PYR. These rates were determined at an assay temperature of 4 °C, and a much higher rate is expected at 37 °C. Using a temperature coefficient (Q10) value of 2 as a rough estimator we assumed an 8 fold higher V_{max} value for these transporters in our model. A final, small correction was made to the values of V_{max} and k_d to include the directionality of the process. Since we use the physiological direction (i.e. monocarboxylate efflux) as positive direction we had to correct for the difference in pH accross the membrane. Note that V_{max} and k_d as measured by Elliot *et al.* [10] include proton concentration implicitly. We scaled the k_d values to maintain the same relative activity to the V_{max} values as at low temperature, resulting in the following values used in the model: $V_{\text{PYRtr}} = 1.0$ and $V_{\text{LACtr}} = 2.8$ μmol·min^{-1} · mg protein^{-1}, $k_{d_{LAC}} = 0.005$, $k_{d_{PYR}} = 0.0007$ min^{-1}, the binding constants for LAC and PYR were not changed.

4.1.15 ATPase

ATP produced in glycolysis is used in a many different processes in the cell, and it is not possible to experimentally characterise each of these reactions and to include each of them explicitly in our model. Therefore, we define a single "ATPase" reaction, which is described by a Hill equation (Eqn. 18). The intracellular ATP:ADP has been experimentally measured to be between 1 (GLC starved) and 5.7 [73, 79–81]. We fitted V_{ATPase} (see Eqn. 18) to a steady state ATP:ADP ratio of 5 giving a value of 1.75 μmol·min^{-1} · mg protein^{-1} and a K_{ATP} of 4.5 mM. We used a large Hill coefficient of 5 to dynamically buffer the ATP:ADP ratio at 5, reflecting an energised state

of the parasite.

$$v\text{ATPase} = \frac{V_{\text{ATPase}} \cdot \left(\frac{\text{atp}}{K_{\text{ATP}}}\right)^5}{1 + \left(\frac{\text{atp}}{K_{\text{ATP}}}\right)^5} \tag{18}$$

4.2   Maximal Specific Activities

In the preceding sections, specific enzyme activities were normalised to their V_{max} values, i.e. presented as (v/V_{max}). Note that these V_{max} values are extrapolated from specific activities that were determined in cell extracts, and are expressed per mg total protein. Thus, these V_{max} values cannot be compared directly with V_{max} values determined for purified enzymes, since these are expressed per mg pure enzyme protein. Our V_{max} values represent the maximal specific activities of the enzymes in the extract and are dependent on the expression levels of the enzymes.

A significant variation in specific activity of the glycolytic enzymes was observed between extracts and the normalisation of enzyme activity to its V_{max} value, compensates for differences in expression level of the enzymes and makes it possible to compare extracts prepared from different cultures. To get a good estimate of its variability, specific activities were determined for a large number of different trophozoite isolations at saturating or near saturating concentrations of substrate (Fig. 15). These specific activities were extrapolated to V_{max} values by substituting the substrate concentrations that were used in the activity assay into the respective rate equations. For the enzymes that exhibited substrate inhibition (i.e. PFK and PK), the V_{max} value could not be determined via extrapolation but needed to be solved from the rate equation. For these enzymes we have given a control rate (V_c) determined under standard conditions in Fig. 15. The V_{max} value for these enzymes were calculated from the respective rate equations and are listed in the tables for the respective enzyme kinetic parameters.

4.3   Model Construction

The kinetic model for *P. falciparum* glycolysis consists of GLC transport into the parasite, 15 reactions in the parasite and 3 transport reactions for lactate, pyruvate and glycerol. The rate equations and kinetic parameter values were given in the preceding sections, and form the core of the mathematical model. A set of ordinary differential equations (ODEs) for the internal metabolites can be defined in terms of these kinetic rate equations from the known reaction network (Fig. 1).
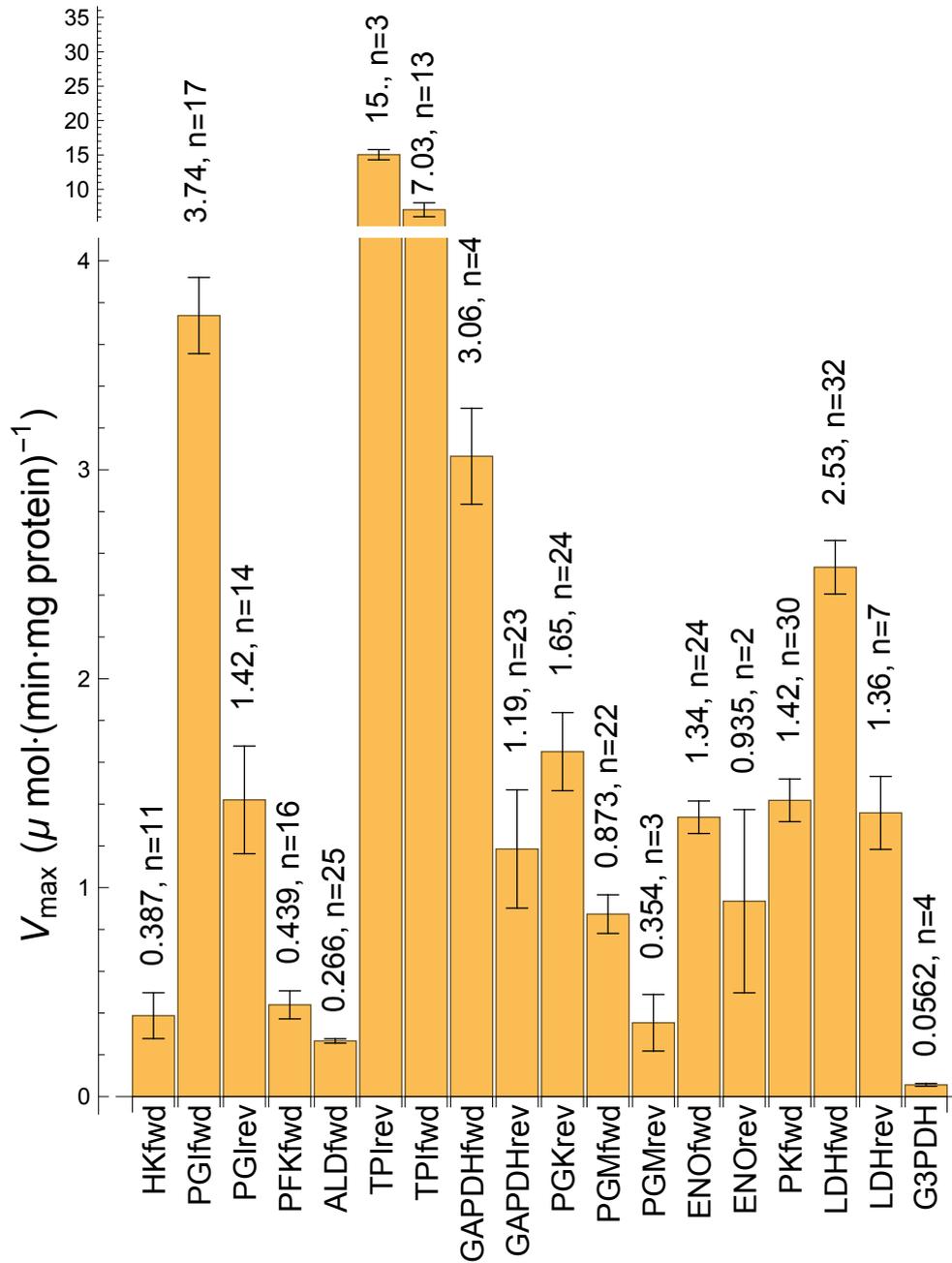
Figure 15: Comparison of the V_{max} values of the *P. falciparum* glycolytic enzymes. The maximal specific activities for each of the glycolytic enzymes of *P. falciparum* were determined from numerous trophozoite isolations to ensure a good representation of the enzyme activities at this stage of parasite development. The enzymes were assayed under standard condition (see Material and Methods) and activities were extrapolated to saturating substrate concentrations to obtain V_{max} values (see text for details). Note that for PFK and PK the control rates are given, see Materials and Methods for assay conditions. The error bars represent SEM, where the number of measurements in different extracts (n) is displayed for each enzyme. The subscript *fwd* and *rev*, refer to the forward and reverse rates respectively.

$$\text{GLC}'[t] = v\text{GLCtr} - v\text{HK} \tag{19}$$
$$\text{G6P}'[t] = v\text{HK} - v\text{PGI} \tag{20}$$
$$\text{F6P}'[t] = v\text{PGI} - v\text{PFK} \tag{21}$$
$$\text{F16BP}'[t] = v\text{PFK} - v\text{ALD} \tag{22}$$
$$\text{DHAP}'[t] = v\text{ALD} - v\text{TPI} - v\text{G3PDH} \tag{23}$$
$$\text{G3P}'[t] = v\text{G3PDH} - v\text{GLYtr} \tag{24}$$
$$\text{GAP}'[t] = v\text{ALD} + v\text{TPI} - v\text{GAPDH} \tag{25}$$
$$\text{B13PG}'[t] = v\text{GAPDH} - v\text{PGK} \tag{26}$$
$$\text{3PG}'[t] = v\text{PGK} - v\text{PGM} \tag{27}$$
$$\text{2PG}'[t] = v\text{PGM} - v\text{ENO} \tag{28}$$
$$\text{PEP}'[t] = v\text{ENO} - v\text{PK} \tag{29}$$
$$\text{PYR}'[t] = v\text{PK} - v\text{LDH} - v\text{PYRtr} \tag{30}$$
$$\text{LAC}'[t] = v\text{LDH} - v\text{LACtr} \tag{31}$$
$$\text{ADP}'[t] = v\text{HK} + v\text{PFK} - v\text{PGK} - v\text{PK} + v\text{ATPase} \tag{32}$$
$$\text{NAD}'[t] = v\text{LDH} - v\text{GAPDH} + v\text{G3PDH} \tag{33}$$

The model variables (metabolites), are defined in terms of fmoles per trophozoite, and time is measured in minutes. Metabolites in the model rate equations are divided by their compartment volume (fL) and the dissociation constants (K values) are given in M. V_{max} values in the model are given in M/min and are multiplied by the compartment volume, which leads to the rate units of fmoles/min per trophozoite, which can be converted to the experimental rates measured in μmoles/min/mg protein, using a cytosolic volume factor of 4.67 μL/mg protein and a trophozoite volume of 28 fL (see Materials and Methods).

For steady state analyses the ODEs were set to zero and solved for metabolite amounts, assuming fixed external concentrations of GLC, LAC, GLY and PYR of respectively 5, 2, 0.15, and 0.2 mM and a total concentration for both the adenosine moiety (ATP + ADP) and the nicotinamide adenosine moiety (NADH + NAD$^+$) of 3 mM. The values for external metabolites are based on plasma concentrations of healthy people and patients with low parasitaemia, (GLC [82, 83], lactate [84, 85], pyruvate [85], glycerol [60, 86]) and we assumed that these concentrations are similar to what Plasmodium experiences inside the RBC, based on the increased permeability of the parasitised erythrocytes to a variety of solutes [87]. These external conditions reflect the conditions in the validation experiments after 30' incubation. For estimation of the moieties we used the following references, adenosine moiety [73, 79, 81], and nicotinamide adenosine moiety [81].

To simulate GLC conversion incubations made with intact trophozoites a second model was constructed for which the set of ODEs was extended with four additional equations for the extracellular metabolites GLC, LAC, PYR and GLY. The ODEs for these extracellular metabolites are equal to the rates of the respective transporters, scaled by the extracellular volume.

The complete model descriptions are given in Supplementary Material, and the models can be simulated and downloaded in SBML format from the JWS Online Model repository: (http://jjj.bio.vu.nl/models/penkler1 and /penkler2).

4.4   Model validation

Two kinetic models were constructed to simulate the experimental conditions: the first with external metabolite concentrations kept constant at the initial concentrations (i.e. to simulate an open system reaching a steady state, penkler1 model), and a second model with the external metabolites as free variables (i.e. simulating a closed system, penkler2 model). Both models are available for simulation on the JWS Online website.

As an initial validation we compared model predictions for substrate consumption and product formation rates with experimental values determined for incubations of intact trophozoites with GLC, (Fig. 16). In addition to LAC, also GLY and PYR were produced by the trophozoites and to be sure that these products were derived from the supplied GLC we used ^{14}C-GLC and obtained a full recovery of label in the measured products. The penkler2 model gives an accurate prediction for substrate consumption and product formation rates, if an initial start-up time of 10 minutes is assumed before the cells reach their maximal rates. Such a slow response of the cells might reflect a de-energised state as they were washed before the incubation with a buffer without GLC. For the model we chose initial concentrations for all metabolites as 0.1 mM, except for external GLC which was set to 5 mM and other external metabolites were set to zero. Conserved moieties ATP + ADP, and NAD$^+$ + NADH were set to 3 mM with initial ratios of 1. The model simulations shown in Fig. 16 were largely independent of the initial conditions of the intracellular metabolites, as long as the initial concentrations were not chosen too low. With strongly de-energized initial conditions (i.e. low concentrations of intermediates and ATP), model simulations show that glycolysis cannot start-up because it lacks ATP for the HK and PFK reactions.

Additional incubations were made with unlabelled GLC and consumption rates for GLC and production rates of LAC, PYR and GLY were determined (see Table 14). In these incubations we also measured intermediate concentrations for G6P, F6P and F16BP after 30 min incubation, assuming that the system has reached a steady state by then (see Table 14). For steady state analysis of the penkler1 model the ODEs were set to zero with fixed concentrations for external metabolites (see Section 4.3). A stable steady state could be calculated for these conditions and fluxes and metabolite concentrations are presented together with the experimentally determined values in Table 14. For the metabolites that could be detected experimentally (G6P, F6P and F16BP) a good agreement between experimental measurement and model prediction was obtained. Both DHAP and GAP could not be detected in our assay, which is in agreement with the model prediction for GAP (0.05 mM), which would be below the detection limit (< 0.1 mM) but is not in agreement with the 1.1 mM prediction of DHAP which should have been detected in the assay.

With these comparisons of model simulations and experimental data we test whether the model can predict the steady state substrate consumption and product formation rates and some of the steady state intermediate concentrations in intact trophozoites on the basis of the kinetics that were measured for the isolated enzymes. The model construction data set consists of initial rate kinetics for each of the enzymes, which is very different from the steady state characteristics of the complete pathway in the intact parasite, which were used as the validation data set. The good agreement between model prediction and experimental validation is quite remarkable given the high dimensionality of the system and the large number of kinetic parameters of the model.

One aspect that automatically follows from the steady state analysis of the mathematical model and which has not been fully appreciated in the literature is the tight coupling of GLY and PYR production. A role in redox metabolism for a G3P-shuttle has been suggested to be important at low oxygen levels [11]. Such a shuttle effectively transfers reducing equivalents from NADH to the electron transport chain via a cytosolic production and subsequent mitochondrial oxidation

of G3P. However this shuttle does not produce glycerol, and it was not clear how *P. falciparum* can produce glycerol and maintain a redox neutral metabolism. In our trophozoite incubations we found a close coupling between PYR and GLY production in a 1:1 ratio, which was predicted by the model and leads to a redox neutral metabolism (see also Fig. 1).

We fully realise that we have tested relatively few of the characteristics of the model and that this certainly does not constitute a full model validation. We are currently preparing a manuscript with further model validation (inhibitor titration of key enzyme) and analyses (sensitivity and metabolic control analysis).

Table 14: Steady state concentrations and fluxes. The steady state metabolite concentrations and fluxes as predicted by the model of *P. falciparum* glycolysis are compared to the experimentally measured values. Metabolites marked with - were not assayed, metabolites marked with n.d. were below the detection limit (< 0.1 mM).

Metabolite	Model (mM)	Experiment (mM)
GLC	1.0	-
G6P	0.97	0.78 ± 0.06
F6P	0.30	0.15 ± 0.01
F16BP	1.4	0.8 ± 0.1
DHAP	1.3	n.d.
G3P	0.56	-
GAP	0.055	n.d.
B13PG	0.001	-
3PG	0.58	-
2PG	0.056	-
PEP	0.061	-
PYR	1.1	-
LAC	2.9	-
ATP	2.5	-
ADP	0.51	-
NADH	0.06	-
NAD$^+$	2.9	-
Flux	Model ($\frac{\mu\text{moles}}{\text{min}\cdot\text{mg protein}}$)	Experiment ($\frac{\mu\text{moles}}{\text{min}\cdot\text{mg protein}}$)
J$_{\text{GLCtr}}$	0.049	0.055 ± 0.004
J$_{\text{LACtr}}$	0.091	0.11 ± 0.01
J$_{\text{GLYtr}}$	0.004	0.005 ± 0.001
J$_{\text{PYRtr}}$	0.004	0.004 ± 0.001

5 General Discussion

Mathematical models are essential tools for the integration of interactions between network components. Such interactions, which can be simple substrate/product links or feedback loops in metabolism, must be taken into account to understand the functional behaviour of these networks [88]. Dependent on the network and on the specific research question, different modelling approaches are used [89]. For large networks, phenomenological models are often used in top-down approaches to describe data sets. These models do not have a strong mechanistic basis but can include many components, and aim for complete descriptions of biological systems. In
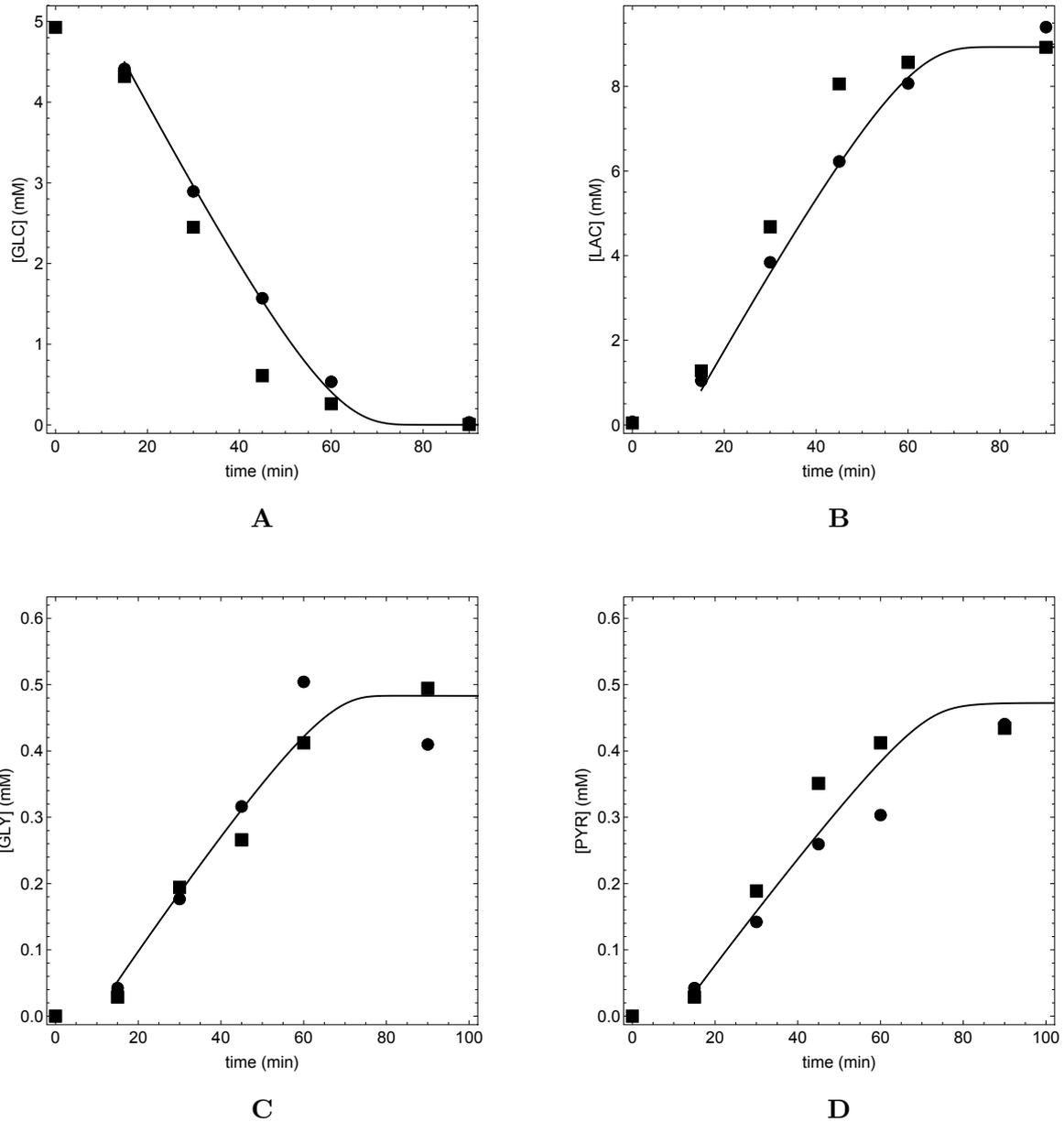
Figure 16: Model predictions of GLC consumption (A) and LAC (B), GLY (C) and PYR production (D). Intact *P. falciparum* trophozoites (cytosolic volume/total volume = 0.106) were incubated with 5 mM GLC (^{14}C labeled) and external metabolite concentrations were determined over a period of 90 minutes. Data points (■ and ●) represent two independent experiments. For the model simulation an initial 10 min startup time is assumed.

contrast to the deductive top-down approach, bottom-up approaches are inductive and aim to predict systems behaviour on the basis of the characteristics of their components. Such models are strong tools for testing of hypotheses, often with core models that capture an essential characteristic. These hypotheses can subsequently be analysed in detailed models to test the actual contribution of the suggested mechanism in models that capture our knowledge of the system more completely. Such Silicon Cell type models should ideally be based on experimental data for the isolated components and not fitted to systemic data sets [14]. If fitting on systemic behaviour is necessary to obtain sufficient information then an independent validation is required.

We have followed a bottom up approach for constructing a detailed kinetic model of *P. falciparum* glycolysis. For the construction we made a kinetic characterisation for each of the glycolytic enzymes and incorporated the resulting rate equations into a detailed kinetic model. In this study, most of the kinetic data were fitted to convenient kinetic equations [18, 19, 90], e.g. simple reversible Michaelis-Menten (uni-uni reactions) or random order (bi-bi reactions). It is not expected that all of the bi-bi reactions follow random order binding, but the kinetic behaviour is well described by these equations. It was not our aim to unravel the kinetic mechanism of each of the glycolytic enzymes, but rather to capture the enzyme kinetics in a biochemically sound rate equation that can be parameterised with a reasonable amount of enzyme kinetic experiments [19, 90]. Thus, although we have not proven that the glycolytic enzymes follow the exact mechanism that underlies our rate equation, we have shown that within physiological ranges of substrates/products and effectors the enzyme rates can adequately be described with our parameterised rate equations. In addition, the mechanistic equations have clearly defined parameters that can be experimentally determined and provide a standard for the comparison of parameters.

For our study we had to characterise the glycolytic enzymes using our own experimental data since most of the enzymes that were characterised before were done so under optimal enzyme conditions, which are not necessarily the same as the conditions under which the enzyme is active in the cell. We tried to mimic the cytosolic conditions in terms of temperature and pH, and measured all enzymes in the same incubation mixture. Five reaction steps were not characterised experimentally in this study: the conversion of glycerol 3-phosphate to GLY and transport of GLY across the membrane; PYR and LAC transport across the membrane; and the ATPase reaction. The GLY production reaction is currently unknown, while for GLY transport an aquaporin has been suggested [60]. We tried and could not detect G3P phosphatase activity or glycerol kinase activity in cell extracts of *P. falciparum*. PYR and LAC transport had been characterised before [10] and we converted the published kinetic rate equation into a form suitable for our model. ATP consuming reactions were grouped into a single reaction and we chose a kinetic form that dynamically buffers the ATP/ADP ratio around 5. The model consists of 88 parameters, of which 11 were taken from the literature and 2 (for the ATPase) were fitted to the physiological ATP/ADP ratio, while all other parameters were experimentally measured in this study. The transport reactions across the parasitic cell membrane were the most difficult to characterise. This is a more general characteristic of transport reactions that do not lead to a chemical conversion, since these reactions are often prone to strong product inhibition and therefore require fast experimentation to acquire so-called "zero-trans kinetics". Working with cells that do not have a sturdy cell-wall adds an additional challenge in preventing lysis when washing the cells to remove extracellular substrate. Obtaining sufficient *P. falciparum* biomass and intact trophozoites, not contaminated with RBC proteins, provided further challenges for extensive enzyme characterisation.

Rate equations that are parameterised in the way described above and more extensively in [14, 91], i.e. based on experimental measurements of the isolated enzymes, are to a large extent independent of the model in which they are used (although limited to the conditions for which

33

they were determined, i.e. pH and temperature). As such these parameterised rate equations can be used in other models, which is important in our hierarchical modelling approach as outlined in the introduction. We plan to merge the validated *P. falciparum* model with a red blood cell model without changing the model parameters when we do so. Despite the more general applicability of models and kinetic rate equations, one must be cautious to directly compare enzyme kinetic parameters, or to use kinetic parameters from the literature, even when they were determined under similar conditions, since reported K_m values might be dependent on the enzyme kinetic mechanism, i.e. the rate equation used to estimate their values. Strictly speaking a K_m value is only defined for the (irreversible, product insensitive) Michaelis-Menten equation. Since the constant is mostly used as a half-saturation constant, i.e. the substrate concentration at which the enzyme shows half-maximal activity, these values can be compared when enzymes show simple hyperbolic saturation curves, but for more complicated kinetic mechanisms, for instance in case of substrate inhibition, it is important to give the rate equation explicitly such that parameter values can be converted to other mechanisms.

To prevent any misinterpretation and to enhance reusability of experimental data, it would be even better to distribute annotated data files for each of the enzyme characterisations. This would allow a user to add complementary data to the data set and/or fit custom equations to the data that might be more suitable for his/her project. For such reuse of (parts of) models, which is essential in modular approaches, where validated models for different parts of metabolism are linked to construct kinetic models of larger systems [92], it is important to use standard description formats and to make data and models publicly available in annotated form.

For this study we have made all experimental data available in RightField annotated spreadsheets [93] using the EuroSEEK platform ([20]) as developed in the FAIRDOM project (http://www.fairdom.org). This investigation (doi:10.15490/seek.1.investigation.56) currently has two studies: "model construction" and "model validation". The model construction study has for each of the enzymes an experimental assay with the kinetic data, a SOP file with the experimental specifications, and a model file that imports the experimental data, specifies the parameterisation methods and produces the manuscript figures (Fig. 17). The model validation study links to the validation experiments and the complete model description file. The model files are available as Mathematica notebooks and as SBML files. In addition, the models can be simulated on JWS online [94], and links to experimental data are available for each of the individual processes via the reaction plot functionality in the model schema. The model can be downloaded in SBML format [95] and is annotated according to MIRIAM standards [96].

The approach we have followed for model construction and validation has been used before for modelling glycolysis in other organisms (e.g. *Trypanosoma brucei* [15], yeast [16] and red blood cells [4]) but these studies relied to a large extent on available data in the literature and experimental data was not made available. In a more recent effort to construct a kinetic model for yeast glycolysis, where the contribution of the different iso-enzymes were taken into account [97], the kinetic data was uploaded to the SABIO-RK database [98], and workflows were used for model construction [99]. However, a user cannot repeat the model construction process that the authors have used. We aimed to make the model construction process completely transparent, making all the experimental data and all the model files that were used for model construction and validation public. The distribution of complete experimental data sets that were used in modelling studies is very rare (for an exception see [39]).

In this first publication we focus on the construction and an initial validation of a detailed kinetic model for glycolysis in the malaria parasite *P. falciparum*; we kinetically characterised 15 enzymes in the pathway, and built a model on the basis of the isolated *in vitro* kinetics and tested the model in its prediction of steady state glycolytic flux and hexose phosphate intermediates in the intact trophozoite stage of the parasite. In a follow up study we will report
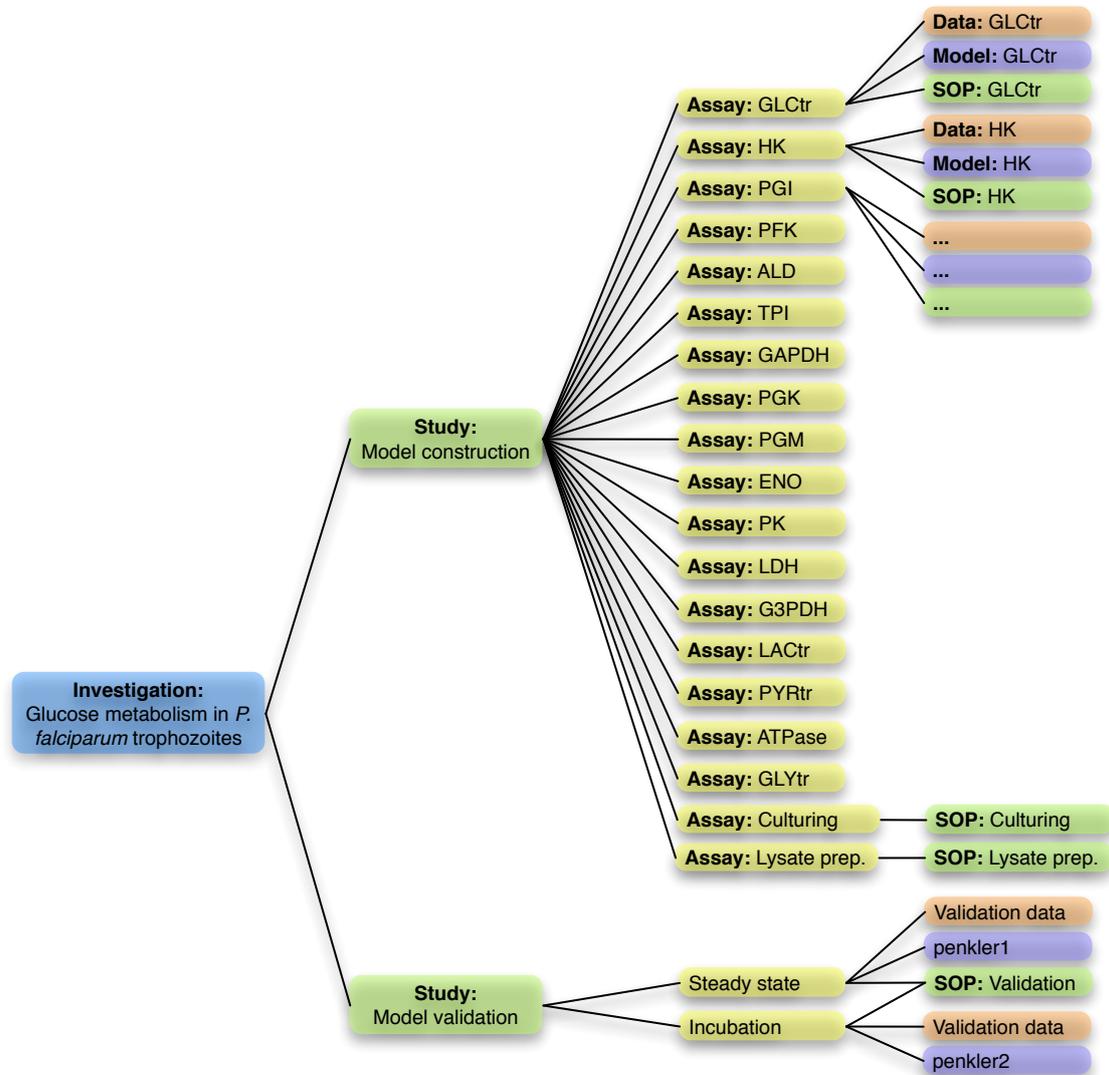
Figure 17: ISA Structure for the "Glucose metabolism in *P. falciparum* trophozoites" investigation in the EuroSEEK platform. The model construction and model validation studies and their linked assays are shown. For each of the reaction steps in the model an experimental data file, SOP document and model file are available. RightField [93] annotated Excel spreadsheets are used for the data files and the "penkler1"and "penkler2" model files are available as MIRIAM annotated [96] SBML files [95].

on additional validation experiments and model analyses.

6   Acknowledgements

7   Materials and Methods

7.1   Culturing and synchronisation of *P. falciparum*

Packed human erythrocytes (A^+, obtained from the Western Province Blood Bank, South Africa) were suspended (3-4 % v/v) in RPMI 1640 culture medium supplemented with Albumax II (0.5% w/v), 22 mM GLC, 25 mM HEPES, 3 mM hypoxanthine, 25 mM sodium bicarbonate and 50 μg/mL gentamycin sulphate, infected with *P. falciparum* D10 and incubated with 3% oxygen, 4% carbon dioxide and 93% nitrogen at 37 °C as described elsewhere [100, 101].

Parasite cultures were synchronised by suspending pelleted infected erythrocytes (750 × g, 3 min), in a 5% w/v sorbitol solution and incubating the suspension at 37°C for 5 min as described by Hoppe *et al.* [102]. Sorbitol treatment leaves the erythrocytes intact, but inactivates all the parasites except the ones in the ring stage.

7.2   Trophozoite Isolation and Lysate Preparation

Approximately 32 hours after invasion, trophozoites were isolated from infected erythrocytes using a saponin lysis protocol [73]. Saponin permeabilises the erythrocyte and parasitophorous vacuolar membranes by interacting with cholesterol found in these membranes [103, 104], but leaves the parasite plasma membrane intact [73, 105], which was verified in trypan blue exclusion tests [105].

After washing isolated trophozoites twice in assay buffer, lysates were prepared by three freeze (liquid nitrogen) - thaw (room temperature) cycles, with a 30 second sonication step in between cycles. After centrifugation (10 000 ×g, 10 min), the supernatant was used for kinetic determinations. Lysates were prepared fresh before enzyme kinetic assays and kept on ice.

7.3   Enzyme Characterisation

Specific activity of the glycolytic enzymes were measured in $NAD(P)H/NAD(P)^+$ linked enzyme assays that were adapted from Teusink *et al.* [16] and measured at 340 nm in 96-well plates (Flat Bottom microplate, Greiner Bio-One, Kremsmünster, Austria) on a spectrophotometer (VarioSkan microplate reader, Thermo Electron Corporation, Waltham, Massachusetts, USA). The same buffer, (20 mM HEPES, 20 mM MgCl, 10 mM KCl and 20 mM NaCl), with an ionic strength close to 0.1 M, was used for all assays, with a pH set to 7.17, matching the cytosolic

pH of *P. falciparum* D10 [74]. All of the linking enzymes were used at a non-limiting, final concentration of 5 U/mL. All reagents and enzymes were obtained from Sigma-Aldrich, St. Louis, Missouri, USA.

For each enzyme the complete experimental data set was fitted with a single rate equation. To compensate for differences in enzyme expression levels in different cell lysates, enzyme activities were normalised to their respective V_{max} values and combined into a single data array for fitting. For fitting we used the NonlinearModelFit function of *Wolfram Mathematica*®, Wolfram Research, Inc. Champaign, Illinois, USA. All data sets and mathematical models of the fitted rate equations for the respective enzymes have been made available in the SEEK platform. Note that for PFK and PK, for which a V_{max} value cannot be estimated via extrapolation due to substrate inhibition, the activities were normalised to standardised substrate concentrations (see the respective enzyme assay methods). The activity measured under these standard conditions was scaled to a V_{max} value after fitting the combined normalised data set.

Hexokinase (HK) was characterised in the forward direction in terms of GLC (0 -10 mM) and ATP (0 - 10 mM) and inhibition by ADP (0 - 20 mM) by linking the production of G6P to the reduction of NADP$^+$ (0.8 mM) via G6PDH. Product inhibition by G6P (0 - 30 mM) was characterised by linking the production of ADP to the oxidation of NADH (0.8 mM) via LDH and PK in the presence of PEP (2 mM).

Phosphoglucoisomerase (PGI) activity was measured via the conversion of G6P (0 - 35 mM) to F6P, which was linked to the oxidation of NADH (0.8 mM) via αGlyPDH, ALD, TPI, PFK in the presence of ATP (2 mM). The reverse isomerisation of F6P (0 - 5 mM) to G6P was linked to reduction of NADP$^+$ (0.8 mM) via G6PDH.

For phosphofructokinase (PFK) activity, the phosphorylation of F6P (0 - 30 mM) by ATP (0 - 5 mM) as well as inhibition by ADP (0 - 5 mM) was linked to the oxidation of NADH (0.8 mM) via αGlyPDH, ALD, TPI. Product inhibition by F16BP (0 - 60 mM) was assayed by linking the production of ADP to the oxidation of NADH (0.8 mM) via LDH, PK in the presence of PEP (2 mM). Since PFK exhibited substrate inhibition, the enzyme rates could not be normalised to maximal specific activity at saturating substrate concentrations. A control rate was determined at 1.25 mM ATP and 1 mM F6P.

Aldolase (ALD) activity was characterised in terms of F16BP saturation (0 - 0.8 mM) by linking the production of DHAP to the oxidation of NADH (0.8 mM) via αGlyPDH in the presence of excess TPI.

Triosephosphate isomerase (TPI) activity was assayed in both directions via αGlyPDH or GAPDH in the presence of NADH (0.8 mM) and GAP (0 - 1.2 mM) or NAD$^+$ (0.8 mM), KH$_2$PO$_4$ (10 mM) and DHAP (0 - 15 mM) respectively.

Glyceraldehyde 3-phosphate dehydrogenase (GAPDH) was assayed with varying substrate concentrations NAD$^+$ (0 - 2.5 mM), GAP (0 - 5 mM) and KH$_2$PO$_4$ (10 mM) and in the reverse direction with NADH (0 - 0.8 mM) and 3PG (0 - 2.5 mM). Since B13PG is not commercially available, 3-phosphoglycerate was varied in a PGK linked assay and equilibrium concentrations for B13PG were calculated by solving the following equation for x: $\frac{(3PG-x)(ATP-x)}{x^2} = K_{eqPGK}$, with 3PG and ATP the initial concentrations in the incubation.

Glycerol 3-phosphate dehydrogenase (G3PDH) activity was assayed by varying substrate con-

centrations NADH (0 - 0.36 mM) and DHAP (0 - 5.55 mM). Product inhibition by G3P (0 - 16.7 mM) in the presence of NADH (0.36 mM) and DHAP (0.22 mM) was measured as well as product inhibition by NAD^+ (0 - 8.4 mM) with DHAP (5.55 mM) and NADH (0.22 mM).

Phosphoglycerate kinase (PGK) activity was assayed in the reverse direction by linking the production of B13PG from ATP (0 - 5 mM) and 3PG (0 - 10 mM) in the presence of ADP (0 - 6 mM) to the oxidation of NADH (0.8 mM) via GAPDH.

Phosphoglycerate mutase (PGM) activity was monitored via the conversion of 3PG (0 - 10 mM) to 2PG, which was linked to the oxidation of NADH (0.8 mM) via LDH, PK, ATP (2 mM) and ENO. The reverse reaction (2PG 0 - 20 mM) was linked to NADH (0.8 mM) oxidation by GAPDH via PGK and ATP (2 mM).

Enolase (ENO) activity was measured via the conversion of 2PG (0 - 10 mM) to PEP, which was linked to NADH oxidation by LDH via PK and ADP (2mM) and in reverse direction via conversion of PEP (0 - 12 mM) to 2PG, which was linked to NADH (0.8 mM) oxidation by GAPDH via PGM, PGK and ATP (2 mM).

Pyruvate kinase (PK) was measured via the conversion of ADP (0 - 5 mM) and PEP (0 - 5 mM) in the presence of ATP (0 - 5 mM) by linking the reaction to NADH oxidation via LDH and in the presence of PYR (0 - 100 mM) by linking the production of ATP to the reduction of $NADP^+$ (0.8 mM) via G6PDH, HK and GLC (10 mM). Since PK exhibited substrate inhibition, the enzyme rates could not be normalised to maximal specific activity at saturating substrate concentrations. A control rate was determined at 1.25 mM PEP and 0.625 mM ADP.

Lactate dehydrogenase (LDH) was characterised via oxidation of NADH (0 - 0.8 mM) in the presence of pyruvate (0 - 2.5 mM) and in the reverse direction via reduction of NAD^+ (0 - 2 mM) in the presence of lactate (0 - 80 mM).

7.4 GLC transport characterisation

GLC uptake rate was measured using a modification of the method by Walsh *et al.* [106, 107]. Isolated trophozoites were washed and suspended in GLC free, modified Ringer buffer (25 mM HEPES, 1 mM $MgCl_2$, 10 mM KCl, 120 mM NaCl, pH 7.1) similar to that described by Wünsch *et al.* [74] and stored on ice. A small aliquot of this suspension was incubated at 37°C in a petri dish and mixed with an equal volume of radiolabelled D-[1-^{14}C] GLC (1 - 20 mM, specific radioactivity 700 to 10 Bq nmol^{-1}, pre-incubated at 37°C) and incubated for 2 s. Uptake was halted by quenching with 10 mL of quench buffer (500 mM GLC, 25 mM HEPES, 1 mM $MgCl_2$, 10 mM KCl, 120 mM NaCl, pH 7.1, incubated at -5°C on a salt-ice mixture). The trophozoites were immediately transferred to a 0.45 μm filter (HVLP, Millipore), covered with a thin layer of filter aid Celite 545, *Sigma-Aldrich*, to prevent clogging) and washed with 10 mL of ice-cold quenching solution, after which the filters were transferred to scintillation vials containing 5 mL scintillation fluid (Flo-Scint III, PerkinElmer, Waltham, Massachusetts, USA). In the negative control experiment the quench fluid was added before the labelled GLC.

In addition, a simple programmable quench-flow device was utilised (see Supplementary Material for a detailed description of the device design, construction and calibration) for GLC uptake experiments with less than 2 s incubation times. For these experiments sample and buffer preparations were identical to the 2 s incubation experiments but now GLC and trophozoites were loaded into separate, temperature (37°C) controlled sample chambers of the quench-flow, and injected through a mixing chamber into a collection vial and at the pre-programmed time the reaction was stopped by injection of the quenching solution.

7.5   Flux and Internal Metabolite Experiments

For the glycolytic flux and metabolite determination experiments, trophozoites were isolated, washed twice and suspended in incubation a modified Ringer buffer (5 or 10 mM GLC, 50 mM HEPES, 1 mM MgCl$_2$, 10 mM KCL, 120 mM NaCl, pH 7.1) similar to that described by Wünsch *et al.*[74]. In this buffer the parasites were able to exclude 0.04% *v/v* trypan blue. Immediately after suspension, two aliquots were taken for cell counting (Improved Neubauer Haemocytometer) and total protein determinations (method of Bradford *et al.* [108]). An intracellular trophozoite volume of 4.67 μL per mg protein was calculated on the basis of cell counts, total protein determination, and a 28 μL volume per trophozoite [109].

External metabolites were determined in two ways i) enzymatically and ii) using a radiolabelled HPLC method with ^{14}C labelled GLC (uniformly labeled and used in a 1:80 ratio with unlabelled glucose) as substrate. For both methods, time point samples of the incubation were centrifuged (5000 $\times$ *g*, 1 min) and the supernatant i) retained for enzymatic determinations or ii) added to acetonitrile (70% *v/v* final) for HPLC determination (see below). For the determination of internal metabolites at specific time intervals, aliquots of the cell suspension were taken and metabolism halted by the addition of 70% *m/v* perchloric acid (12% *m/v* final concentration). Following 1 min sonication and centrifugation (10 min, 20 000x*g*, 4 °C), the supernatant was retained for the enzymatic determination of the glycolytic metabolites. The supernatant was neutralised with 10 M KOH. Samples were stored at -80°C until analysis.

7.6   Enzymatic GLC, Lactate, Pyruvate and Glycerol determinations

Extracellular D-GLC was assayed by linking it to NADP reduction via HK and G6PDH. Samples and standards were incubated at room temperature in HEPES buffer (50 mM, pH 7.5) containing HK (5 U/mL), ATP (0.2 mM), G6PDH (10 U/mL) and NADP$^+$ (0.5 mM). After a 15 minute incubation period the absorbance at 340 nm was measured. Extracellular L-lactate was assayed by using an LDH and NAD$^+$ linked assay. After a 20 min incubation period at room temperature in HEPES buffer (50 mM, pH 7.5) containing LDH (10 U/mL), NAD$^+$ (0.2 mM) and hydrazine (16 μL/mL), samples and standards were measured at 340 nm. Hydrazine binds to pyruvate and thus thermodynamically drives the unfavourable LDH reaction (reverse) to completion. Glycerol was measured using the method developed by Eggstein and Kuhlmann [110]. Glycerol samples and standards were incubated in assay buffer (150 mM HEPES (150 mM), MgSO$_4$ (15 mM), pH 7.5) with glycerol kinase (8.4 U/ mL), PEP (1 mM), NADH (0. 4 mM), ATP (1 mM), pyruvate kinase (3 U/mL) and lactate dehydrogenase (3.6 U/ mL) and the oxidation of NADH after 10 min was measured at 340 nm. Pyruvate samples and standards were incubated in HEPES buffer (50 mM, pH 7.5) containing LDH (10 U/mL) and NADH (0.1 mM) and the absorbance after 10 minutes measured at 340 nm.

7.7   Enzymatic Determination of Metabolites

The intermediates of upper glycolysis (G6P, F6P, F16BP, DHAP and GAP) were all assayed within a single sample (180 μL) by linking the metabolite assays to the reduction of NADP$^+$ via G6PDH or oxidation of NADH via α-glycerolPDH. G6P was determined by adding G6PDH (1U/mL final) and NADP$^+$ (5 mM final). Total change in absorbance at 340 nm was determined upon completion of the reaction. A spike of G6P (20 μM) was added and change in absorbance determined once the reaction was complete. To the same sample, PGI (1U/mL final) was added for assaying F6P and again the total change in absorbance determined. After completion, a 20 μM F6P spike was added to the mixture. In a similar stepwise (sample/spike) manner, DHAP, GAP and FBP were determined via NADH (0.8 mM final) and α-glycerolPDH (1U/mL final,

TPI (1U/mL) and aldolase (1U/mL) respectively. Under these experimental conditions there is a linear dependency between absorbance (340 nm) and metabolite (G6P, F6P and F16BP) concentration (2 - 200 μM). The change in absorbance for the 20 μM intermediate spike was thus used as an internal standard to determine the concentration of each intermediate within the sample. The intermediates of lower glycolysis could not be determined due to high concentrations of lactate and pyruvate in the samples. This prevented the linked determination of PEP and the phosphoglycerates via LDH and NADH. Trophozoite counts and the assumption of a trophozoite cytosolic volume of 28 fL [109] were used to calculate the intracellular concentration of each metabolites.

7.8   GLC, Lactate, Pyruvate and Glycerol HPLC Determinations

The method of Antonio *et al.* [111] was employed to determine the concentrations of the radiolabelled extracellular GLC, lactate, pyruvate and glycerol. Antonio *et al.* [111] did not detect glycerol as it ionises poorly in an ESI (electro-spray ionisation) source. GLC, lactate, pyruvate and glycerol eluted at 13.4, 6.5, 10.1 and 10.4 min respectively. We confirmed that the eluent at 10.4 min was glycerol using enzyme determination assays. Briefly, separation occurred on a ZIC®-HILIC column (150×7.5 mm, 5 μm, 200 Å, SeQuant™, Merck, Darmstadt, Germany) fitted with a guard column (20×2.1mm, 5 μm, SeQuant™, Merck, Darmstadt, Germany) on a HPLC system. The system consists of a SpectraSYSTEM P4000 pump (Thermo Separation™ products, San Jose, CA, USA), a SpectraSYSTEM AS3000 autosampler (Thermo Separation™ products, San Jose, CA, USA) and a Flo-One liquid scintillation spectrophotometer (Radiomatic, Tampa, FL, USA). A flow rate of 1.0 mL/min and an injection volume of 100 μL were used. Separation occurred at room temperature (25°C). Mobile phase A consisted of acetonitrile (0.1% *m/v* formic acid) and mobile phase B of 5 mM ammonium acetate, pH 4 (0.1% *m/v* formic acid). The method was slightly modified by pumping 90% *v/v* A through the system for 1 min, prior to the initiation of the gradient elution profile. The analogue intensity (V) data were integrated and analysed with *Mathematica*®.

7.9   Computational Modelling

All computational analyses were made with *Wolfram Mathematica*® version 10. Parameter estimations for the individual rate equations were performed using the NonlinearModelFit function with either the default method or the NMinimize method, as is indicated in the Mathematica notebooks for the individual reaction steps available on OpenSEEK. The kinetic models were formulated as sets of ordinary differential equations (ODEs) on the basis of known reaction stoichiometry of the Embden-Meyerhof-Parnas pathway. The ODEs were solved using the NDSolve function. Steady state was calculated using the FindRoot function. The numerical simulations were confirmed in Copasi [112]. The models are available as Mathematica notebooks and SBML files, and can be simulated in a browser via JWS Online [94].

References

[1] Menard R, Tavares J, Cockburn I, Markus M, Zavala F, et al. (2013) Looking under the skin: the first steps in malarial infection and immunity. Nat Rev Micro 11: 701–712.

[2] Planche T, Dzeing A, Ngou-Milama E, Kombila M, Stacpoole P (2005) Metabolic complications of severe malaria. Curr Top Microbiol Immunol 295: 105-136.

[3] Mulquiney PJ, Bubb WA, Kuchel PW (1999) Model of 2,3-bisphosphoglycerate metabolism in the human erythrocyte based on detailed enzyme kinetic equations: *in vivo* kinetic characterization of 2,3-bisphosphoglycerate synthase/phosphatase using ^{13}C and ^{31}P NMR. Biochem J 342: 567-580.

[4] Mulquiney P, Kuchel P (1999) Model of 2,3-bisphosphoglycerate metabolism in the human erythrocyte based on detailed enzyme kinetic equations: equations and parameter refinement. Biochem J 342: 581-596.

[5] Hornberg J, Bruggeman F, Bakker B, Westerhoff H (2007) Metabolic control analysis to identify optimal drug targets. Prog Drug Res 64: 171, 173-89.

[6] Sherman IW (1979) Biochemistry of *Plasmodium* (malarial parasites). Microbiol Rev 43: 453-495.

[7] Pattanaik P, Raman J, Balaram H (2002) Perspectives in drug design against malaria. Curr Top Med Chem 2: 483-505.

[8] Sherman I (1998) Carbohydrate metabolism of asexual stages. In: Sherman I, editor, Malaria: Parasite biology, pathogenesis and protection, Washington, D.C.: ASM Press. pp. 135-143.

[9] Olszewski K, Mather M, Morrisey J, Garcia B, Vaidya A, et al. (2010) Branched tricarboxylic acid metabolism in *Plasmodium falciparum*. Nature 466: 774-778.

[10] Elliott JL, Saliba KJ, Kirk K (2001) Transport of lactate and pyruvate in the intraerythrocytic malaria parasite, *Plasmodium falciparum*. Biochem J 355: 733-739.

[11] Lian LY, Al-Helal M, Roslaini A, Fisher N, Bray P, et al. (2009) Glycerol: an unexpected major metabolite of energy metabolism by the human malaria parasite. Malar J 8: 38.

[12] Becker K, Tilley L, Vennerstrom JL, Roberts D, Rogerson S, et al. (2004) Oxidative stress in malaria parasite-infected erythrocytes: host-parasite interactions. Int J Parasitol 34: 163-189.

[13] van Eunen K, Bouwman J, Daran-Lapujade P, Postmus J, Canelas A, et al. (2010) Measuring enzyme activities under standardized *in vivo*-like conditions for systems biology. FEBS J 277: 749 -760.

[14] Snoep J, Westerhoff H (2004) The silicon cell initiative. Current Genomics 5: 687-697.

[15] Bakker BM, Michels PA, Opperdoes FR, Westerhoff HV (1997) Glycolysis in bloodstream form *Trypanosoma brucei* can be understood in terms of the kinetics of the glycolytic enzymes. J Biol Chem 272: 3207-3215.

[16] Teusink B, Passarge J, Reijenga C, Esgalhado E, van der Weijden C, et al. (2000) Can yeast glycolysis be understood in terms of *in vitro* kinetics of the constituent enzymes? testing biochemistry. Eur J Biochem 267: 5313-5329.

[17] Visser D, Heijnen JJ (2003) Dynamic simulation and metabolic re-design of a branched pathway using linlog kinetics. Metabolic Engineering 5: 164 - 176.

[18] Liebermeister W, Klipp E (2006) Bringing metabolic networks to life: convenience rate law and thermodynamic constraints. Theor Biol Med Model 3: 41.

[19] Rohwer J, Hanekom A, Crous C, Snoep J, Hofmeyr J (2006) Evaluation of a simplified generic bi-substrate rate equation for computational systems biology. Syst Biol (Stevenage) 153: 338-341.

[20] Wolstencroft K, Owen S, Preez F, Krebs O, Mueller W, et al. (2011) The seek: A platform for sharing data and models in systems biology. Methods in Enzymology 500: 629-655.

[21] Roth EF, Jr (1987) Malarial parasite hexokinase and hexokinase-dependent glutathione reduction in the *Plasmodium falciparum*-infected human erythrocyte. J Biol Chem 262: 15678-15682.

[22] Boyer PD, Robbins EA (1957) Determination of the equilibrium of the hexokinase reaction and the free energy of hydrolysis of adenosine triphosphate. JBiol Chem 224: 121-135.

[23] Staples J, Suarez R (1997) Honeybee flight muscle phosphoglucose isomerase: matching enzyme capacities to flux requirements at a near-equilibrium reaction. J Exp Biol 200: 1247-1254.

[24] Goldberg R, Tewari Y, Bhat T (2004) Thermodynamics of enzyme-catalyzed reactions-a database for quantitative biochemistry. Bioinformatics 20: 2874-2877.

[25] Srivastava IK, Schmidt M, Grall M, Certa U, Garcia AM, et al. (1992) Identification and purification of glucose phosphate isomerase of *Plasmodium falciparum*. Mol Biochem Parasitol 54: 153-64.

[26] Buckwitz D, Jacobasch G, Gerth C (1990) Phosphofructokinase from *Plasmodium berghei*: a kinetic model of allosteric regulation. Mol Biochem Parasitol 40: 225-232.

[27] Buckwitz D, Jacobasch G, Gerth C (1990) Phosphofructokinase from *Plasmodium berghei*. influence of Mg^{2+}, ATP and Mg^{2+}-complexed ATP. Biochem J 267: 353-357.

[28] Buckwitz D, Jacobasch G, Gerth C, Holzhutter HG, Thamm R (1988) A kinetic model of phosphofructokinase from *Plasmodium berghei*. influence of ATP and fructose-6-phosphate. Mol Biochem Parasitol 27: 225-232.

[29] Buckwitz D, Jacobasch G, Kuckelkorn U, Plonka A, Gerth C (1990) Glucose-6-phosphate dehydrogenase from *Plasmodium berghei*: kinetic and electrophoretic characterization. Exp Parasitol 70: 264-275.

[30] Mony B, Mehta M, Jarori G, Sharma S (2009) Plant-like phosphofructokinase from *Plasmodium falciparum* belongs to a novel class of atp-dependent enzymes. Int J Parasitol 39: 1441-1453.

[31] Döbeli H, Trzeciak A, Gillessen D, Matile H, Srivastava IK, et al. (1990) Expression, purification, biochemical characterization and inhibition of recombinant *Plasmodium falciparum* aldolase. Mol Biochem Parasitol 41: 259-268.

[32] Helfert S, Estevez A, Bakker B, Michels P, Clayton C (2001) Roles of triosephosphate isomerase and aerobic metabolism in *Trypanosoma brucei*. Biochem J 357: 117-125.

[33] Hoefnagel M, Starrenburg M, Martens D, Hugenholtz J, Kleerebezem M, et al. (2002) Metabolic engineering of lactic acid bacteria, the combined approach: kinetic modelling, metabolic control and experimental analysis. Microbiology 148: 1003-1013.

[34] Holzhutter H (2004) The principle of flux minimization and its application to estimate stationary fluxes in metabolic networks. Eur J Biochem 271: 2905-2922.

[35] Lowry O, Passonneau J (1964) The relationship between substrates and enzymes of glycolysis in brain. J Biol Chem 239: 31-42.

[36] Singh SK, Maithal K, Balaram H, Balaram P (2001) Synthetic peptides as inactivators of multimeric enzymes: inhibition of *Plasmodium falciparum* triosephosphate isomerase by interface peptides. FEBS Lett 501: 19-23.

[37] Maithal K, Ravindra G, Nagaraj G, Singh S, Balaram H, et al. (2002) Subunit interface mutation disrupting an aromatic cluster in *Plasmodium falciparum* triosephosphate isomerase: effect on dimer stability. Protein Eng 15: 575-584.

[38] Lambeir AM, Loiseau A, Kuntz D, Vellieux F, Michels P, et al. (2005) The cytosolic and glycosomal glyceraldehyde-3-phosphate dehydrogenase from *Trypanosoma brucei*. Eur J Biochem 198: 429-435.

[39] Kouril T, Esser D, Kort J, Westerhoff HV, Siebers B, et al. (2013) Intermediate instability at high temperature leads to low pathway efficiency for an *in vitro* reconstituted system of gluconeogenesis in *Sulfolobus solfataricus*. FEBS J 280: 4666-4680.

[40] Grüning NM N-M, Du D, Keller M, Luis B, Ralser M (2014) Inhibition of triosephosphate isomerase by phosphoenolpyruvate in the feedback-regulation of glycolysis. Open Biology 4: 130232.

[41] Blacklow SC, Raines RT, Lim WA, Zamore PD, Knowles JR (1988) Triosephosphate isomerase catalysis is diffusion controlled. appendix: Analysis of triose phosphate equilibria in aqueous solution by ^{31}P NMR. Biochemistry 27: 1158-1167.

[42] Campanale N, Nickel C, Daubenberger C, Wehlan D, Gorman J, et al. (2003) Identification and characterization of heme-interacting proteins in the malaria parasite, *Plasmodium falciparum*. J Biol Chem 278: 27354-27361.

[43] Byers LD, She HS, Alayoff A (1979) Interaction of phosphate analogues with glyceraldehyde-3-phosphate dehydrogenase. Biochemistry 18: 2471-80.

[44] Roth E, Joulin V, Miwa S, Yoshida A, Akatsuka J, et al. (1988) The use of enzymopathic human red cells in the study of malarial parasite glucose metabolism. Blood 71: 1408-1413.

[45] Pal B, Pybus B, Muccio DD, Chattopadhyay D (2004) Biochemical characterization and crystallization of recombinant 3-phosphoglycerate kinase of *Plasmodium falciparum*. Biochim Biophys Acta 1699: 277-280.

[46] Bergmeyer H (1974) Methods of enzymatic analysis. Verlag Chemie.

[47] Hills T, Srivastava A, Ayi K, Wernimont A, Kain K, et al. (2011) Characterization of a new phosphatase from plasmodium. Mol Biochem Parasitol 179: 69-79.

[48] Pal-Bhowmick I, Sadagopan K, Vora H, Sehgal A, Sharma S, et al. (2004) Cloning, overexpression, purification and characterization of *Plasmodium falciparum* enolase. Eur J Biochem 271: 4845-4854.

[49] Chan M, Sim T (2005) Functional analysis, overexpression and kinetic characterisation of pyruvate kinase from *Plasmodium falciparum*. Biochem Biophys Res Comm 326: 188-196.

[50] Chan M, Tan DH, Sim TS (2007) *Plasmodium falciparum* pyruvate kinase as a novel target for antimalarial drug-screening. Travel Med Infect Dis 5: 125-131.

[51] Shoemark D, Cliff M, Sessions R, Clarke A (2007) Enzymatic properties of the lactate dehydrogenase enzyme from *Plasmodium falciparum*. FEBS J 274: 2738-2748.

[52] Gomez MS, Piper RC, Hunsaker LA, Royer RE, Deck LM, et al. (1997) Substrate and cofactor specificity and selective inhibition of lactate dehydrogenase from the malarial parasite *P. falciparum*. Mol Biochem Parasitol 90: 235-246.

[53] Racker E (1950) Crystalline alcohol dehydrogenase from baker's yeast. J Biol Chem 184: 313-319.

[54] Dawkins P, Dickens F (1965) The oxidation of d- and l-glycerate by rat liver. Biochem J 94: 353-367.

[55] Young H, Pace N (1958) Some physical and chemical properties of crystalline alpha-glycerophosphate dehydrogenase. Arch Biochem Biophys 75: 125 -141.

[56] Olszewski KL, Llinás M (2011) Central carbon metabolism of *Plasmodium* parasites. Mol Biochem Parasitol 175: 95-103.

[57] Schnick C, Polley S, Fivelman Q, Ranford-Cartwright L, Wilkinson S, et al. (2009) Structure and non-essential function of glycerol kinase in *Plasmodium falciparum* blood stages. Mol Microbiol 71: 533-545.

[58] Naidoo K, Coetzer T (2013) Reduced glycerol incorporation into phospholipids contributes to impaired intra-erythrocytic growth of glycerol kinase knockout plasmodium falciparum parasites. Biochimica et Biophysica Acta 1830: 5326–5334.

[59] Gardner MJ, Hall N, Fung E, White O, Berriman M, et al. (2002) Genome sequence of the human malaria parasite *Plasmodium falciparum*. Nature 419: 498-511.

[60] Hansen M, Kun J, Schultz J, Beitz E (2002) A single, bi-functional aquaglyceroporin in blood-stage *Plasmodium falciparum* malaria parasites. J Biol Chem 277: 4874-4882.

[61] Kirk K, Horner H, Kirk J (1996) Glucose uptake in *Plasmodium falciparum*-infected erythrocytes is an equilibrative not an active process. Mol Biochem Parasitol 82: 195-205.

[62] Goodyer ID, Hayes DJ, Eisenthal R (1997) Efflux of 6-deoxy-D-glucose from *Plasmodium falciparum*-infected erythrocytes via two saturable carriers. Mol Biochem Parasitol 84: 229-239.

[63] Krishna S, Woodrow CJ, Burchmore RJS, Saliba KJ, Kirk K (2000) Hexose transport in asexual stages of *Plasmodium falciparum* and *Kinetoplastidae*. Parasitol Today 16: 516-521.

[64] Woodrow CJ, Penny JI, Krishna S (1999) Intraerythrocytic *Plasmodium falciparum* expresses a high affinity facilitative hexose transporter. J Biol Chem 274: 7272-7277.

[65] Woodrow CJ, Burchmore RJ, Krishna S (2000) Hexose permeation pathways in *Plasmodium falciparum*-infected erythrocytes. Proc Natl Acad Sci U S A 97: 9931-9936.

[66] Joët T, Chotivanich K, Silamut K, Patel A, Morin C, et al. (2004) Analysis of *Plasmodium vivax* hexose transporters and effects of a parasitocidal inhibitor. Biochem J 381: 905-909.

[67] Joët T, Eckstein-Ludwig U, Morin C, Krishna S (2003) Validation of the hexose transporter of *Plasmodium falciparum* as a novel drug target. Proc Natl Acad Sci U S A 100: 7476-7479.

[68] Joët T, Holterman L, Stedman TT, Kocken CH, Van Der Wel A, et al. (2002) Comparative characterization of hexose transporters of *Plasmodium knowlesi, Plasmodium yoelii* and *Toxoplasma gondii* highlights functional differences within the apicomplexan family. Biochem J 368: 923-929.

[69] Manning S, Woodrow C, Zuniga F, Iserovich P, Fischbarg J, et al. (2002) Mutational analysis of the hexose transporter of *Plasmodium falciparum* and development of a three-dimensional model. J Biol Chem 277: 30942-30949.

[70] Saliba K, Krishna S, Kirk K (2004) Inhibition of hexose transport and abrogation of pH homeostasis in the intraerythrocytic malaria parasite by an O-3-hexose derivative. FEBS Lett 570: 93-96.

[71] Kotyk A (1967) Mobility of the free and of the loaded monosaccharide carrier in *Saccharomyces cerevisiae.* Biochim Biophys Acta 135: 112-119.

[72] Halestrap AP, Price N (1999) The proton-linked monocarboxylate transporter (mct) family: structure, function and regulation. Biochem J 343: 281-299.

[73] Saliba K, Kirk K (1999) pH regulation in the intracellular malaria parasite, *Plasmodium falciparum.* H^+ extrusion via a v-type H^+-ATPase. J Biol Chem 274: 33213-33219.

[74] Wünsch S, Sanchez C, Gekle M, Grosse-Wortmann L, Wiesner J, et al. (1998) Differential stimulation of the Na^+/H^+ exchanger determines chloroquine uptake in *Plasmodium falciparum.* J Cell Biol 140: 335-345.

[75] Bosia A, Ghigo D, Turrini F, Nissani E, Pescarmona GP, et al. (1993) Kinetic characterization of Na^+/H^+ antiport of *Plasmodium falciparum* membrane. J Cell Physiol 154: 527-534.

[76] Hayashi M, Yamada H, Mitamura T, Horii T, Yamamoto A, et al. (2000) Vacuolar H(+)-ATPase localized in plasma membranes of malaria parasite cells, *Plasmodium falciparum*, is involved in regional acidification of parasitized erythrocytes. J Biol Chem 275: 34353-34358.

[77] Wünsch S, Sanchez C, Gekle M, Kersting U, Fischer K, et al. (1997) A method to measure the cytoplasmic pH of single, living *Plasmodium falciparum* parasites. Behring Inst Mitt 99: 44 -50.

[78] Cranmer S, Conant AR, Gutteridge WE, Halestrap AP (1995) Characterization of the enhanced transport of L- and D-lactate into human red blood cells infected with *Plasmodium falciparum* suggests the presence of a novel saturable lactate proton cotransporter. J Biol Chem 270: 15045-15052.

[79] Choi I, Mikkelsen R (1990) *Plasmodium falciparum*: ATP/ADP transport across the parasitophorous vacuolar and plasma membranes. Exp Parasitol 71: 452-462.

[80] Fry M, Webb E, Pudney M (1990) Effect of mitochondrial inhibitors on adenosinetriphosphate levels in *Plasmodium falciparum.* Comp Biochem Physiol B 96: 775-782.

[81] Teng R, Junankar P, Bubb W, Rae C, Mercier P, et al. (2009) Metabolite profiling of the intraerythrocytic malaria parasite *Plasmodium falciparum* by ^{1}H NMR spectroscopy. NMR Biomed 22: 292-302.

[82] Agbenyega T, Angus BJ, Bedu-Addo G, Baffoe-Bonnie B, Guyton T, et al. (2000) Glucose and lactate kinetics in children with severe malaria. J Clin Endocrinol Metab 85: 1569-1576.

[83] Evans ML, Matyka K, Lomas J, Pernet A, Cranston IC, et al. (1998) Reduced counterregulation during hypoglycemia with raised circulating nonglucose lipid substrates: evidence for regional differences in metabolic capacity in the human brain? J Clin Endocrinol Metab 83: 2952-2959.

[84] Travis S, Morrison A, Clements RJ, Winegrad A, Oski F (1971) Metabolic alterations in the human erythrocyte produced by increases in glucose concentration. the role of the polyol pathway. J Clin Invest 50: 2104-2112.

[85] Krishna S, Waller DW, ter Kuile F, Kwiatkowski D, Crawley J, et al. (1994) Lactic acidosis and hypoglycaemia in children with severe malaria: pathophysiological and prognostic significance. Trans R Soc Trop Med Hyg 88: 67-73.

[86] Pukrittayakamee S, White NJ, Davis TM, Supanaranond W, Crawley J, et al. (1994) Glycerol metabolism in severe *falciparum* malaria. Metabolism 43: 887-892.

[87] Kirk K (2001) Membrane transport in the malaria-infected erythrocyte. Physiol Rev 81: 495-537.

[88] Snoep J, Westerhoff H (2005) From isolation to integration, a systems biology approach for building the silicon cell. In: Alberghina L, Westerhoff H, editors, Systems Biology: Definitions and Perspectives, Springer-Verlag.

[89] Bruggeman FJ, Hornberg JJ, Boogerd FC, Westerhoff HV (2007) Introduction to systems biology. EXS 97: 1–19.

[90] Cornish-Bowden A, JHS H (2005) Kinetic characterization of enzymes for systems biology. The Biochemist 27: 11-14.

[91] Snoep JL (2005) The silicon cell initiative: working towards a detailed kinetic description at the cellular level. Curr Opin Biotechnol 16: 336–343.

[92] Snoep J, Bruggeman F, Olivier B, Westerhoff H (2006) Towards building the silicon cell: a modular approach. Biosystems 83: 207-216.

[93] Wolstencroft K, Owen S, Horridge M, Krebs O, Mueller W, et al. (2011) Rightfield: embedding ontology annotation in spreadsheets. Bioinformatics 27: 2021-2022.

[94] Olivier B, Snoep J (2004) Web-based kinetic modelling using JWS Online. Bioinformatics 20: 2143-2144.

[95] Hucka M, Finney A, Bornstein B, Keating S, Shapiro B, et al. (2004) Evolving a lingua franca and associated software infrastructure for computational systems biology: the systems biology markup language (sbml) project. Systems Biology 1: 41-53.

[96] Le Novere N, Finney A, Hucka M, Bhalla US, Campagne F, et al. (2005) Minimum information requested in the annotation of biochemical models (miriam). Nat Biotechnol 23: 1509–1515.

[97] Smallbone K, Messiha H, Carroll K, Winder C, Malys N, et al. (2013) A model of yeast glycolysis based on a consistent kinetic characterisation of all its enzymes. FEBS Lett 587: 2832-2841.

[98] Wittig U, Kania R, Golebiewski M, Rey M, Shi L, et al. (2012) Sabio-rk—database for biochemical reaction kinetics. Nucleic Acids Research 40: D790-D796.

[99] Li P, Dada J, Jameson D, Spasic I, Swainston N, et al. (2010) Systematic integration of experimental data and models in systems biology. BMC Bioinformatics 11: 582.

[100] Cranmer S, Magowan C, Liang J, Coppel R, Cooke B (1997) An alternative to serum for cultivation of *Plasmodium falciparum in vitro*. Trans R Soc Trop Med Hyg 91: 363-365.

[101] Trager W, Jensen J (1976) Human malaria parasits in continuous culture. Science 193: 673-675.

[102] Hoppe H, Verschoor J, Louw A (1991) *Plasmodium falciparum*: a comparison of synchronisation methods for *in vitro* cultures. Exp Parasitol 72: 464-467.

[103] Ansorge I, Benting J, Bhakdi S, Lingelbach K (1996) Protein sorting in *Plasmodium falciparum*-infected red blood cells permeabilized with the pore-forming protein streptolysin O. Biochem J 315: 307-314.

[104] Ansorge I, Paprotka K, Bhakdi S, Lingelbach K (1997) Permeabilization of the erythrocyte membrane with streptolysin O allows access to the vacuolar membrane of *Plasmodium falciparum* and a molecular analysis of membrane topology. Mol Biochem Parasitol 84: 259-261.

[105] Saliba K, Horner H, Kirk K (1998) Transport and metabolism of the essential vitamin pantothenic acid in human erythrocytes infected with the malaria parasite *Plasmodium falciparum*. J Biol Chem 273: 10190-10195.

[106] Walsh MC, Smits HP, Scholte M, Smits G, van Dam K (1994) Rapid kinetics of glucose uptake in *Saccharomyces cerevisiae*. Folia Microbiol (Praha) 39: 557-559.

[107] Walsh MC, Smits HP, Scholte M, van Dam K (1994) Affinity of glucose transport in *Saccharomyces cerevisiae* is modulated during growth on glucose. J Bacteriol 176: 953-958.

[108] Bradford M (1976) A rapid and sensitive method for the quantitation of microgram quantities of protein utilizing the principle of protein-dye binding. Anal Biochem 72: 248-254.

[109] Allen R, Kirk K (2004) Cell volume control in the *Plasmodium*-infected erythrocyte. Trends Parasitol 20: 7-10.

[110] Eggstein M, Kuhlmann E (1974) Methods of Enzyme Analysis, volume 29. Academic Press Inc., 2nd edition, 1825-1831 pp.

[111] Antonio C, Larson T, Gilday A, Graham I, Bergström E, et al. (2008) Hydrophilic interaction chromatography/electrospray mass spectrometry analysis of carbohydrate-related metabolites from *Arabidopsis thaliana* leaf tissue. Rapid Commun Mass Spectrom 22: 1399 -1407.

[112] Hoops S, Sahle S, Gauges R, Lee C, Pahle J, et al. (2006) COPASI- COmplex PAthway SImulator. Bioinformatics 22: 3067-3074.

List of References

1. World Health Organization. *World Malaria Report: 2013*. WHO Press, 2013.

2. G. P. Penkler. *A kinetic model of glucose catabolism in Plasmodium falciparum*. PhD thesis, University of Stellenbosch & Vrije Universiteit Amsterdam, Department of Biochemistry, University of Stellenbosch, Private Bag X1, 7602 Matieland, South Africa, December 2013. Supervisors: Prof. J. L. Snoep and Prof. M. Rautenbach.

3. R. Heinrich and T. Rapoport. A linear steady-state treatment of enzymatic chains. General properties, control and effector strength. *European Journal of Biochemistry*, 42(1):89–95, 1974.

4. H. Kacser and J. A. Burns. The control of flux. *Symposia of the Society for Experimental Biology*, 27:65–104, 1973.

5. T. Rapoport, R. Heinrich, G. Jacobasch, and S. Rapoport. A linear steady-state treatment of enzymatic chains. A mathematical model of glycolysis of human erythrocytes. *European Journal of Biochemistry*, 42(1):107–120, 1974.

6. B. M. Bakker, H. V. Westerhoff, F. R. Opperdoes, and P. A. Michels. Metabolic control analysis of glycolysis in trypanosomes as an approach to improve selectivity and effectieffect of drugs. *Molecular and Biochemical Parasitology*, 106(1): 1–10, 2000.

7. J. Hornberg, F. Bruggeman, B. Bakker, and H. Westerhoff. Metabolic control analysis to idaction optimal drug targets. *Progress in Drug Research*, 64:171,173–189, 2007.

8. I. Sherman. *Malaria: Parasite biology, pathogenesis and protection*. ASM Press, 1998.

9. L. H. Miller, D. I. Baruch, K. Marsh, and O. K. Doumbo. The pathogenic basis of malaria. *Nature*, 415:673–679, 2002.

10. I. Coppens, D. J. Sullivan, and S. T. Prigge. An update on the rapid advances in malaria parasite cell biology. *Trends in Parasitology*, 26:305–310, 2010.

11. A. Ghosh, M. J. Edwards, and M. Jacobs-Lorena. The journey of the malaria parasite in the mosquito: hopes for a new century. *Parasitology Today*, 16: 196–201, 2000.

12. N. Lang-Unnasch and A. D. Murphy. Metabolic changes of the malaria parasite during the transition from the human to the mosquito host. *Annual Review of Microbiology*, 52:561–590, 1998.

13. K. L. Olszewski and M. Llinás. Central carbon metabolism of *Plasmodium* parasites. *Molecular and Biochemical Parasitology*, 175(2):95–103, 2011.

14. N. P. Balabaskaran, J. M. Morrisey, S. M. Ganesan, H. Ke, A. M. Pershing, M. W. Mather, and A. B. Vaidya. ATP synthase complex of *Plasmodium falciparum*: dimeric assembly in mitochondrialmembranes and resistance to genetic disruption. *The Journal of Biological Chemistry*, 286(48):41312–41322, 2011.

15. N. Fisher, P. G. Bray, S. A. Ward, and G. A. Biagini. The malaria parasite type ii NADH:quinone oxidoreductase: An alternative enzyme for an alternative lifestyle. *Trends in Parasitology*, 23(7):305–310, 2007.

16. M. Fry, E. Webb, and M. Pudney. Effect of mitochondrial inhinhibit on adenosinetriphosphate levels in *Plasmodium falciparum*. *Comparative Biochemistry and Physiology B*, 96(4):775–782, 1990.

17. S. Déchamps, S. Shastri, K. Wengelink, and H. J. Vial. Glycerophospholipid acquisition in *Plasmodium*: A puzzling assembly of biosynthetic pathways. *International Journal of Parasitology*, 40:1347–1367, 2010.

18. G. L. Nixon, C. Pidathala, A. E. Shone, T. Antoine, N. Fisher, S. A. Ward, and G. A. Biagini. Targeting the mitochondrial electron transport chain of *Plasmodium falciparum*: new strategies towards the development of improved aantimalarial for the elimination era. *Future Medicinal Chemistry*, 5(13):1573–1591, 2013.

19. G. P. Penkler. Construction and validation of a detailed kinetic model of glycolysis in asexual *Plasmodium falciparum*: A feasibility study. Master's thesis, University of Stellenbosch, Department of Biochemistry, University of Stellenbosch, Private Bag X1, 7602 Matieland, South Africa, December 2009. Supervisors: Prof. J. L. Snoep and Prof. M. Rautenbach.

20. M. Hansen, J. F. J. Kun, J. E. Schultz, and E. Beitz. A single, bi-functional aquaglyceroporin in blood-stage *Plasmodium falciparum. The Journal of Biological Chemistry*, 277(7):4874–4882, 2002.

21. E. Beitz, S. Pavlovic-Djuranovic, M. Yasui, P. Agre, and J. E. Schultz. Molecular dissection of water and glycerol permeability of the aquaglyceroporin from *Plasmodium falciparum* by mutational analysis. *Proceedings from the National Academy of Science USA*, 101(5):1153–1158, 2004.

22. L.-Y. Lian, M. Al-Helal, A. M. Roslaini, N. Fischer, P. G. Bray, S. A. Ward, and G. A. Biagini. Glycerol: An unexpected major metabolite of energy metabolism by the human malaria parasite. *Malaria Journal*, 8:38, 2009.

23. G. Penkler, F. du Toit, W. Adams, M. Rautenbach, D. Palm, D. van Niekerk, and J. L. Snoep. Construction and validation of a detailed kinetic model of glycolysis in *Plasmodium falciparum. FEBS Journal*, in press 2015.

24. S. Cranmer, A. R. Conant, W. E. Gutteridge, and A. P. Halestrap. Characterization of the enhanced transport of l- and d-lactate into human red blood cells infected with *Plasmodium falciparum* suggests the presence of a novel saturable lactate proton cotransporter. *Journal of Biological Chemistry*, 270(25): 15045–15052, 1995.

25. J. L. Elliott, K. J. Saliba, and K. Kirk. Transport of lactate and pyruvate in the intraerythrocytic malaria parasite *Plasmodium falciparum. Biochemical Journal*, 355:733–739, 2001.

26. J. W. Choe, D. Guerra, P. A. M. Miches, and W. G. J. Hol. *Leishmania mexicana* glycerol 3-phosphate dehydrogenase showed conformational changes upon binding a bi-substrate adduct. *Journal of Molecular Biology*, 3329:335–349, 2003.

27. J. Albertyn, A. van Tonder, and B. A. Prior. Purification and characterization of glycerol 3-phosphate dehydrogenase of *Saccharomyces cerevisiae. FEBS Letters*, 308(2):130–132, 1992.

28. G. Klöck and K. Kreuzberg. Kinetic properties of a *sn*-glycerol-3-phosphate dehydrogenase purified from the unicellular alga *Chlamydomonas reinhardtii. Biochimica et Biophysica Acta*, 991:347–352, 1989.

29. J. R. Merkel, M. Straume, S. A. Sajer, and R. L. Hopfer. Purification and some properties of *sn*-glycerol 3-phosphate dehydrogenase from *Saccharomyces cerevisiae. Analytical Biochemistry*, 122:180–185, 1982.

30. A. Nilsson and L. Adler. Purification and characterization of glycerol-3-phosphate dehydrogenase (NAD$^+$) in the salt-tolerant yeast *Debaryomyces hansenii*. *Biochimica et Biophysica Acta*, 1034:180–185, 1990.

31. Y. Zheng, L. Zhao, J. Zhang, H. Zhang, X. Ma, and D. Wei. Production of glycerol from glucose by coexpressing glycerol-3-phosphate dehydrogenase and glycerol-3-phosphatase in *Klebsiella pneumoniae*. *Journal of Bioscience and Bioengineering*, 105:508–512, 2008.

32. S. Marché, P. A. M. Michels, and F. R. Opperdoes. Comparative study of *Leishmania mexicana* and *Trypanosoma brucei* NAD-dependent glycerol-3-phosphate dehydrogenase. *Molecular and Biochemical Parasitology*, 106:83–91, 2000.

33. C. E. Stebeck, U. Frevert, T. P. Mommsen, E. Vassella, I. Roditi, and T. W. Pearson. Molecular characterization of glycosomal NAD+ -dependent glycerol 3-phosphate dehydrogenase from *Trypanosoma brucei rhodesiense*. *Molecular and Biochemical Parasitology*, 76:145–158, 1996.

34. S. Suresh, S. Turley, F. R. Opperdoes, P. A. M. Michels, and W. G. J. Hol. A potential target enzyme for trypanocidal drugs revealed by the crystal structure of NAD-dependent glycerol-3-phosphate dehydrogenase from *Leishmania mexicana*. *Structure*, 8:541–552, 2000.

35. J. D. Cheng and J. de Vellis. Oligodendrocytes as glucocorticoid target cells: Functional analysis of the glycerol phosphate dehydrogenase gene. *Journal of Neuroscience Research*, 59:436–445, 2000.

36. P. B. Chock and H. Gutfreund. Reexamination of the kinetics of the transfer of NADH between its complexes with glycerol 3-phosphate dehydrogenase and with lactate dehydrogenase. *Proceedings from the National Academy of Science*, 85:8870–8875, 1988.

37. T. P. Fondy, J. Solomon, and C. R. Ross. Comparison of cytoplasmic glycerol 3-phosphate dehydrogenase from rat liver and muscle. *Archives of Biochemistry and Biophysics*, 145:604–611, 1971.

38. T. C. Koekemoer, D. Litthauer, and W. Oelofsen. Isolation and characterization of adipose tissue glycerol-3-phosphate dehydrogenase. *International Journal of Biochemistry and Cell Biology*, 27:625–632, 1995.

39. J. Kömpf, H. Ritter, and J. Schmitt. Genetic polymorphism of glycerol 3-phosphate dehydrogenase (E.C.: 1.1.1.8): I. Transspecific variability of G-3-PD subunit B in primates. *Humangenetik*, 13:75–77, 1971.

40. J. F. McGinnis and J. de Vellis. Differential hormonal regulation of L-glycerol 3-phosphate dehydrogenase in rat brain and skeletal muscle. *Archives of Biochemistry and Biophysics*, 179:682–689, 1977.

41. J. F. McGinnis and J. de Vellis. Glycerol-3-phosphate dehydrogenase isoenzymes in human tissues: Evidence for a heart-specific form. *Journal of Molecular and Cellular Cardiology*, 11:795–802, 1979.

42. C. R. Ross, S. Curry, A. Wesson Swartz, and T. P. Fondy. Multiple molecular forms of cytoplasmic glycerol-3-phosphate dehydrogenase in rat liver. *Archives of Biochemistry and Biophysics*, 145:591–608, 1971.

43. C. Aurrecoechea, J. Brestelli, B. P. Brunk, J. Dommer, S. Fisher, B. Gajria, X. Gao, A. Gringle, G. Grant, O. S. Harb, M. Heiges, F. Innamorato, J. Iodice, J. C. Kissinger, E. Kraemer, W. Li, J. A. Miller, V. Nayak, C. Pennington, D. F. Pinney, D. S. Roos, C. Ross, Jr. C. J. Stoeckert, C. Treatman, and H. Wang. PlasmoDB: A functional genomic datadata for malaria parasites. *Nucleic Acids Research*, 37(Database issue):D539–D543, 2009.

44. Z. Bozdech and H. Ginsburg. Data mining of the tratranscript of *Plasmodium falciparum*: the pentose phosphate pathway and ancillary processes. *Malaria Journal*, 4:17, 2005.

45. R. W. Brosemer and R. W. Kuhn. Comparative structural properties of honeybee and rabbit α-glycerophosphate dehydrogenases. *Biochemistry*, 8(5):2095–2105, 1969.

46. H. B. White, III. The molecular weights of glycerol-3-p dehydrogenases from chicken, rabbit, and honey bee. *Archives of Biochemistry and Biophysics*, 147: 123–128, 1971.

47. K. Naidoo and T. L. Coetzer. Reduced glycerol incorporation into phospholipids contributes to impaired intra-erythrocytic growth of glycerol kinase knockout *Plasmodium falciparum* parasites. *Biochimica et Biophysica Acta*, 1830:5326–5334, 2013.

48. C. Schnick, S. D. Polley, Q. L. Fivelman, L. C. Ranford-Cartwright, S. R. Wilkinson, J. A. Brannigan, A. J. Wilkinson, and D. A. Baker. Structure and non-essential function of glycerol kinase in *Plasmodium falciparum* blood stages. *Molecular Microbiology*, 71(2):533–545, 2009.

49. P. M. Durand, K. Naidoo, and T. L. Coetzer. Evoevolution patterning: A novel approach to the identification of potential drug target sites in *Plasmodium falciparum. PLoS One*, 3:e3685, 2008.

50. T. Hills, A. Srivastava, K. Ayi, A. K. Wernimont, K. Kain, A. P. Waters, R. Hui, and J. C. Pizarro. Characterization of a new phosphatase from *Plasmodium. Molecular and Biochemical Parasitology*, 179:69–79, 2011.

51. Z. E. R. Newby, J. O'Connell, III, Y. Robes-Colmenares, S. Khademi, L. J. Miercke, and R. M. Stroud. Crystal structure of the aquaglyceroporin pfaqp from the malarial parasite *Plasmodium falciparum. Nature Structural & Molecular Biology*, 15(6):619–625, 2008.

52. Jr. G. G. Holz. Lipids and the malarial parasite. *Bulletin of the World Health Organization*, 55(2-3):237–248, 1977.

53. H. J. Vial, M. J. Thuet, and J. R. Philippot. Phospholipid biosynthesis in synchronous *Plasmodium falciparum* cultures. *Journal of Protozoology*, 29(2): 258–263, 1982.

54. N. M. Q. Palacpac, Y. Hiramine, F. Mi-ichi, M. Torii, K. Kita, R. Hiramatsu, T. Horii, and T. Mitamura. Developmental-stage-specific triacylglycerol biosynthesis, degradation and trafficking as lipid bodies in *Plasmodium falciparum*-infected erythrocytes. *Journal of Cell Science*, 117:1469–1480, 2004.

55. T. C. Santiago, R. Zufferey, R. S. Mehra, R. A. Coleman, and C. B. Mamoun. The *Plasmodium falciparum* pfgatp is an endoplasmic reticulum membrane protein important for the initial step of malarial glycerolipid synthesis. *The Journal of Biological Chemistry*, 279(10):9222–9232, 2004.

56. V. Choubey, M. Guha, P. Maity, S. Kumar, R. Raghunandan, P. R. Maulik, K. Mitra, U. C. Halder, and U. Bandyopadhyay. Molecular characterization and localization of *Plasmodium falciparum* choline kinase. *Biochimica et Biophysica Acta*, 1760:1027–1038, 2006.

57. S. Déchamps, K. Wengelink, L. Berry-Sterkers, R. Cerdan, H. J. Vial, and L. Gannoun-Zaki. The kennedy phospholipid biosynthesis pathways are refractory to genetic disruption in *Plasmodium berghei* and therefore appear essential in blood stages. *Molecular and Biochemical Parasitology*, 173:69–80, 2010.

58. F. Gibellini and T. K. Smith. The Kennedy pathway—*De novo* synthesis of phosphatidylenthanolamine and phosphatidylcholine. *IUBMB Life*, 62(6):414–428, 2010.

59. N. Kresge, R. D. Simoni, and R. L. Hill. The Kennedy pathway for phospholipid synthesis: the work of Eugene Kennedy. *The Journal of Biological Chemistry*, 280(25):e22–e24, June 2005.

60. G. Pessi, G. Kociubinski, and C. B. Mamoun. A pathway for phosphatidylcholine biosynthesis in *Plasmodium falciparum* involving phosphoethanolamine methylation. *Proceedings of the National Academy of Sciences of the USA*, 101(16): 6206–6211, 2004.

61. S. Shastri, A.-M. Zeeman, L. Berry, R. J. Verburgh, C. Braun-Breton, A. W. Thomas, L. Gannoun-Zaki, C. H. M. Kocken, and H. J. Vial. *Plasmodium* CDP-DAG synthase: An atypical gene with an essential N-terminal extension. *International Journal for Parasitology*, 40:1257–1268, 2010.

62. P. Sen, H. J. Vial, and O. Radulescu. Kinetic modelling of phospholipid synthesis in *Plasmodium knowlesi* unravels crucial steps and relative importance. *BMC Systems Biology*, 7:123, 2013.

63. H. Bisswanger. *Enzyme kinetics: Principles and methods.* Wiley-VCH Verlag GmbH and Co. KGaA, Weinheim, Germany, 2 edition, 2008.

64. I. H. Segel. *Enzyme kinetics: Behaviour and analysis of rapid equilibrium and steady-state enzyme systems.* Wiley-Interscience, 1 edition, 1974.

65. A. Cornish-Bowden. *Fundamentals of enzyme kinetics.* Portland Press Ltd., London, revised edition, 1995.

66. G. E. Briggs and J. B. S. Haldane. A note on the kinetics of enzyme action. *Biochemistry Journal*, 19:338–339, 1925.

67. D. A. Fell. Metabolic control analysis: A survey of its theoretical and experimental development. *Biochemical Journal*, 286(Pt 2):313–330, 1992.

68. J.-H. S. Hofmeyr. Metabolic control analysis in a nutshell. In *Proceedings of the ICSB*, 291-300, Pasedena, California, 2000.

69. H. V. Westerhoff. Systems biology left and right. In J. N. Abelsen and M. I. Simon, editors, *Methods in Enzymology*, volume 500, chapter 01, pages 3–11. Elsevier Inc., 1st edition, 2011.

70. H. G. Holzhutter, G. Jacobasch, and A. Bisdorff. Mathematical modelling of metabolic pathways affected by an enzyme deficiency. A mathematical model of glycolysis in normal and pyruvate-kinase-deficient red blood cells. *European Journal of Biochemistry*, 149(1):101–111, 1985.

71. W. Trager and J. B. Jensen. Human malaria parasites in continuous culture. *Science*, 193(4254):673–675, 1976.

72. S. L. Cranmer, C. Magowan, J. Liang, R. L. Coppel, and B. M. Cooke. An alternative to serum for cultivation of *Plasmodium falciparum* in vitro. *Transactions of the Royal Society of Tropical Medicine and Hygiene*, 91(3):363–375, 1997.

73. H. C. Hoppe, J. A. Verschoor, and A. I. Louw. *Plasmodium falciparum*: A comparison of synchronisation methods for in vitro cultures. *Experimental Parasitology*, 72(4):464–467, 1991.

74. K. J. Saliba, H. A. Homer, and K. Kirk. Transport and metabolism of the essential vitamin pantothenic acid in human erythrocytes infected with the malaria parasite *Plasmodium falciparum*. *Journal of Biological Chemistry*, 273 (17):10190–10195, 1998.

75. M. Eggstein and E. Kuhlmann. Triglycerides and glycerol: Determination after alkaline hydrolysis. In H. Bergmeyer, editor, *Methods in Enzymatic Analysis*, pages 1825–1831. Academic Press, Inc., 2nd edition, 1974.

76. O. Wieland. Glycerol. In H. Bergmeyer, editor, *Methods in Enzymatic Analysis*, pages 211–214. Academic Press, Inc., 2nd edition, 1974.

77. J. E. G. Barnett, R. E. Brice, and D. L. Corina. A colorimetric determination of inositol monophosphates as an assay for D-glucose 6-phosphate-L-*myo*inositol 1-phosphate cyclase. *Biochemistry Journal*, 119:183–186, 1970.

78. J. L. Snoep and B. G. Olivier. JWS Online cellular systems modelling and microbiology. *Microbiology*, 149(Pt 11):3045–3047, 2003.

79. B. Olivier and J. Snoep. Web-based kinetic modelling using jws online. *Bioinformatics*, 20(13):2143–2144, 2004.

80. K. Wolstencroft, S. Owen, F. du Preez, O. Krebs, W. Mueller, C. Goble, and J. L. Snoep. The SEEK: A platform for sharing data and models in systems biology. In J. N. Abelsen and M. I. Simon, editors, *Methods in Enzymology*, volume 500, chapter 29, pages 629–655. Elsevier Inc., 2011.

81. P. Hemström and K. Irgum. Hydrophilic interaction chromatography. *Journal of Separation Science*, 29(12):1784–1821, 2006.

82. C. Antonio, T. Larson, A. Gilday, I. Graham, E. Bergström, and J. Thomas-Oates. Hydrophilic interaction chromatography/electrospray mass spectrometry

analysis of carbohydrate-related metabolites from *Arabidopsis thaliana* leaf tissue. *Rapid Communications in Mass Spectrometry*, 22:1399–1407, 2008.

83. S. M. Nilapwar, M. Nardelli, H. V. Westerhoff, and M. Verma. Absorption spectroscopy. In J. N. Abelsen and M. I. Simon, editors, *Methods in Enzymology*, volume 500, chapter 4, pages 59–75. Elsevier Inc., 1st edition, 2011. D. Jameson and M. Verma and H. V. Westerhoff (eds of volume 500). Abelsen and Simon are editors-in-chief.

84. M. M. Bradford. A rapid and sensitive method for the quantitation of microgram quantities of protein utilizing the principle of protein-dye binding. *Analytical Biochemistry*, 72:248–254, 1976.

85. J. M. Rohwer, A. J. Hanekom, C. Crous, J. L. Snoep, and J.-H. S. Hofmeyr. Evaluation of a simplified generic bi-substrate rate equation for computational systems biology. *IEE Proceedings Systems Biology*, 153:338–341, 2006.

86. R. N. Goldberg, Y. B. Tewari, D. Bell, K. Fazio, and E. Anderson. Thermodynamics of enzyme-catalyzed reactions: Part 1. Oxidoreductases. *Journal of Physical Chemistry*, 22(2):515–582, 1993.

87. G. T. Santora, R. Gee, and N. E. Tolbert. Isolation of a *sn*-glycerol 3-phosphate: NAD oxidoreductase from spinach leaves. *Archives of Biochemistry and Biophysics*, 196:403–411, 1979.

88. J. L. Snoep, M. H. N. Hoefnagel, and H. V. Westerhoff. *Metabolic engineering in the post-genomic era*, chapter Metabolic engineering of branched systems: Redirecting the main pathway flux, pages 357–375. Horizon Bioscience, 2004.

89. H. M. Sauro. *Control Theory for Biologists and Bioengineers*, electronic Branched and cyclic systems, pages 307–318. May 2012. URL `http://sys-bio.org/control-theory-for-biologists/`.

90. H. M. Sauro, J. R. Small, and D. A. Fell. Metabolic control analysis: Extensions to the theory and matrix method. *European Journal of Biochemistry*, 165: 215–221, 1987.

91. D. A. Fell and H. M. Sauro. Metabolic control and its analysis: Additional relationships between elasticities and control coefficients. *European Journal of Biochemistry*, 148:555–561, 1985.

92. B. M. Bakker, P. A. M. Michels, F. R. Opperdoes, and H. V. Weterhoff. What controls glycolysis in bloodstream form *Trypanosoma brucei*? *The Journal of Biological Chemistry*, 274(21):14551–14559, 1999.

93. J. L. Krakow and C. C. Wang. Purification and characterization of glycerol kinase from *Trypanosoma brucei. Molecular and Biochemical Parasitology*, 43: 17–26, 1990.

94. I. Králová, D. J. Rigden, F. R. Opperdoes, and P. A. M. Michels. Glycerol kinase of *Trypanosoma brucei*: Cloning, molecular characterization and mutagenesis. *The European Journal of Biochemistry*, 267:2323–2333, 2000.

95. B. Teusink, J. Passarge, C. A. Reijenga, E. Esgalhado, C. C. van der Weijden, M. Schepper, M. C. Walsh, B. M. Bakker, K. van Dam, H. V. Westerhoff, and J. L. Snoep. Can yeast glycolysis be underunder in terms of *in vitro* kinetics of the constituent enzymes? Testing biochemistry. *European Journal of Biochemistry*, 267(17):5313–5329, 2000.

96. B. M. Bakker, P. A. M. Michels, F. R. Opperdoes, and H. V. Westerhoff. Glycolysis in bloodstream form *Trypanosoma brucei* can be underunder in terms of the kinetics of glycolytic enzymes. *The Journal of Biological Chemistry*, 272 (6):3207–3215, 1997.

97. A. G. Dawson and G. J. Cooney. Reconstruction of the α-glycerophosphate shuttle using rat kidney mitochondria. *FEBS Letters*, 91(2):169–172, 1978.

98. R. M. Njogu and M. Nyindo. Presence of a peculiar pathway of glucose metabolism in infective forms of *Trypanosoma brucei* cultured from salivary glands of tsetse flies. *The Journal of Parasitology*, 67(6):847–851, 1981.